DESIGN AND OPTICAL EVALUATION OF SECONDARY OPTICS FOR OPTIMIZING ELECTRICAL PERFORMANCE OF DENSE-ARRAY CONCENTRATOR PHOTOVOLTAIC SYSTEM

YEW TIONG KEAT

DOCTOR OF PHILOSOPHY IN ENGINEERING

LEE KONG CHIAN FACULTY OF ENGINEERING AND SCIENCE
UNIVERSITI TUNKU ABDUL RAHMAN
SEPTEMBER 2016

DESIGN AND OPTICAL EVALUATION OF SECONDARY OPTICS FOR OPTIMIZING ELECTRICAL PERFORMANCE OF DENSE-ARRAY CONCENTRATOR PHOTOVOLTAIC SYSTEM

By

YEW TIONG KEAT

A thesis submitted to the Department of Electrical and Electronic Engineering,
Lee Kong Chian Faculty of Engineering and Science,
Universiti Tunku Abdul Rahman,
in partial fulfillment of the requirements for the degree of
Doctor of Philosophy in Engineering
September 2016

ABSTRACT

DESIGN AND OPTICAL EVALUATION OF SECONDARY OPTICS FOR OPTIMIZING ELECTRICAL PERFORMANCE OF DENSE-ARRAY CONCENTRATOR PHOTOVOLTAIC SYSTEM

Yew Tiong Keat

A secondary concentrator had been designed to increase the packing factor of dense-array concentrator photovoltaic (DACPV) module. Array of dielectric filled CCPC lenses is selected as secondary concentrator due to high acceptance angle, larger entrance aperture to provide more space for high flexibility of inter-connection among CPV cells, and square exit aperture that match well with the shape of commercial CPV cell. Optical characterization is carried out to study its optical performance. The uniformity is measured by peak-to-average ratio (PAR), which ranges from 2.08 to 2.35. The optical efficiency of CCPC lens is evaluated with experiment under the sun. The solar concentration ratio of CCPC is found to be ranging from 3.96-4.22. Electrical performance of integrated CPV cells with CCPC lenses (CPV + CCPC) assembly module is analyzed for different pointing errors: 0°, 0.1°, 0.2°, 0.3° & 0.4°, and the results are compared to that of dense-array CPV (DACPV) module. It was found that overall electrical performance of CPV + CCPC assembly module is better than that of DACPV module despite using 77% less CPV cells than that of DACPV module. CPV + CCPC assembly module is connected to load to measure its maximum output. The maximum power is 503W when DNI is 789 W/m^2 and GSI is 973 W/m^2. Therefore system efficiency of the DACPV system is calculated as 17%.

ACKNOWLEDGEMENT

I would like to dedicate the work to my father and late mother who had always offered me encouragement and support in all my endeavours.

First thanks goes to my supervisor, Prof. Dr. Chong Kok Keong for his guidance, invaluable advice and encouragement over the years of my study. I would like to express my gratitude to my co-supervisor, Dr Yap Vooi Voon for his continuous help and support that enable me to complete my study.

I would like to specially thank my research team parteners, Wong Chee Woon, Tan Ming Hui, Tan Woei Chong and Siaw Fei Lu for their assistances in discussing ideas and hands for helping out in some experimental work. Furthermore, I would like to show my appreciation to none forgetting all of the lab officers and lab assistants of Lee Kong Chian Faculty of Engineering and Science, University Tunku Abdul Rahman for their assistance in making some hardware for my experimental works.

Many thanks also to my family members who had been always understanding and encouraging through the years.

APPROVAL SHEET

This dissertation/thesis entitled "**DESIGN AND OPTICAL EVALUATION OF SECONDARY OPTICS FOR OPTIMIZING ELECTRICAL PERFORMANCE OF DENSE-ARRAY CONCENTRATOR PHOTOVOLTAIC SYSTEM"** was prepared by YEW TIONG KEAT and submitted as partial fulfillment of the requirements for the degree of Doctor of Philosophy in Engineering at Universiti Tunku Abdul Rahman.

Approved by:

_____

(Prof. Dr. Chong Kok Keong)
Date:……..
Supervisor
Department of Electrical and Electronic Engineering
Lee Kong Chian Faculty of Engineering and Science
Universiti Tunku Abdul Rahman

_____

(Dr. Yap Vooi Voon)
Date:……..
Co-supervisor
Department of Electronic Engineering
Faculty of Engineering and Green Technology
Universiti Tunku Abdul Rahman

LEE KONG CHIAN FACULTY OF ENGINEERING AND SCIENCE

UNIVERSITI TUNKU ABDUL RAHMAN

Date: 20 September 2016

SUBMISSION OF THESIS

It is hereby certified that **YEW TIONG KEAT** *(*ID No: **12UED05809**) has completed this thesis entitled "**DESIGN AND OPTICAL EVALUATION OF SECONDARY OPTICS FOR OPTIMIZING ELECTRICAL PERFORMANCE OF DENSE-ARRAY CONCENTRATOR PHOTOVOLTAIC SYSTEM**" under the supervision of **Prof. Dr. CHONG KOK KEONG** (Supervisor) from the Department of Electrical and Engineering, Lee Kong Chian Faculty of Engineering and Science, and **Dr. YAP VOOI VOON** (Co-Supervisor) from the Department of Electronic Engineering, Faculty of Engineering and Green Technology.

I understand that University will upload softcopy of my thesis in pdf format into UTAR Institutional Repository, which may be made accessible to UTAR community and public.

Yours truly,

_____

(Yew Tiong Keat)

DECLARATION

I hereby declare that the dissertation is based on my original work except for quotations and citations which have been duly acknowledged. I also declare that it has not been previously or concurrently submitted for any other degree at UTAR or other institutions.

Name _____Yew Tiong Keat _____ __

Date _____20 September 2016_____

TABLE OF CONTENTS

CHAPTER **Page**

LIST OF TABLES

LIST OF FIGURES

LIST OF ABBREVIATIONS

2-D	2-Dimensional
3-D	3-Dimensional
ADC	Analog-to-Digital Converter
CCPC	Crossed Compound Parabolic Concentrator
CPC	Compound Parabolic Concentrator
CPV	Concentrator Photovoltaic
DACPV	Dense Array Concentrator Photovoltaic
DBC	Direct Bond Copper
DNI	Direct Normal Irradiance
FF	Fill Factor
GSI	Global Solar Irradiance
I-V	Current-Voltage
MJ	Multi-junction
NIDC	Non-Imaging Dish Concentrator
NIPC	Non-Imaging Planar Concentrator
P-V	Power-Voltage
PAR	Peak-to-Average Ratio
PV	Photovoltaic
SCR	Solar Concentration Ratio
SOE	Secondary Optical Element
USB	Universal Serial Bus
UTAR	Universiti Tunku Abdul Rahman

CHAPTER 1

INTRODUCTION

1.1 Research Background and Motivation

The advancement of science and technology has greatly changed the way of life of our modern society. The demand for electrical energy has surged significantly to suit our new lifestyle. The largest source of electrical energy generation is from fossil fuel, which includes coal, oil, natural gas, etc. Burning fossil fuel emits carbon dioxide that has contributed substantially to climate change. Renewable energy is the best way to reduce our reliance for energy on fossil fuel, but sometimes it comes at a higher cost depending on the type of collecting system used. A lot of research has been ongoing to find ways to produce electrical energy from renewable energy such as solar, wind, wave, geothermal heat, etc. at a lower cost. Solar energy is the most abundant renewable energy source available. Scientists have estimated that the maximum solar energy derivable over land is 16,300 terawatts, which is about 1,000 times of the current energy usage of the whole world (Buchanan, 2015).

Conversion efficiency as high as 46% recorded by multi-junction solar cells had given boast to the development of the solar concentrator system as multi-junction solar cells can be used under a concentrated condition (Green et al., 2015). The idea to use solar concentrator is to replace the solar cell

material with a relatively cheap optical device that can focus the solar energy up to thousands folds on multi-junction solar cells in order to reduce the cost of producing electrical energy from solar energy. Numerous types of solar concentrator systems had been developed in the past 30 to 40 years to achieve this target, but there are still room for improvement to achieve a better outcome.

1.2 The Challenge

Fresnel lens is one the most widely used optical devices in the CPV system wherein each Fresnel lens focuses sunlight onto a single CPV cell (Sonneveld et al., 2011 and Ryu et al., 2006). One of the shortcomings of most Fresnel lens CPV systems is its ineffectiveness in recollection of thermal waste that is not converted to electricity. In this design, each solar cell is attached to a passive heat sink for rejecting the waste heat to the surroundings without any heat recapturing mechanism in order to maintain the cell at optimal operating temperature. For large point focus systems, a parabolic dish is employed to concentrate sunlight onto a receiver plane whereby either the thermal convertor or the CPV receiver can be placed for energy conversion. In the case of a CPV receiver in a dish system, an active cooling system is required to maintain the operating temperature of the CPV cell by circulating cooling fluid through the heat sink for heat removal. The waste heat collection via the cooling fluid can then be utilized for thermal applications or power generation. This centralized waste heat is higher than if heat is gathered from

each individual cell in a Fresnel type system, due to the lost heat in the transport links between cells. Therefore, the overall system efficiency can be much higher as compared to that of flat PV panels or Fresnel lens CPV systems and so on, when both electricity and thermal outputs are considered. In spite of the parabolic dish system being capable of generating both electrical and thermal powers simultaneously, the nature of its optical property is not so suitable for the application of the CPV system that requires uniform illumination (Baig et al., 2012). A parabolic dish is an imaging device that produces sharp, circular shaped, and non-uniform Gaussian distribution focusing spot.

In order to overcome the challenges faced by the parabolic dish, Chong and colleagues invented a computer generated dish geometry that is constituted of many flat facet mirrors aimed to produce a uniform focusing spot, the non-imaging dish concentrator (NIDC) (Chong et al., 2012, 2013a, 2013b, and Tan et al., 2014). A dense-array CPV (DACPV) receiver is placed at the focal plane of the NIDC to convert concentrated sunlight into electricity. The assembly of the DACPV module requires a small gap among solar cells for interconnection both in parallel and series, and thus there will be some physical area illuminated by the concentrated sunlight without active solar cell material. Furthermore, the presence of build-in bus bars on the surface of the CPV cell (about 1 mm on both sides of the CPV cell) has further increased the non-active area of the incident surface. Figure 1.1 illustrates that a blank gap is required in the assembly of DACPV for interconnection.

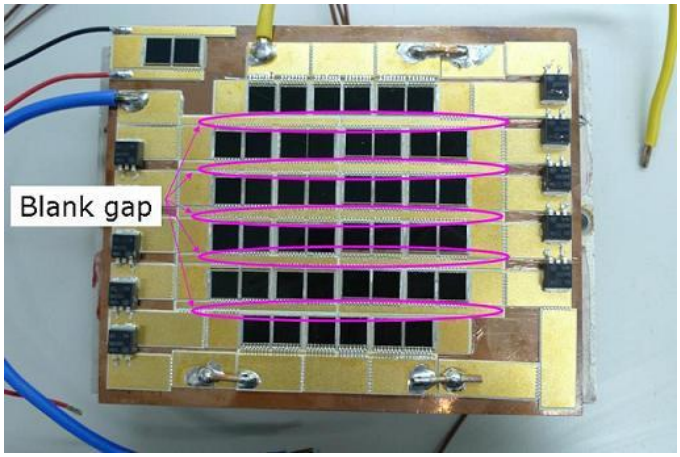

Figure 1.1: A blank gap occurred due to the need of interconnection between CPV modules in the assembly of DACPV.

As a result, it is impossible to achieve 100% packing factor whereby the packing factor of the DACPV module is defined as the ratio of usable active area of solar cells to the total solar illumination area on the incident surface. A low packing factor will affect the overall conversion efficiency of the whole system since the concentrated sunlight fallen on non-active area of the receiver will not be converted to electricity. In this thesis, a method to increase the percentage of incident rays that impinge on the active area of solar cells has been proposed by the introduction of a secondary concentrator. The solar cell is attached directly to the exit aperture of the secondary concentrator, which acts as an optical funnel tailored to guide the concentrated sunlight from the primary concentrator to the solar cells. In addition to that, the introduction of a secondary concentrator can provide more space for the interconnection among solar cells that allows more flexibility in the ways to connect solar cells in both series and parallel for minimizing the current mismatch in the circuitry of DACPV cells. Each CPV cell can also have an

individual by-pass diode for protecting the cell and improving the fill factor of the CPV system.

1.3 Objectives

In order to overcome the above-mentioned packing factor problem, the use of secondary optics in the DACPV system had been proposed and explored. The main objectives are as follows:

1. To design a secondary concentrator for the Non-Imaging Dish Concentrator (NIDC).
2. To study the performance of the secondary concentrator with ray tracing simulation.
3. To validate the simulated results of the secondary concentrator via testing under the sun testing.

1.4 Contributions

Improvements to the packing factor of the dense-array CPV receiver can be done by adding a secondary concentrator to the receiver. The addition of a secondary concentrator reduces the usage of solar cell material due to the utilization of less costly optical devices. The secondary concentrator is found to be still operational under a concentration of more than 300×. The

introduction of a secondary concentrator also provides the possibility to incorporate a by-pass diode to each CPV cell in the receiver module to protect the CPV cell when non-uniform illumination occurs. By integrating a secondary concentrator, more space for a more flexible way of interconnecting CPV cells in the receiver module is made possible. The study found that by using a secondary concentrator, the amount of solar cells used was reduced significantly while still giving a similar output power.

1.5 Outline of the Thesis

The organization of the thesis is outlined as follows:

- Chapter 1 of this thesis gives an introduction to the research's background and motivation in developing a secondary concentrator for the dense array CPV system. This section also identifies the challenges in the development of a secondary concentrator for the DACPV system. Besides that, the project's objectives and contributions are clarified in this chapter.

- In Chapter 2, a literature review about the various types of solar concentrators including linear focusing lens, two-dimensional focusing lens, linear focusing reflector, two-dimensional focusing reflector, and central receiver system is presented.

- At the beginning of Chapter 3, the working principle of the primary concentrator, the non-imaging dish concentrator is briefly explained. Next, the procedure of designing a secondary concentrator and the optical characterization of the secondary concentrator is discussed in detail. The optical efficiency evaluation of the secondary concentrator with an experiment is also discussed in the later part of the chapter.

- At first, Chapter 4 explains the assembly process of a secondary concentrator. Next, the electrical performance of the dense array CPV is analysed via simulation. At the end of this chapter, an experimental study of the electrical performance is presented.

- Chapter 5 ends the thesis with the conclusion and future work. The thesis concludes with the outcomes of the overall research achievements and the advantages of the developed system.

1.6 Publications

Based on the findings from this research, several papers have been published in peer-reviewed journals and international conference proceedings. A full list of publications is presented in Table 1.1.

Table 1.1: Papers published in peer-reviewed journals and international conference proceedings.

Appendix	Paper title	Year	Journal/ conference	Impart factor of journal
A	"Design and development in optics of concentrator photovoltaic system" **(Published)**	2013	Renewable and Sustainable Energy Reviews	5.901
B	"Dense-Array Concentrator Photovoltaic System Utilising Non-Imaging Dish Concentrator And Array Of Crossed Compound Parabolic Concentrators" **(Pending)**	2014	U.S. Patent	N/A
C	"Dense-Array Concentrator Photovoltaic System using Non-Imaging Dish Concentrator and Crossed Compound Parabolic Concentrator" **(Published)**	2014	National Physics Conference (PERFIK 2014)	N/A
D	"Performance study of crossed compound parabolic concentrator as secondary optics in non-imaging dish concentrator for the application of dense-array concentrator photovoltaic system" **(Published)**	2015	Solar Energy	3.469

CHAPTER 2

LITERATURE REVIEW

Concentrating solar power has been getting more importance as an alternative green solution to reduce the cost of electrical and thermal power generation. The recent achievement in the technology of multi-junction concentrator photovoltaic (CPV) cell with a conversion efficiency of more than 46% and still in the stage of improving have stimulated the development of concentrator optics (Green et al., 2015). Solar concentrators with an appropriate optical design is deployed to concentrate sunlight onto the CPV cell that is capable to work efficiently under highly concentrated solar irradiance to generate electricity (Zubi et al., 2009 and Chong et al., 2013b). Solar concentrators made of less costly materials can offset the price of highly efficient CPV cells made from more expensive semiconductor materials, so that the whole system can be more cost effective.

2.1 Types of Solar Concentrators and Optical Designs

Solar concentrator systems employ either lenses or reflectors or a combination of both types associated with a tracking system to concentrate a large area of sunlight onto a small beam. Some concentrator systems also employ secondary concentrators or even tertiary concentrators to enhance the

solar concentration ratio as well as to homogenize the distribution of solar flux on the receiver. The output power of the CPV module is directly affected by the distribution of focused sunlight on the module. Therefore, it is important that the concentrator is designed to focus sunlight uniformly over the receiver module's surface. Although a wide range of concentrating technologies exist, all of these optical technologies can be fundamentally categorized into five major groups based on their primary focusing method: linear focusing lens, two-dimensional focusing lens, linear focusing reflector, two dimensional focusing reflector, and central receiver system. The architectural designs and optical principles for various solar concentrators specially tailored for the CPV systems are depicted and presented in the following section.

2.1.1 Linear Focusing Lens

By using the edge ray principle, Leutz et al. (1999) designed an optimum convex shaped non-imaging Fresnel lens. With a secondary concentrator and a diffuser, it is possible to operate the system without tracking the sun with the irradiance still well distributed over the photovoltaic panel. The flux concentration in this system is around 15–20 times and the schematic diagram is given in Figure 2.1. The proposed truncated non-imaging Fresnel lens requires only passive tracking and seasonal tilt.

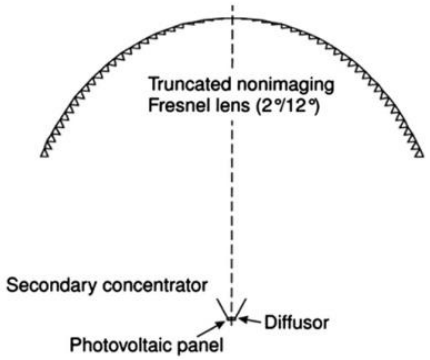

Figure 2.1: Schematic of the truncated non-imaging Fresnel lens with a secondary concentrator for application in photovoltaic systems. (Leutz et al., 1999).

Chemisana and colleagues proposed a photovoltaic-thermal module for the Fresnel linear concentrator by combining a domed linear Fresnel lens as the primary concentrator (5×), a compound parabolic reflector as the secondary concentrator (2×), and a photovoltaic-thermal module (Chemisana et al., 2011).

O'Neill patented a "high efficiency, extremely light-weight, and robust stretched Fresnel lens solar concentrator" coupled to a photovoltaic concentrator array for generating power in space (O'Neill, 2000). The stretched Fresnel lens solar concentrator consists of a flexible Fresnel lens attached to end supports to maintain its proper position and shape as shown in Figure 2.2.

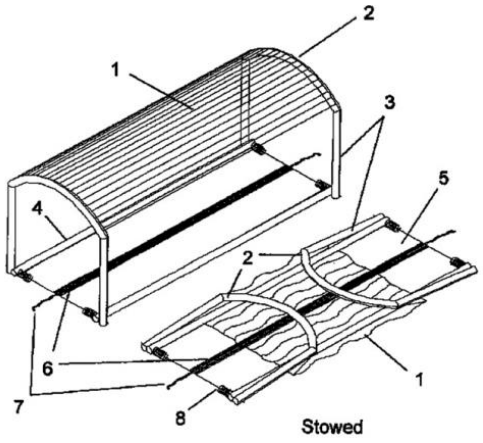

Figure 2.2: A perspective view of a deployable embodiment of a stretched Fresnel lens solar concentrator for generating power in space. (O'Neill, 2000).

2.1.2 Two-Dimensional Focusing Lens

Jebens and Skillman patented a Fresnel lens concentrator that is formed by a specially designed Fresnel lens and a solar cell located on the axis of the lens at its focal plane (Jebens and Skillman, 1989). The lens is designed so that its central facets' project the light from the sun towards the outer periphery of the cell and facets progressively towards the periphery of the lens which would project light progressively toward the centre of the cell to obtain a uniform distribution of light on the cell. Adjacent groups of facets of the lens project the light alternatively in front and beyond the cell to maintain a constant light intensity for a certain depth of focus of the lens.

Davies studied the design of single-surface spherical lens as a secondary concentrator in the two-stage concentrator with the Fresnel lens as the primary stage (Davies, 1993). Figure 2.3 shows a cross section view of a

two-stage, axially-symmetric concentrator with Fresnel lens as the primary with a flat first surface and a single-surface spherical lens as the secondary in the form of a domed pillar glued to the cell. In this design, a Fresnel lens with a maximum concentration of about 100 times at f/1.37 has been improved in the two-stage concentrator system to a maximum concentration of 530 times at optimal f-number of f/2.84.

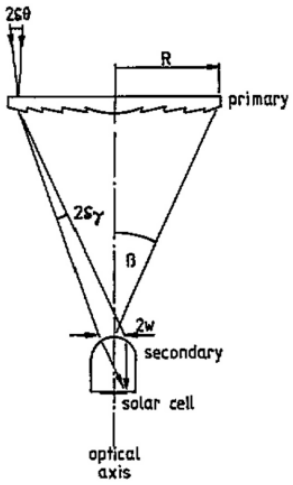

Figure 2.3: Sketch showing a cross section through a two-stage, axially-symmetric concentrator with Fresnel lens as the primary and a single-surface spherical lens as the secondary. (Davies, 1993).

Terao et al. (2000) proposed a non-imaging optics design for a flat-plate CPV system. As shown in Figure 2.4, the system uses the aspheric and TIR lens components as the primary optics and a secondary optical element to focus sunlight onto the solar cells. The primary optics design can reduce the focal length and hence the thickness of the whole module. The ray-tracing simulations had shown that the acceptable angle of more than ±2.61° can be achieved, hence making it suitable for light-weight, low-cost tracking systems.

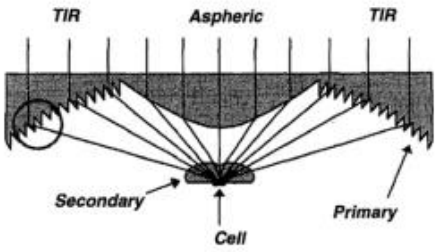

Fig. 5. TIR-R concentrator with detail of TIR lens.

Figure 2.4: TIR-R concentrator with details of the TIR lens. (Terao et al., 2000).

Chen patented a stationary solar photovoltaic array module design, which constitutes a three or four steps of optical concentrations of the photovoltaic power generation system (Chen, 2003, 2004). The concentrator can have either a one layer (2004) or two layers (2003) Fresnel lens concentrating sunrays. A compound parabolic concentrator (CPC) is mounted under a first or second Fresnel lens to further concentrate the intensity of the sunlight twenty times more. Then, the concentrated sunlight is homogenized as it passes through a third or fourth optical concentrator glass lens with an anti-reflection coating on the top surface just before the incident on the multi-junction solar cell. Figure 2.5 shows the combination of a multi-stage Fresnel lens and optical reflectors, which can concentrate solar intensity 300 to 1,000 times within a six-inch distance.

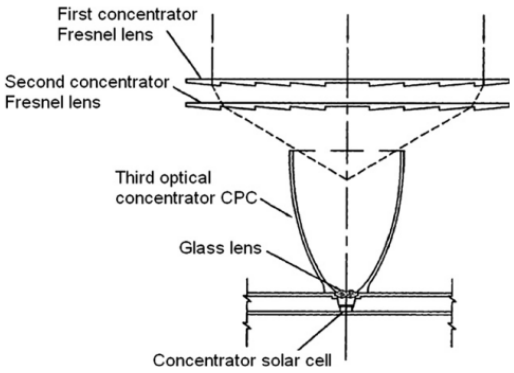

Figure 2.5: A stationary photovoltaic array module's design sequence from top to bottom: first concentrator Fresnel lens for focusing sunrays 5 to 10 times; second concentrator Fresnel lens; third optical concentrator CPC; fourth optical concentrator; a specially shaped glass lens; and a concentrator solar cell with a 45% conversion efficiency. (Chen, 2003, 2004).

Andreev et al. (2004) proposed a modified structure of the high concentration all glass PV module for a solar-powered Thermo-Photovoltaic (TPV) system with III–V solar cells. The system consists of Fresnel lenses with a small aperture area and short focal length as the primary concentrator while the secondary optics is a smooth-surface convex lens inserted between the primary lens and the solar cell as shown in Figure 2.6. Both primary and secondary lenses are made up of composite (glass-silicone) structures. The advantages are the module can be fabricated with a large total area and the environmental protection of the solar cells can be improved.

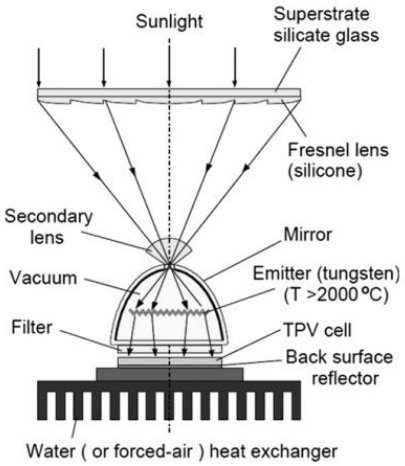

Figure 2.6: Optical design concept of a modified structure of the high concentration all glass PV module for the solar-powered TPV system with high temperature (T>2000°C) vacuum bulb emitter. (Andreev et al., 2004).

Ryu and team proposed "a new configuration of solar concentration optics utilizing modularly faceted Fresnel lenses to achieve a uniform intensity on the receiver plane with moderate concentration ratio" (Ryu et al., 2006). Figure 2.7 reveals that the uniform illumination is obtained by the superposition of flux distribution resulting from modularly faceted Fresnel lens. The flux distribution at the cell plane is estimated to be uniform within ~20% with a transmission efficiency larger than 65% for 3×3, 5×5, and 7×7 arrays of Fresnel lenses. With f/1.2, the intensity levels of the various concentration ratios are 7 suns for the 3×3 array, 19 suns for the 5×5 array, 31 suns for the 7×7 array, 47 suns for the 9×9 array, and 60 suns for the 11×11 array.

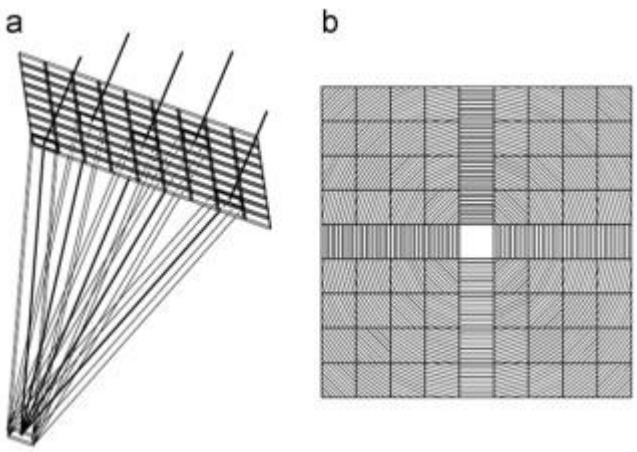

Figure 2.7: Optical design concept of the modular Fresnel lenses for solar flux concentration: (a) 3-D of the concentration optics; (b) facet directions of the modularly faceted Fresnel lenses. (Ryu et al., 2006).

Winston and Ritschel patented an optical device that produces efficient electrical output as illustrated in Figure 2.8. The device consists of a primary Fresnel lens and a secondary non-imaging optics to concentrate high solar flux onto a multi-junction solar cell (Winston and Ritschel, 2008). The primary Fresnel lens with an f-number of greater than 1 (e.g., between 1 and 4 or greater) is configured to focus light from a distant source onto the entry aperture of the secondary concentrator. The solar cell is located at the exit aperture of the secondary concentrator. The optical device has an optical acceptance angle of about ±5° or greater and with an optical efficiency of about 80%–85%. It can be configured with a 125 × 125 mm entry aperture and a depth of about 230 mm to provide a geometric concentration of about 500× for a 5.5 × 5.5 mm multi-junction cell and 150× for a 10 × 10 mm Si cell.

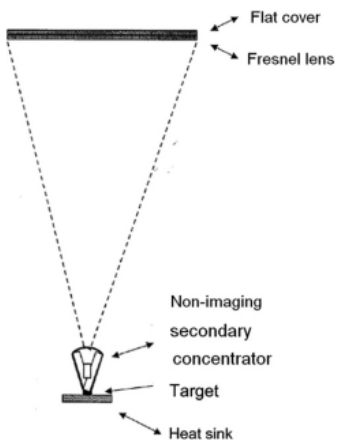

Figure 2.8: A concentrating photovoltaic system using Fresnel lens and non-imaging secondary optics. (Winston and Ritschel, 2008).

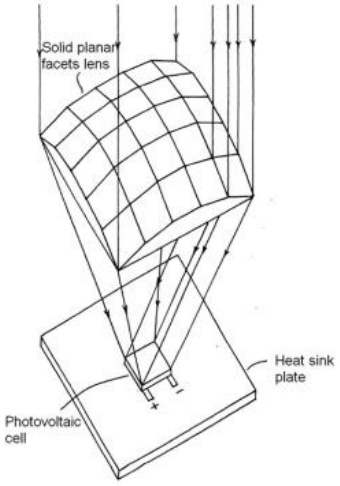

Figure 2.9: A perspective view showing a solid lens with 25 planar facets on the top side facing the sun and a planar surface on the bottom side facing the photovoltaic cell mounted on a heat sink plate. (Schwartzman, 2008).

Schwartzman designed a solar energy concentrator lens formed by a prism array (Schwartzman, 2008). Figure 2.9 shows how each prism of the 25 planar facet is designed to deflect the incident solar rays and fully illuminate a

rectangular photovoltaic cell with uniform intensity. The combination of multiple prisms uniformly illuminating a common target area yields a concentrated uniform illumination across the target area.

Araki and colleagues patented a concentrator solar photovoltaic apparatus including a primary optics for concentrating sunlight, a columnar optical member, and a transparent resin member, and the solar cell (refer to Figure 2.10) (Araki et al., 2008). A columnar optical member or homogenizer acting as the secondary optics was used for guiding the sunlight, which is concentrated by the primary optics to the solar cell.

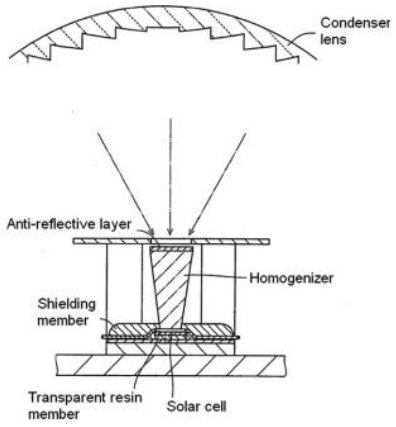

Figure 2.10: A generation module of a concentrator solar photovoltaic apparatus, which comprises of a plurality of generation modules disposed within in an enlarged cross sectional view. (Araki et al., 2008).

Ota and Nishioka developed a 3-D simulation for calculating the operating characteristics of a CPV module. The simulation was done by connecting the ray-trace simulation for an optics model and a 3D equivalent circuit simulation for a triple-junction solar cell. It has been used to study a

typical flat Fresnel lens (110 × 110 mm in the entry aperture area and a focal length of 150 mm) and homogenizer (9 × 9 mm in the entry aperture area, 4.5 × 4.5 mm in the exit aperture area, and 35 mm in height) set in the vicinity of the focal length of the Fresnel lens to have an effective geometrical concentration ratio of 597 times (Ota and Nishioka, 2012).

2.1.3 Linear Focusing Reflector

Singh and Liburdy presented a reflective concentrator capable of concentrating a collimated beam of light onto a flat receiver to obtain a uniform flux distribution with the maximum theoretical concentration ratio of 22.79 (Singh and Liburdy, 1993). The benefit of this design is it enables the use of commercially available plane mirror of various sizes as the reflector, as shown in Figure 2.11. Measurement of the flux on its receiver indicates a quite uniform flux distribution in about 80% of the receiver area.

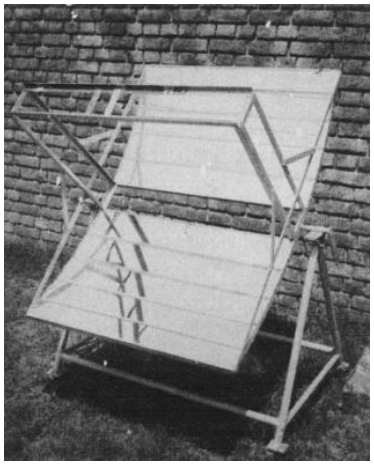

Figure 2.11: Experimental solar concentrator consisting of a series of flat panels of different sizes. (Singh and Liburdy, 1993).

Lamb and Lawrence patented a multiple-reflector concentrator to concentrate sunlight onto a panel of photovoltaic cells in a solar electric power system as shown in Figure 2.12 (Lamb and Lawrence, 1994). The power system consists of multiple reflectors, mounted PV cells, and a heat dissipation component mounted on a tracker that keeps the system directed to the sun. The system can operate on either a single or dual axis tracker with active or passive tracking.

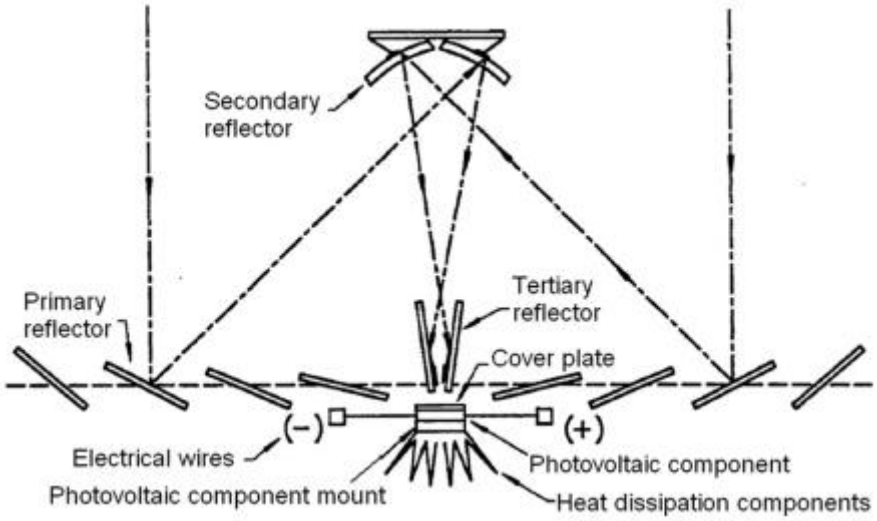

Figure 2.12: A cross sectional schematic of the multiple-reflector-concentrator module with the secondary reflector placed at the focal line of the primary reflector. (Lamb and Lawrence, 1994).

Gordon presented the optical design for a high-efficiency linear photovoltaic solar concentrator assembled from readily available inexpensive components (Gordon, 1996). Accounting for all geometric and material-related optical losses, he found that it should easily produce flux levels of 50–100 suns with homogeneous irradiance of the absorber. The specification of the system components is as follows: the parabolic focal length is 1.49 m and

the parabola entrance aperture width is 2.47 m; the solar cell's width is 0.033 m; the secondary V-trough has a depth of 0.072 m and an entrance width of 0.176 m.

For the project EUCLIDES (EUropean Concentration Light Intensity Development of Energy Sources), Sala and colleagues developed a one axis horizontal tracking, North/South oriented parabolic trough reflector for the CPV system (Sala et al., 1996). The geometric concentration ratio is 32 and the overall efficiency of the 14 series connected receiving modules is 15% at 25°C. Such modules consist of fully encapsulated 12 BP solar SATURN concentrator cells.

Clemens disclosed a light weight photovoltaic concentrator having a "foldable, easily deployed structure" for concentrating sunrays on solar cells for generating electricity (Clemens, 1997). The concentrator can be inflated to a shape of a parabolic trough for focusing sunlight onto the solar cells at the ratio of 20 suns. The inflatable concentrator is supported by pumping up the gas in the central arm. The gas is pumped up until the epicentres of the front and rear surfaces achieve a specified distance as shown in Figure 2.13.

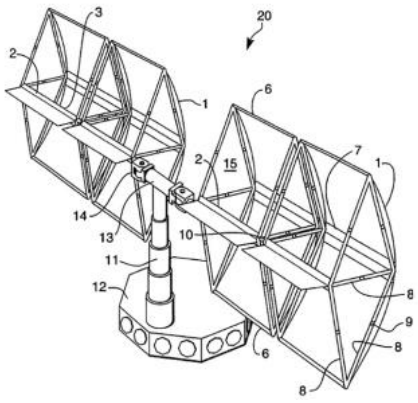

Figure 2.13: Photovoltaic concentrator (20) with foldable struts (8) extended to form the triangular frame section (15): end arms (6) are connected at the top and bottom of the triangular frame section (15) and are used to attach a reflective concentrator (1) to the structure. The reflective concentrator is an inflatable concentrator made of silvered Kapton films. (Clemens, 1997).

Frazier patented a double reflecting solar concentrator utilizing a primary reflective surface (parabolic mirror), which reflects incident light towards a secondary surface (directrix plane) (Frazier, 2001). The incident light is reflected by the primary reflective surface to the secondary surface where it will be focused towards the secondary focal point located on the surface of the primary reflector. The invention provides an exemplary double reflecting style of the parabolic trough structure that is substantially more rigid than a simple parabolic surface where the photovoltaic cell can be placed along the focal line as shown in Figure 2.14.

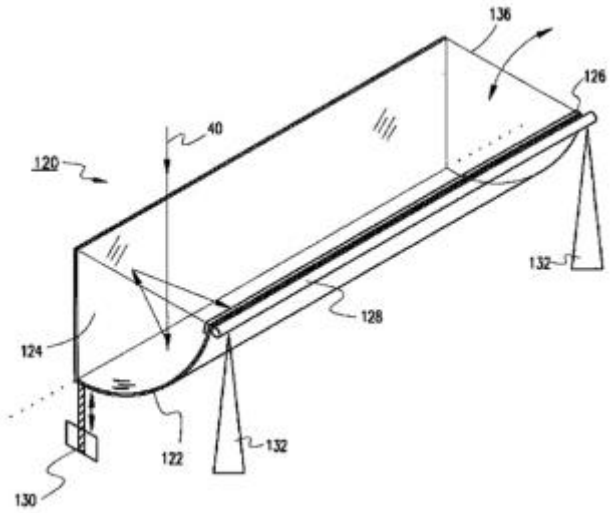

Figure 2.14: A three-dimensional view of a double reflecting solar concentrator (1 2 0) mounted on a support structure (1 3 2) and connected to a hydraulic driving system (1 3 0): incident light (40) reflects off the primary reflective surface (1 2 2) towards the secondary reflective surface (1 2 4) and then towards a solar collector or photovoltaic (1 2 6) located at the focal line. (Frazier, 2001).

Hein et al. (2003) achieved a high geometrical concentration ratio of 300 suns using a parabolic trough mirror and a three-dimensional second stage consisting of compound parabolic concentrators (CPC). In the design, the geometrical concentration of the first stage concentrator and the CPC are 39.7 and 7.7 times, respectively, leading to the concentration ratio of more than 300 times. Figure 2.15 shows the prototype of this concentrator system built at the Fraunhofer Institute for Solar Energy (ISE).

Figure 2.15: Picture of a prototype of the concentrator module on a tracker. Two GaAs cells with CPCs have been mounted on heat sinks and installed in the focal line. (Hein et al., 2003).

Coventry published the performance of a prototype parabolic trough photovoltaic/thermal collector with a geometric concentration of 37 suns constructed at the Australian National University (Coventry, 2005). Measured results under typical operating conditions show a thermal efficiency of around 51% and an electrical efficiency of around 11% to result in a combined efficiency of 69%. The measured illumination flux profile along the length showed a significant variation with the peak flux intensities shown to be around 100 suns, even though a large part of the mirror area had a mirror shape error of less than 1 mm. Mirror shape error, shading of receiver holding arm, and gaps between mirrors caused non-uniform illumination that heavily affected the overall electrical output.

Straka patented a non-imaging reflective trough that receives and linearly reflects spectral energy onto a smaller area on one side of the device with a geometric concentration of seven suns (Straka, 2006). The linearly

reflecting trough concentrator has the geometry of a single slope-relief interval in a Fresnel lens, and in a preferred embodiment comprises an array of plane facet reflectors connected continuously to form the base of the trough, a non-imaging focal point where a photovoltaic receiver is located, and a relief surface to connect the mirror arrays to the receiver location. The concentrator comprises of arrays of plane mirrors oriented according to the negative profile of two interleaved linear Fresnel lens, where the slope of one is the relief of the other.

2.1.4 Two-Dimensional Focusing Reflector

Jorgensen and Wendelin designed a multi-step-molded-dish concentrator capable of producing a uniform flux profile on a flat target plane (Jorgensen and Wendelin, 1992). Concentration levels of 100–200 suns, which are uniform over an area of several square inches, can be directly achieved for collection apertures of a reasonable size of approximately 1.5 m in diameter. As for the arrangement, as shown in Figure 2.16, there are five concentric annular regions with each region made up of 20% of the total aperture area. Each step section was offset along the optical axis and specified to be a spherical element with a curvature of 1/2f.

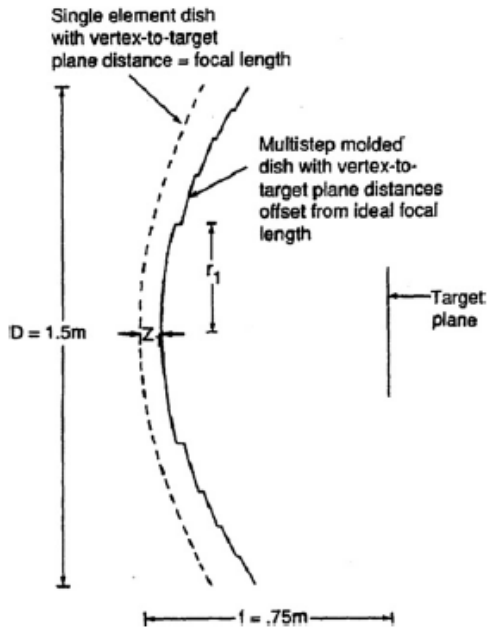

Figure 2.16: Cross sectional geometry of a 5-element molded dish (Jorgensen and Wendelin, 1992).

Ries and colleagues proposed and analysed sample designs for a high flux photovoltaic concentrator comprised of a large-aperture paraboloidal-dish primary concentrator, and a second-stage kaleidoscope flux homogenizer (Ries et al., 1997). In reference to Figure 2.17, the design satisfied highly uniform irradiance on the solar cell absorber, high collective efficiency, and a solar concentration ratio of below 500 suns. The solution is to move the absorber out of the nominal focal plane, away from the dish, to a plane where the average concentration is 500 suns.

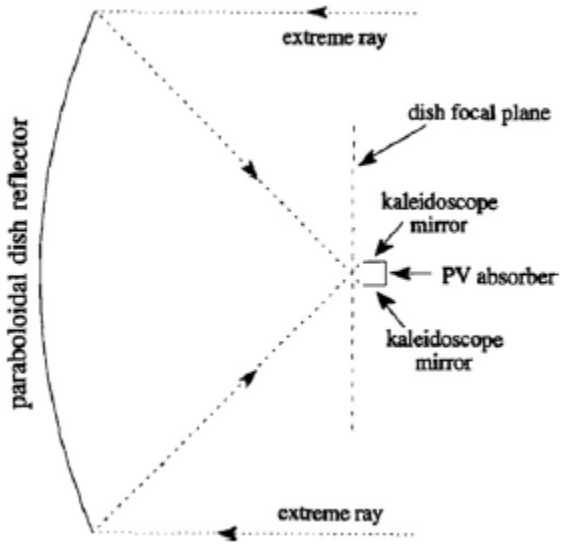

Figure 2.17: Side view of the paraboloidal dish, its focal plane, and the recessed kaleidoscope. The extreme rays from the dish cut the smallest waist in the focal plane, which defines its average concentration (e.g., 10,000). The kaleidoscope is recessed to a plane where the area delimited by the extreme rays corresponds to the prescribed concentration ratio (e.g., 500). (Ries et al., 1997).

Feuermann and Gordon proposed a high concentration photovoltaic design based on the miniature paraboloidal dish and kaleidoscope to achieve 1,000 suns (Feuermann and Gordon, 2001). The collection unit is a miniature parabolic dish with a diameter of the order of 10 cm that concentrates sunlight onto a short glass rod called the kaleidoscope. The flux distribution of the transported light is homogenized in a miniature glass kaleidoscope that is optically coupled to a small, high-efficiency solar cell as illustrated in Figure 2.18. The cell resides behind the dish and can be cooled adequately with a passive heat sink.

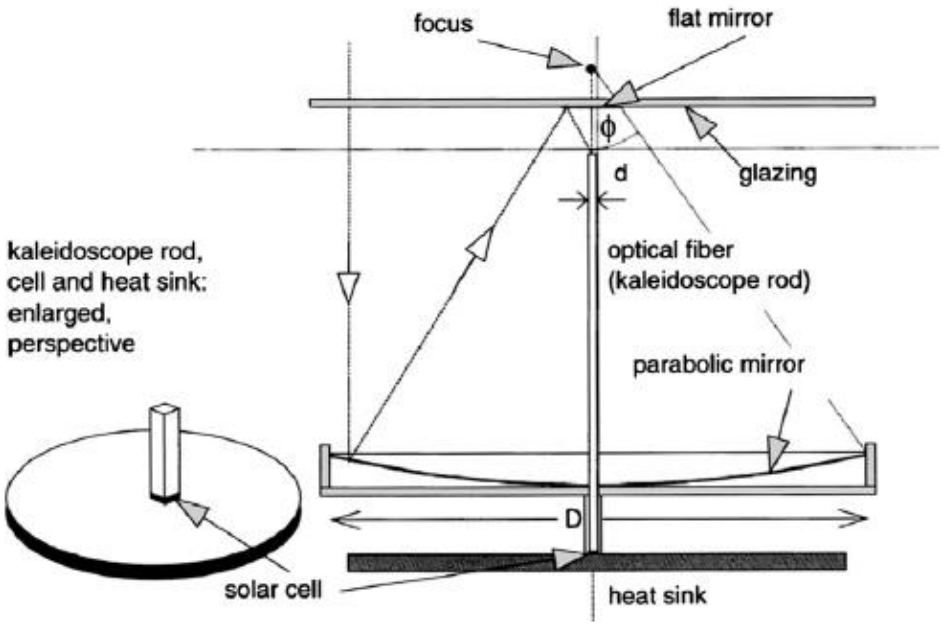

Figure 2.18: Schematic illustration of a solar mini-dish photovoltaic concentrator: the parabolic mini-dish sits in an opaque encasement, except for the protective glazing. A small mirror deposited on the glazing redirects rays reflected from the mini-dish to the fibre's proximate tip, which is sited at a prescribed recession below the focal plane. A square cross section kaleidoscope optically couples the distal end of the fibre and the solar cell. (Feuermann and Gordon, 2001).

Kreske developed an optical solution to redistribute light over an approximately 1 m^2 plane with a rectangular receiver box with reflective sidewalls (i.e., a kaleidoscope or solar flux homogenizer) (Kreske, 2002). The primary concentrator is a 400 m^2 paraboloidal solar concentrating dish and the solar cell will be installed at the output of the receiver box. The ray analysis done had shown the possibility of achieving a flux uniformity suitable for the photovoltaic application with a concentration ratio around 500 suns.

Vasylyev et al. (2003) patented a non-imaging energy flux transformation system that includes a concentrator incorporating a set of nested, ring-like, concave reflective elements, and a receiver as shown in Figure 2.19. The system efficiently concentrates sunlight by means of focusing the energy striking the entrance aperture of the concentrator to the receiver located on the side of the concentrator's exit aperture. The mirror surface of the reflective elements having appropriate individual non-imaging profiles represented by curved or straight lines are positioned so that the energy portions reflected from individual surfaces are directed, focused, and superimposed on one another to cooperatively form a common focal region on the receiver. The receiver can be an energy absorbing device (e.g., photovoltaic array), a secondary energy concentrating transformer, or a flux homogenizer. Vasylyev then published the prototype of a non-imaging reflective lens concentrator, which provides a solar concentration ratio of 1,000 suns and a flux uniformity on the rear of the concentrator (Vasylyev, 2005).

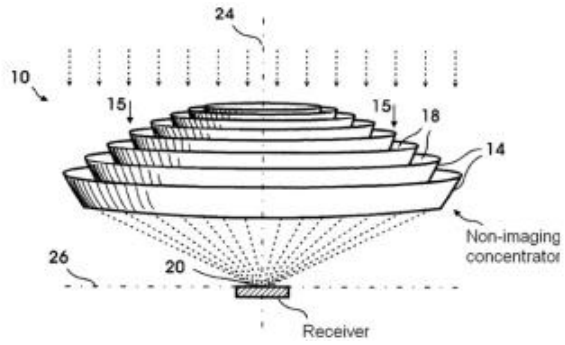

Figure 2.19: Schematic view of the non-imaging system (10), which includes a non-imaging concentrator comprising of a plurality of coaxial ring-like elements (14) having inner reflective surface (18) and a receiver. Surfaces (18) receive incident sunlight (15) on the entrance aperture of the concentrator and form a concentrated energy spot (20) on the target plane (26). (Vasylyev et al., 2003).

Terao and Krippendorf patented a compact micro-concentrator for the photovoltaic cells that comprises of partial parabolic reflectors arranged in rows and columns with each reflector directing radiation to a photovoltaic cell (Terao and Krippendorf, 2007). In a compact photovoltaic cell arrangement, each cell is shielded from direct radiation by the adjacent reflector. A secondary optical element, either reflective or refractive, can be provided to each cell receiver to further concentrate the reflected radiation to a photovoltaic cell at a more accessible location in the array.

Benitez and team developed a two-mirror high concentration non-imaging optics as shown in Figure 2.20 that can operate at a 15 mrad tolerance level without using a kaleidoscope while having an average concentration of over 800 suns (local concentration is below 2000 suns) (Benitez et al., 2006).

This is an advantage over the imaging systems that only operate below 175 suns at the same acceptance angle.

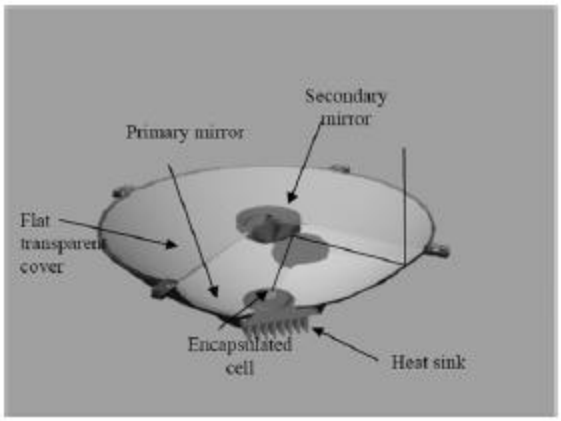

Figure 2.20: CAD modal of the prototype design (a quarter of the primary, secondary, and cover have been removed). (Benitez et al., 2006).

As illustrated in Figure 2.21, Lichy patented an asymmetric, three dimensional, non-imaging, light concentrator designed to concentrate sunlight onto a solar cell (Lichy, 2006). The proposed solar concentrator has three stages of optical components. The first stage optics is formed by arranging two pairs of compound parabolic concentrators (CPC) orthogonally to form a hollow reflector with a rectangular aperture. A solid second stage optics is placed below the hollow reflector; it was formed by a similar method and is coated with reflective material on the side wall. The solid reflector is placed on top of a solid, cuboid shaped light diffuser with reflective coating on the side walls, which is optically coupled to a solar cell. The whole concentrator is mounted on a metal substrate for thermal management. The proposed concentrator can operate efficiently with only a single axis tracking the sun

because its acceptance angle in the north-south direction is greater than the range of the sun's azimuth.

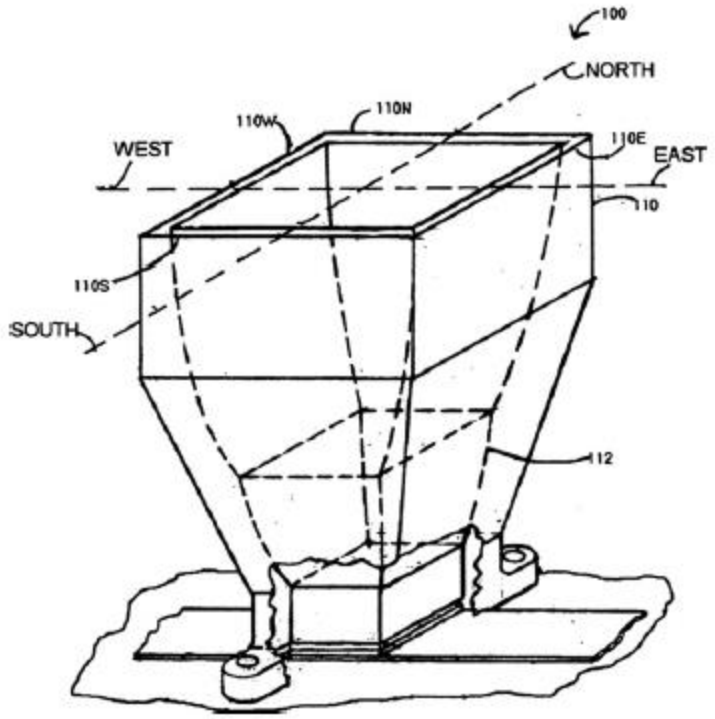

Figure 2.21: Schematic illustration of an asymmetric, three-dimensional, non-imaging, compound parabolic concentrator (1 0 0): the hollow reflector (1 1 0) partially encloses and contains a solid reflector (1 1 2). (Lichy, 2006).

Fork and Maeda patented a Cassegrain-type concentrating solar collector cell that employed primary and secondary mirrors with opposing convex and concave surfaces (Fork and Maeda, 2006). Light entering the concentrator is reflected by the primary mirror towards the secondary mirror, which then reflects the light onto a solar cell located at the bottom centre of the primary mirror.

Neubauer and Gibson patented a solar concentrator consisting of a "first reflective surface formed parabolic along a first axis and a second reflective surface formed parabolic along a second axis", which is perpendicular to the first axis (Neubauer and Gibson, 2007). The focal length of the second reflective surface is shorter than the focal length of the first reflective surface, for crossing the focal lines of the first and second reflective surfaces at a point as shown in Figure 2.22. In other words, the whole concentrator consists of two parabolic troughs that are aligned along an optical axis. Hence, each parabolic trough can take parallel sunrays and focus them to a line. The parabolic axis of the first parabolic trough is oriented perpendicular to the parabolic axis of the second parabolic trough to focus the light from a line to a point.

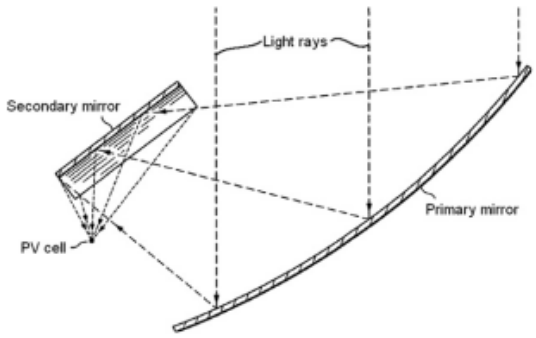

Figure 2.22: A ray diagram illustrating an optical path for concentrated sunlight: parallel rays are shown striking a primary mirror and reflecting towards a reflective surface, which serves as a secondary mirror, and then to a focal point where the PV cell is located. (Neubauer and Gibson, 2007).

Maeda patented a beam integration for concentrating solar collectors to concentrate sunlight onto a PV cell. The system consists of an array of first optical elements that divide the sunlight into separate beams and a secondary optical system that integrates the separate beams in a defocused state at the image plane in order to form a uniform light distribution pattern on the CPV cell (Maeda, 2007). The secondary optical system is positioned at a distance from the aperture plane, whereby the rays of each separate beam leaving the secondary optical element are parallel. The image plane (CPV cell) is located at the back focal point of the second imaging system, whereby all of the separate beams are superimposed on the PV cell in a defocused state.

Fork and Horne patented a laminated solar concentrating photovoltaic device as shown in an exploded view in Figure 2.23, in which the concentrator elements (optics, CPV cells, and wiring) are laminated to form a composite, substantially planar structure (Fork and Horne, 2007). Primary and secondary mirrors are disposed on convex and concave surfaces, respectively. Both primary and secondary mirrors are arranged such that the sunrays travel perpendicular to the aperture surface, as shown in Figure 2.23. Sunrays entering the optical element through a specific region of the aperture surface is reflected by a corresponding region of the primary mirror to an associated region of the secondary mirror and from the secondary mirror to the CPV cell. The top coversheet serves to protect the secondary mirror from the harsh outdoor environment by providing a thin, optically transparent layer (glass) over the aperture surface and secondary mirror.

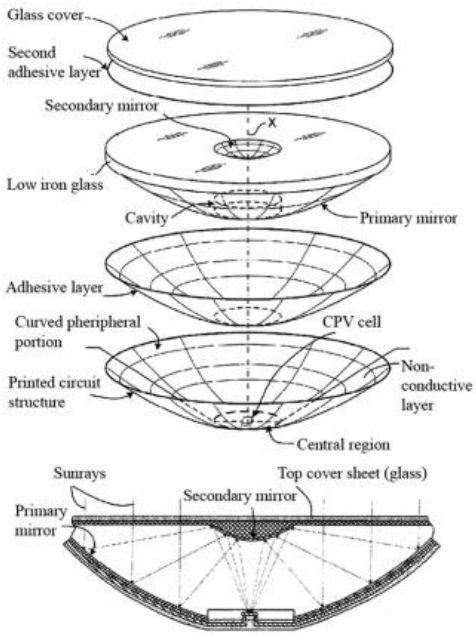

Figure 2.23: An exploded perspective view (upper diagram) and a cross-sectional side-view (lower diagram) showing a laminated solar concentrating photovoltaic device. (Fork and Horne, 2007).

Shifman patented a solar energy utilization system comprising of a Cassegrain-type concentrator and two solar radiation receiver components (Shifman, 2008). The first receiver component is designed to convert the first part of the solar spectral energy into electrical energy, and the second receiver component is designed to convert the second part of the solar spectral energy into electrical energy. The solar radiation concentrating optics comprises of a concave primary reflector and a convex secondary reflector. The secondary reflector is a beam splitter, which reflects visible light towards fibre optics light guide and transmits concentrated infrared towards an array of solar cells mounted behind the secondary reflector.

Draganov patented a solar concentrator with folded beam optical configuration allowing for compact, lightweight construction (Draganov, 2009). Reflective optics is employed, including dichroic mirror and antireflection coating, to remove unwanted infrared radiation from reaching the solar cell. As shown in Figure 2.24, the solar concentrator comprises of three reflecting surfaces. The primary mirror (concave surface) reflects solar radiation upward to the second reflecting surface (plane reflector) that is optically coupled to the primary mirror for reflecting the solar radiation downward to the tertiary mirror (concave surface). The tertiary mirror is configured to reflect the solar radiation upward again to the second reflecting surface in such a way that the solar radiation is then reflected from the second reflecting surface towards the focal plane where the photovoltaic cell is located.

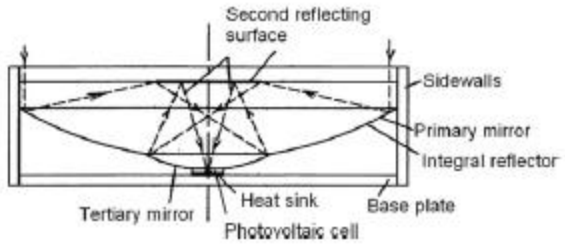

Figure 2.24: The primary and tertiary mirrors form the integral reflector, which is also known as the unitary reflector. The second reflecting surface is a planar surface and is disposed between the primary mirror and the focal plane of the primary mirror. The PV cell is mounted on a heat sink with a base plate. On top of the solar concentrator, a piece of flat glass is spaced apart from the double curved reflector with sidewalls. (Draganov, 2009).

Chong and colleagues proposed a non-imaging planar concentrator consisting of numerous square flat mirrors capable of producing uniform sunlight and at a reasonably high concentration ratio (Chong et al., 2009, 2010). The uniform concentrated light is formed from the superposition of the flat mirror images into one as illustrated in Figure 2.25. The prototype consisted of 360 flat mirrors, each with a dimension of 4.0 × 4.0 cm, to achieve the solar concentration ratio of 298 suns at a focal distance of 78 cm.

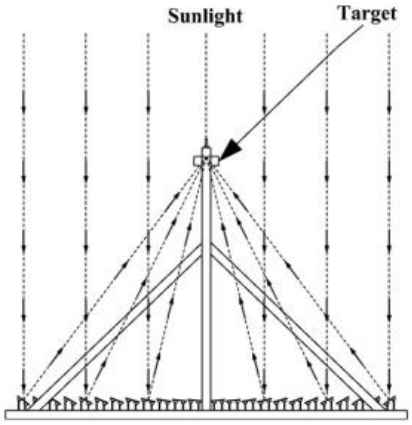

Figure 2.25: Conceptual layout design of the non-imaging planar concentrator: cross-sectional view of the planar concentrator to show how the individual mirror directs the solar rays to the target. (Chong et al., 2009).

Tsadka et al. (2009) patented the optical design of a new concentrator with a plurality of reflectors to reflect sunrays directly onto the solar receiver or the CPV panel for electricity and heat generation as shown in Figure 2.26. Plurality of reflectors are arranged on a support surface and each reflector is configured as well as aligned to reflect solar radiation with a high degree of uniformity onto the solar receiver.

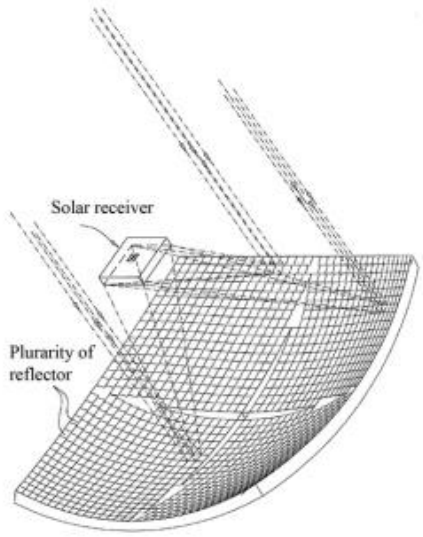

Figure 2.26: Solar concentrator by Tsadka et al. (2009): a simplified pictorial illustration of beam paths from some of the mirrors of the reflector portion to the receiver portion of the solar energy converter assembly.

Chong and team has filed the patent for a non-imaging dish concentrator that provides uniform solar flux, which matches the square or rectangular solar images to the square or rectangular dimension of the photovoltaic receiver, and produces a high solar concentration ratio (Chong et al., 2012). The non-imaging dish concentrator consists of a plurality of optical assembly sets (see Figure 2.27(a)) and each optical assembly set comprises of four flat mirrors placed together and sharing one common pivot point at the centre (see Figure 2.27(b)). In reference to Figure 2.27(b), flat facet mirrors are used to ensure a rectangular and uniform solar flux in which the superposition of all the images of the four facet mirrors of each optical assembly set into one is done by inclining them relative to the pivot at the centre.

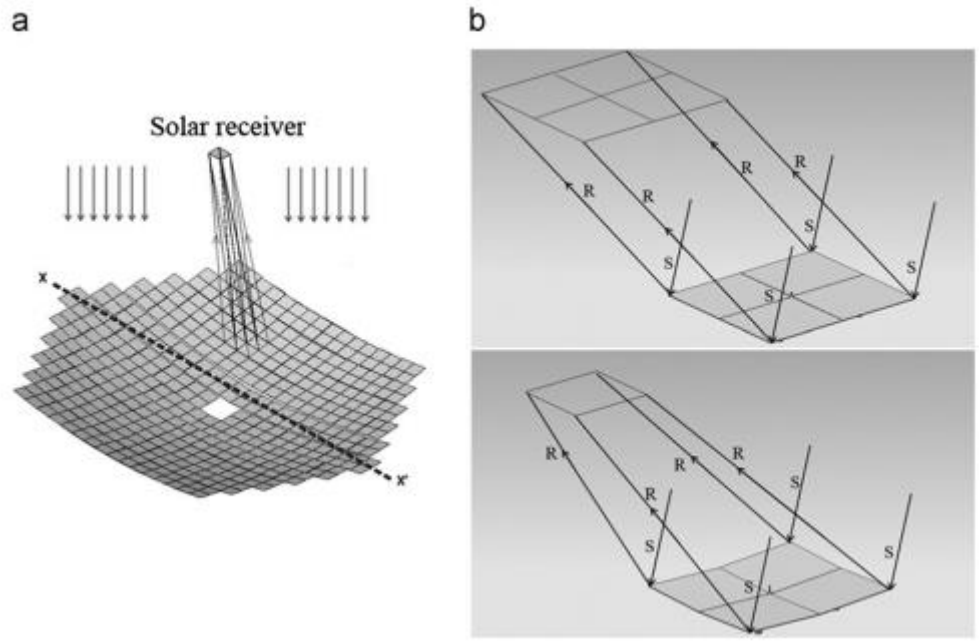

Figure 2.27: (a) a non-imaging dish concentrator by Chong et al. (2012) consisting of an optical assembly set in which the solar concentration ratio is dependent on the applications by simply increasing or decreasing the total number of optical assembly sets; (b) the superposition of all the images of the four flat component mirrors of each optical assembly set into one by inclining them relative to the pivot at the centre. Four flat mirrors are placed together to form one optical assembly set and they share one common pivot point at the meeting point. The shape of each mirror is either rectangular or square depending on the solar cells' arrangement at the photovoltaic receiver. The mechanism of inclining the four flat mirrors' arrangement with reference to the common pivot point at the centre results in the solar images of the four component mirrors to superpose or overlap into one. (Chong et al., 2012).

2.1.5 Central Receiver System

Ittner proposed an array of directable mirrors as a photovoltaic concentrator (Ittner, 1980). The mirror field consists of a two dimensional matrix of mirrors, which may be plane or focused. For simplicity, it is assumed that the centres of the mirrors all lie in a plane which is centred on the photovoltaic target normal and is parallel to the plane of the target. The photovoltaic target normal, thus defined as the target mirror frame axis that may be either fixed to a direction or arranged to track the sun in one or two dimensions (for instance, by rotating the arrangement as shown in the east-west direction about a vertical axis and by tilting the target-heliostat axis relative to the plane of the horizon). Independently, the individual mirrors may be moved so that they direct the sun's rays onto the plane of the target. Mirrors are positioned in two dimensions within the plane as shown in the cross section in Figure 2.28.

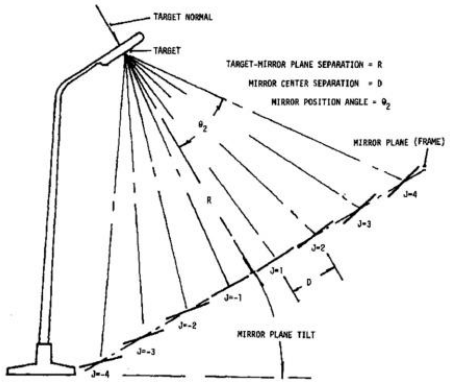

Figure 2.28: Cross section of target-mirror geometries. Centres of mirrors lie in the mirror frame plane. Mirrors may be moved individually (or in groups) to direct the sun's image. In addition to that, the target-mirror plane structure could be rotated and tilted to track the sun. (Ittner, 1980).

As illustrated in Figure 2.29, Segal et al. (2004) presented the option to use the beam down optics of a solar tower system for large-scale and grid-connected CPV cells. Two optical approaches for a large scale hybrid CPV and thermal power conversion at different spectral bands are proposed. In the first approach, the hyperboloid-shaped tower reflector is used as the spectrum splitter. Its mirrors can be made of transparent fused silica glass, coated with a dielectric layer, functioning as a band-pass filter. The transmitted band reaches the upper focal zone, where an array of PV modules is placed. The location of these modules and their interconnections depend on the desirable concentration level and the uniformity of the flux distribution. The reflected band is directed to the second focal zone near the ground, where a compound parabolic concentrator is required to recover and enhance the concentration to a level depending on the operating temperature at this target. In the second approach, the total solar spectrum is reflected down by the tower reflector. Before reaching the lower focal plane, the spectrum is split and filtered. One band can be reflected and directed horizontally to a PV array and the rest of the spectrum is transmitted to the lower focal plane. The system is intended to be operated under concentrated solar radiation in the range of 200–800 suns. The study showed that 6.5 MW from the PV array and 11.1 MW from a combined cycle can be generated starting from a solar heat input of 55.6 MW.

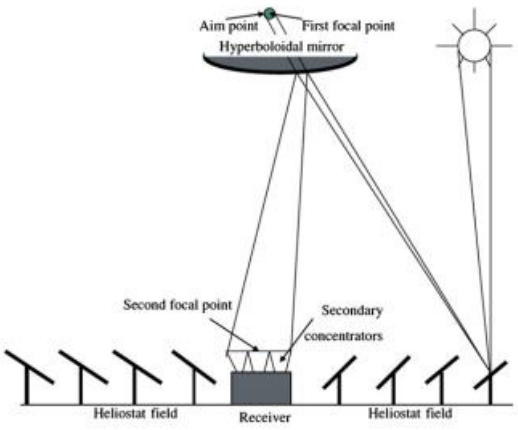

Figure 2.29: The principle of tower reflector optics. (Segal et al., 2004).

2.2 Compound Parabolic Concentrator (CPC)

Compound parabolic concentrator (CPC) was first invented by Welford and Winston (1978). CPC is a type of non-imaging concentrator that can concentrate all the incident sunrays from the entrance aperture within the acceptance angle to the exit aperture. Compound parabolic concentrator has been long used as a solar collector for both photovoltaic and thermal applications (Mallick et al., 2004 and Oommen and Jayaraman, 2002). As most of the commercially available CPV cells are in the shape of either square or rectangle, the design of the secondary concentrator must take the shape of the receiver into consideration. Mammo et al. (2012), Sellami et al. (2010), Sellami and Mallick (2013), and Baig et al. (2014) discussed on how to match the exit aperture of a reflective 3-D crossed compound parabolic concentrator (CCPC) to a solar cell in both size and shape.

Micheli et al. (2014) had discussed technical issues and challenges in the fabrication of the densely packed concentrating photovoltaic receiver in which one compound parabolic concentrator coupled with a homogenizer is placed on top of each cell, but there was no detailed study on the optical design.

In their study, an array of 3-D dielectric filled CCPCs as secondary concentrators with each of them coupled to a single CPV cell to form a good optical combination with NIDC was proposed and filed for patent (Chong et al., 2012, 2013a, 2013b, 2014a, and Chong 2014b, 2014c). In the thesis, both optical and electrical performances of the integrated optical system of NIDC and dielectric filled CCPC have been analysed and studied in the application of the CPV system. Then, the performance of the integrated optical system is compared with that of the NIDC without the secondary concentrator in the DACPV system.

CHAPTER 3

DESIGN AND OPTICAL EVALUATION OF SECONDARY OPTICS OF DENSE-ARRAY CONCENTRATOR PHOTOVOLTAIC SYSTEM

3.1 Primary Optics: Non-Imaging Dish Concentrator

Non-imaging dish concentrators (NIDCs) with the aim of producing uniform flux distribution across rectangular focusing spot was first proposed by Chong and colleagues and further analysed by Tan et al. (Chong et al., 2012, 2013a, 2013b, 2014a, 2014b, 2014c, and Tan et al., 2014). Figure 3.1 shows the primary concentrator NIDC comprising of 96 identical flat facet mirrors acting as optical apertures to gather solar irradiance from the sun and to superimpose all the facet images at the focal plane to form a primary focused image.

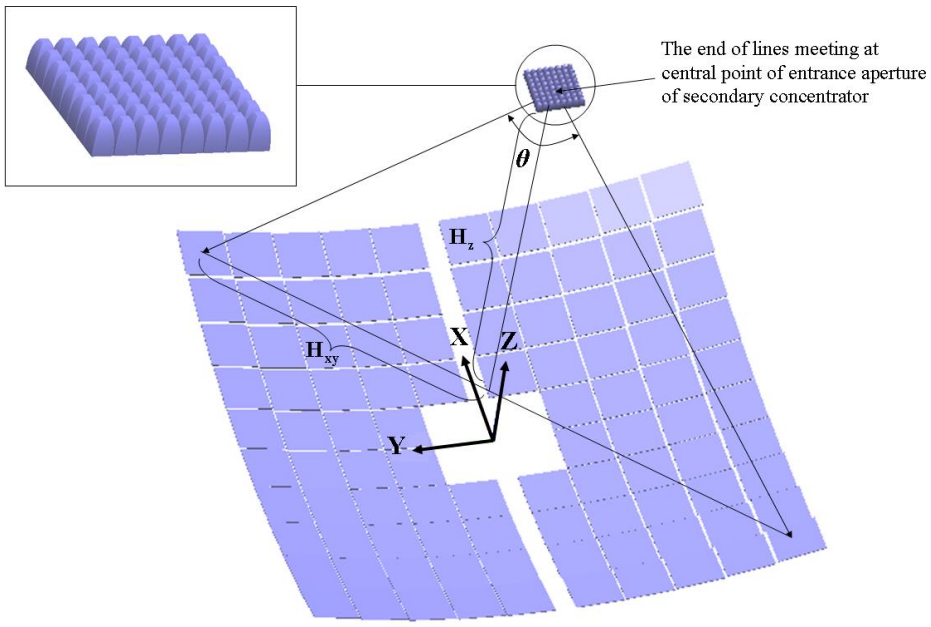

Figure 3.1: Schematic diagram to show an integrated optical system consisting of two major elements: the primary concentrator, non-imaging dish concentrator (NIDC), and the secondary concentrator, an array of dielectric filled crossed compound parabolic concentrator, where the rim angle of NIDC is defined as θ.

The geometrical configuration of the facet mirrors was determined using a newly developed computational algorithm, which is capable of eliminating blocking and shadowing effects among the adjacent facet mirrors (Chong et al., 2012, 2013a, 2013b, and Tan et al., 2014). It can be done by gradually increasing the height of facet mirrors located in the central to peripheral regions as shown in Figure 3.2. Due to the gradual elevation of the facet mirrors at the outer ring of the concentrator, the final optical configuration of the facet mirrors forms a reflective surface of the dish's contour.

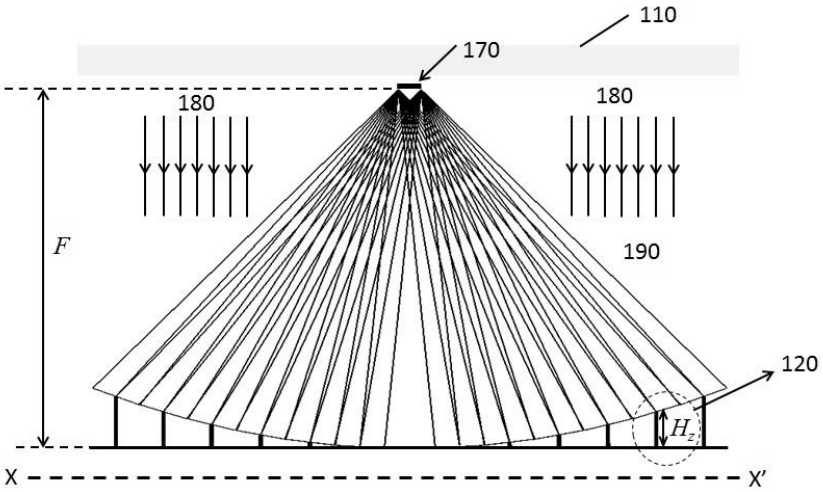

Figure 3.2: Cross-sectional view of the non-imaging dish concentrator showing gradual elevation of facet mirrors located in the central to peripheral regions.

In this study, we consider the NIDC configuration to consist of an array of 10 × 10 facet mirrors with a dimension of 20 × 20 cm each and the four facet mirrors in the central region are omitted due to shadowing by the receiver. As shown in Figure 3.3, each mirror were mounted on a pole with a triangle flat metal plate on top. Three screws were attached to the back of each mirror and springs were inserted to each screw. The mirror, screws, and springs set were then mounted on the triangle metal plate with three holes that acted as the slots for the three screws attached to the mirror. The three screws were fastened with nuts at different force intensities. This is to enable each flat facet mirror to be tilted at two orientation angles based on its location in the NIDC to reflect incident sunrays to a common target. Therefore, sunrays reflected by different facet mirrors were with different angles of reflection.

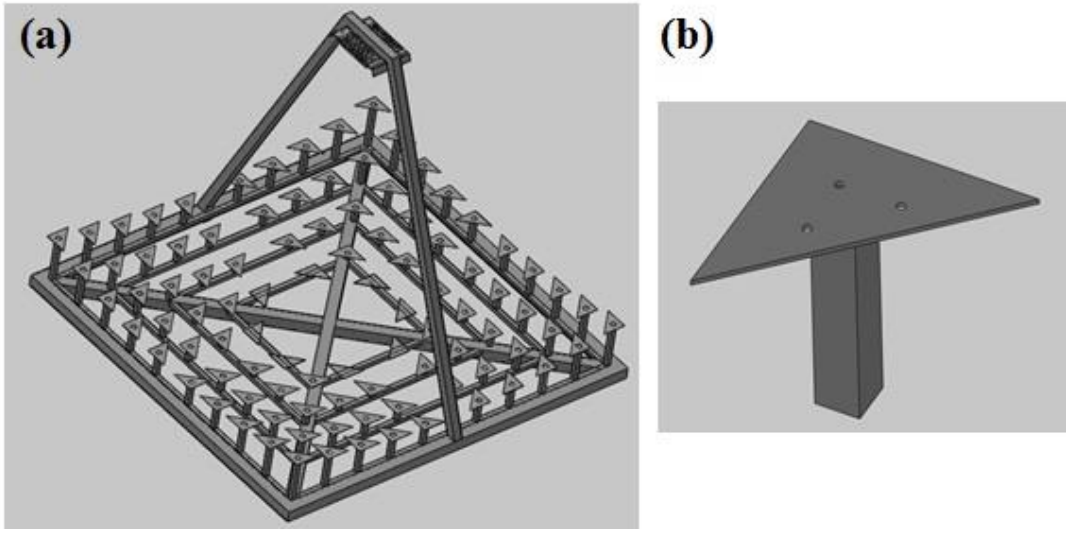

Figure 3.3: (a) aluminium frame with mirror and receiver holders; (b) single mirror holder with a triangle plate mounted at the top of the aluminium square hollow bar. Three through holes acted as slots for mirror installation.

Referring to Figure 3.4, the Cartesian coordinate system was applied to represent the main coordinate system (x, y, z) attached to the dish concentrator and the sub-coordinate system (x', y', z') attached to the i, j-facet mirror, where i and j refer to the mirror location at i-th row and j-th column of the dish concentrator. The origins of the main coordinate and sub-coordinate systems were located at the centre of the concentrator, ***O*** (0, 0, 0), and the centre of i, j-facet mirror, $(H_{Cx}, H_{Cy}, H_{Cz})_{ij}$, respectively. The incident angle (θ_{ij}) of the sunray, relative to the i, j-facet mirror, and the tilted angles of the i, j-facet mirror about x'-axis (γ_{ij}) and y'-axis (σ_{ij}) were derived as follow:

$$\theta_{ij} = \frac{1}{2}\arctan\left[\frac{\sqrt{H_{Cx}^2 + H_{Cy}^2}}{f - H_{Cz}}\right]_{ij} \tag{3.1}$$

$$\gamma_{ij} = \arctan\left[\frac{H_{Cx}}{\left(f - H_{Cz}\right) + \sqrt{H_{Cx}^2 + H_{Cy}^2 + \left(f - H_{Cz}\right)^2}}\right]_{ij} \tag{3.2}$$

$$\sigma_{ij} = \arctan\left[\frac{H_{Cx}}{\sqrt{\left(\begin{array}{l} H_{Cx}^2 + 2H_{Cy}^2 + 2\left(f - H_{Cz}\right)^2 \\ +2\left(f - H_{Cz}\right)\sqrt{H_{Cx}^2 + H_{Cy}^2 + \left(f - H_{Cz}\right)^2} \end{array}\right)}}\right]_{ij} \tag{3.3}$$

where f is the focal length of the dish concentrator or the perpendicular distance of central points between the dish concentrator and the receiver.

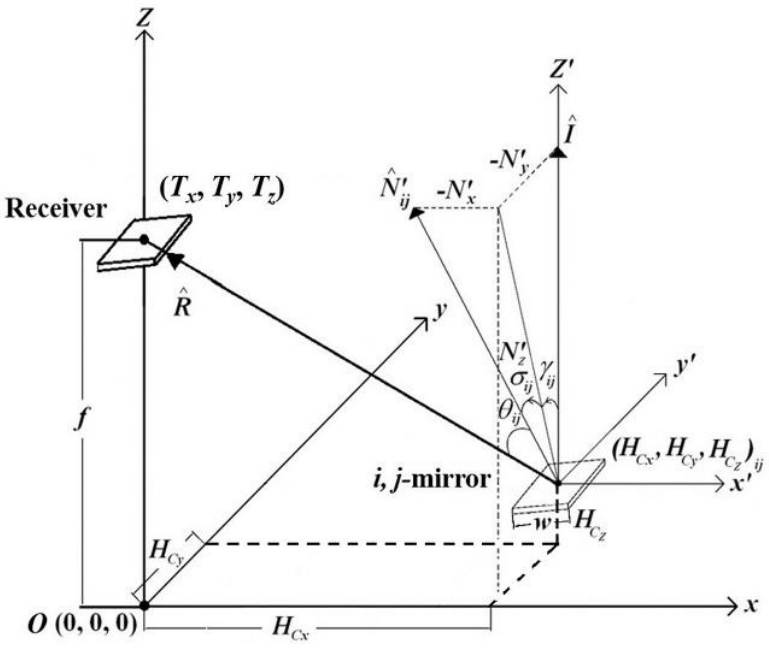

Figure 3.4: The Cartesian coordinate system was used to represent the main coordinate system (x, y, z) attached to the plane of the dish concentrator and the sub-coordinate system (x', y', z') is defined as attached to the i, j-facet mirror.

The total reflective area of the NIDC was 3.84 m^2, the projection area of the facet mirrors was 3.76 m^2, and the focal distance of the NIDC was 210 cm. A two-axis sun-tracking system was employed to ensure that the incident sunlight was always aligned with the optical axis of the NIDC. The two-axis sun-tracking system is an open-loop tracking system, which employs algorithm to calculate the sun's position according to date, time, and geographical information.

The sunrays reflected by the facet mirrors at the four corners had the largest incident angle relative to the receiver plane and thus, the rim angle of the NIDC is defined as the angle subtended by the light rays reflected by the two most distant facet mirrors, which were located at the top-left and bottom-right corners. Figure 3.1 shows a facet mirror located at one corner of the NIDC where its distance from centre of the NIDC in *X*-direction and *Y*-direction were 92.25 cm and 96.25 cm, respectively. The shortest vertical distance in the *Z*-direction from the central point of the entrance aperture of the secondary optics to the line joining the central points of the two most distant facet mirrors was 183.86 cm. The rim angle was calculated as 71.9° using the following equation:

$$\text{Rim angle, } \theta = 2\tan^{-1}\left(\frac{H_{xy}}{H_z}\right) = 2\tan^{-1}\left(\frac{\sqrt{92.25^2 + 96.25^2}}{183.86}\right) \qquad (3.4)$$

Table 3.1: Specifications of the non-imaging dish concentrator.

Primary concentrator: non-imaging dish concentrator (NIDC)	
Type of reflector	3 mm mirror with back metallic coating
Number of facet mirror	96 units
Dimension of facet mirror	20 × 20 cm
Array arrangement	Facet mirrors arranged into 10 rows and 10 columns with 4 facet mirrors in the central region removed
Focal distance	210 cm
Total reflective area	3.84 m^2
Total projection area of reflector	3.76 m^2
Range of solar rays reflected angle	8.6°–36.7°

The NIDC was oriented by two stepper motors in azimuth-elevation axes. Two worm gear reducers with a gear ratio of 60:1 were used to drive the solar concentrator frame along the azimuth and elevation axes. Compared with ordinary gear trains using spur gears, the direction of the worm gear transmission is irreversible because a larger friction is involved between the worm and worm-wheel. In other words, worm gear configurations in which the gear cannot drive the worm are said to be *self-locking*. In this way, there is no motor energy consumption on stationary positions and the usage of complex load brake mechanisms is not required.

As sunlight is concentrated on the solar cell, the non-converted sunlight will generate heat that will raise the solar cell's temperature. If the temperature of the solar cell is higher than the standard operating temperature, the energy conversion efficiency will drop significantly. Therefore, a copper cooling block was installed as a receiver to obtain better heat dissipation effect

and to prevent the solar cell from operating at a higher temperature. Besides that, an automotive radiator cooling system was applied in the prototype for heat management purposes that is to lower down the temperature of the solar cells (Chong et al., 2012a). Figure 3.5 shows the automotive radiator from the commercial automobile model "Proton Wira 1500 cc". The materials of the automotive radiator casing and tubes are aluminium alloy with high heat conductivity and light weight. It is easy to be installed into the prototype of the NIDC with minimum load added to the driving system. The external fins sandwiched between the ducts in the radiator are made of copper in order to have higher heat conductivity for increasing the heat dissipation rate.

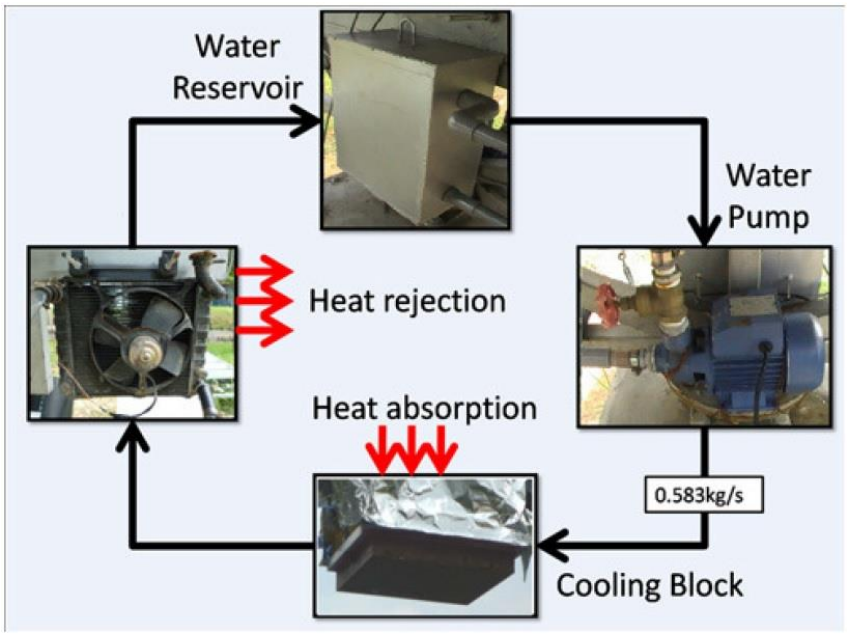

Figure 3.5: Automotive radiator cooling system (Chong et al., 2012a).

3.2 Secondary Optics: Dielectric Filled Crossed Compound Parabolic Concentrator

There are two major requirements for the geometrical design of a secondary concentrator. The first requirement is to ensure that the exit aperture can match well with the shape and dimension of the CPV cell. The second requirement is to ensure that the acceptance angle of the secondary concentrator is larger than the rim angle of the NIDC so that the aperture of the secondary optics is sufficiently large to subtend all the sunrays reflected by the NIDC and to maximize the sunlight to be concentrated onto the CPV cell.

The high efficiency multi-junction CPV cell, which is commercially available, is mostly either square or rectangle in shape. The CPV cells used in our study are the product of Spectrolab with the mechanical dimension of 11 × 10 mm and an active area of 9.85 × 9.89 mm, and the detailed specifications are listed in Table 4.1 (Spectrolab, 2010). A square exit aperture is highly recommended instead of a circular exit aperture in order to map the concentrated sunrays across the CPV cell for aiming to produce a uniform illumination throughout the active surface area.

For this reason, a typical candidate for the secondary concentrator with a square exit aperture would be the crossed compound parabolic concentrator (CCPC), which is formed by intersecting two symmetrical 2-D compound parabolic concentrators (CPC) orthogonally. In the perspective of geometrical

optics for the CCPC, all the sunrays that successfully enter the CCPC within the acceptance angle will emerge at the exit aperture.

A dielectric filled CCPC with square cross sections in both the entrance and exit apertures were tailored to match the dimension of the CPV cell assembly as shown in Figure 3.6. Each CPV cell assembly consisted of a CPV cell, a by-pass diode, and a direct bonded copper with Au/Ni surface plating (front and back surfaces) on an Al_2O_3 substrate. On the other hand, B270 super white was selected as the dielectric material for the CCPC lens as it is a clear high transmission crown glass (modified soda-lime glass) available in various forms and is affordable.

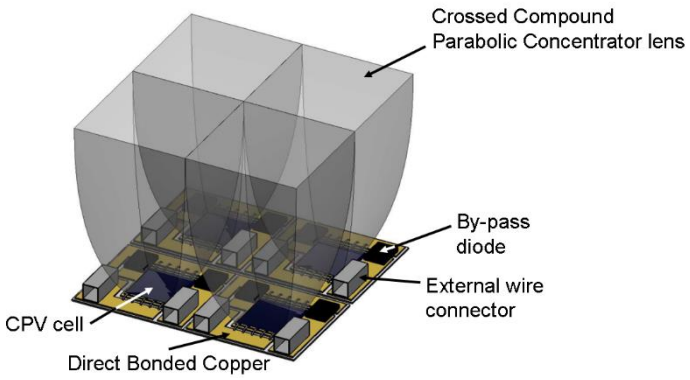

Figure 3.6: A 2 × 2 array of CPV + CCPC assembly sets. Each CPV + CCPC assembly set is an integrated concentrator photovoltaic cell assembly and crossed compound parabolic concentrator lens. Each concentrator photovoltaic (CPV) cell assembly consisted of a triple-junction CPV cell, a by-pass diode, and a direct bonded copper with Au/Ni surface plating (front and back surfaces) on an Al_2O_3 substrate.

A systematic process as shown in the flow chart described in Figure 3.7 was applied to design the dimension of the CCPC lens well-tailored to our application.

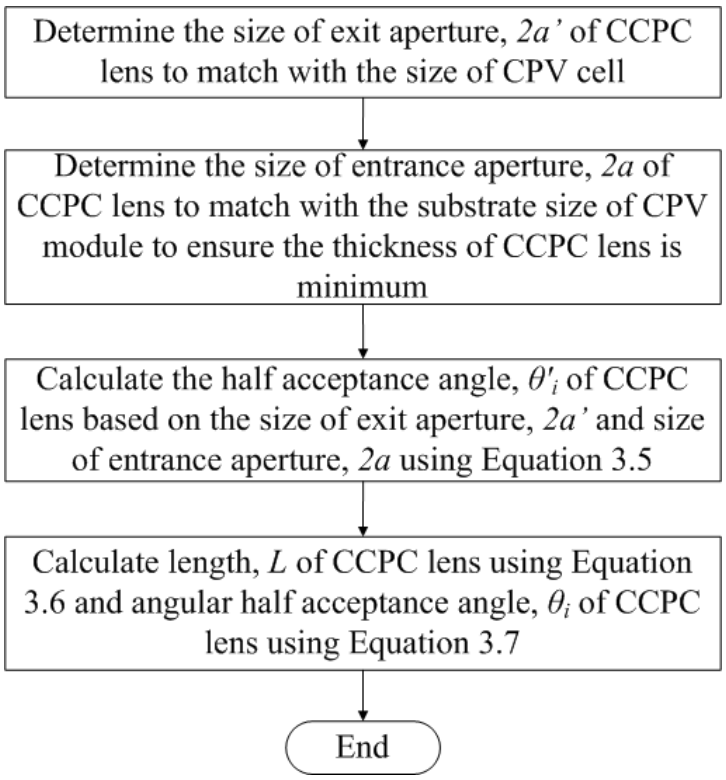

Figure 3.7: Flow chart showing the systematic process in designing the dielectric filled CCPC geometry.

In reference to Figure 3.7, Eqs. (3.5), (3.6), and (3.8) were derived by Winston et al. (2005) and Eq. (3.7) was derived from the Snell Law (Winston et al., 2005).

$$2a = \frac{2a'}{\sin\theta'_i} \tag{3.5}$$

$$L = \frac{a'\left(1+\sin\theta'_i\right)\cos\theta'_i}{\sin^2\theta'_i} \tag{3.6}$$

$$\theta_i = \sin^{-1}\left(n \sin \theta_i'\right) \tag{3.7}$$

$$C_R = \left(\frac{a}{a'}\right)^2 = \left(\frac{1}{\sin \theta_i'}\right)^2 = \left(\frac{n}{\sin \theta_i}\right)^2 \tag{3.8}$$

In our design, the CCPC lens had an exit aperture size ($2a'$ = 9.8 mm), which was slightly smaller than the active area of the solar cell, (9.85 × 9.89 mm), so that all the sunrays arriving at the exit aperture can reach the active area of the solar cell, including the sunlight exiting near the edge of the exit aperture. In the case study, the size of the entrance aperture, $2a$ = 24 mm, was selected in order to match the dimension of the CPV cell assembly, 25 × 21 mm, as listed in Table 3.2 with the configuration as shown in Figure 3.8.

Table 3.2: Specifications of crossed the compound parabolic concentrator lens and the secondary concentrator.

Crossed compound parabolic concentrator (CCPC) lens	
Dimension of entrance aperture	24 × 24 mm
Dimension of exit aperture	9.8 × 9.8 mm
Length, L	37.78 mm
Geometrical concentration ratio	5.998
Half acceptance angle, θ'_i	24.1°
Angular half acceptance angle, θ_i	37.77°
Dielectric material	B270 super white
Refractive index of the dielectric material	1.5
Transmittivity of the dielectric material	87.5%
Secondary concentrator: Array of CCPC lenses	
Array of CCPC lenses	8 × 8
Size of the entrance aperture	195.5 × 195.5 mm
Gap between CCPC lenses	0.5 mm

The purpose of this selection is to ensure that the CPV cell assembly can be arranged closely to each other with a small tolerance of 0.5 mm in every side and to minimize the thickness of the CCPC lens because the absorptivity of sunlight by the dielectric material of CCPC is proportional to the thickness of the lens. The size of the CCPC entrance aperture must be either the same or larger than the size of the CPV cell assembly so that all the CCPC lenses can be arranged tightly to each other. The integrated design of the CCPC and CPV is more efficient compared to that of the DACPV in terms of packing factor by reducing the percentage of the sunlight fallen on non-active areas that incurs losses to the whole system.

The final geometrical design of the CCPC lens is shown in Figure 3.8.

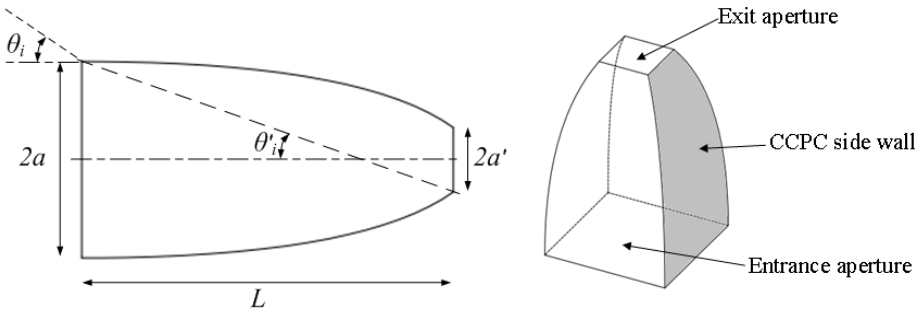

Figure 3.8: Dielectric filled crossed compound parabolic concentrator with an angular half acceptance angle, θ_i of 37.77°. The square entrance aperture size, $2a$, is 24 mm; the square exit aperture size, $2a'$, is 9.8 mm; and the total length, L, is 37.78 mm.

The half acceptance angle, θ'_i of the CCPC geometry was 24.1° and was computed using Eq. (3.5). For the dielectric filled CCPC lens made of B270 glass material with a refractive index, n, of 1.5, the angular half acceptance angle, θ_i of the CCPC lens was calculated to be 37.77° using Eq. (3.7). There are two advantages of the CCPC lens against the reflector: it increases the acceptance angle due to the refraction effect at the air-dielectric interface and it allows total internal reflection without any reflectivity loss. Since the focal distance is inversely proportional to the rim angle based on Eq. (3.4), the rim angle can be reduced by increasing the focal distance in the case of the rim angle (θ) being larger than the acceptance angle of the CCPC ($2\theta_i$). By fixing the acceptance angle of the CCPC, the adjustment of the focal length is necessary to ensure that all the concentrated sunlight from the NIDC can be fully guided to the exit aperture. The length, L, of the lens was 37.78 mm, calculated using Eq. (3.6). The geometrical concentration ratio of CCPC, defined as CR, is expressed in Eq. (3.8) and was determined to be 5.998. The sunlight concentrated by the NIDC was further concentrated by the CCPC lens.

3.2.1 Preliminary Ray Tracing

Preliminary ray tracing had been carried out to study the behaviour of the dielectric filled 2-D CPC to understand its feasibility to be used as the secondary of the NIDC system. It is important that light rays that incident on the entrance aperture of the CCPC will be guided to the exit aperture with

minimal loss. The 2-D ray trace was carried out with the optical simulation software, LightTools, to investigate the behaviour of the light ray incident from 0° to 37.8°. All light rays with an incident angle of 0° to 26° was transmitted to the exit aperture. When the incident angle of the light rays was more than 26°, the ray tracing analysis revealed that part of the incoming light rays did not undergo total internal reflection, even within the half acceptance angle of the CPC. Those light rays escaped from the side walls, which were near the exit aperture without reaching the exit aperture as shown in Figure 3.9(c). The percentage of light rays which escaped gradually increased from 0 to 13.8% as the incident angle increased from 26.0° to 37.8°.

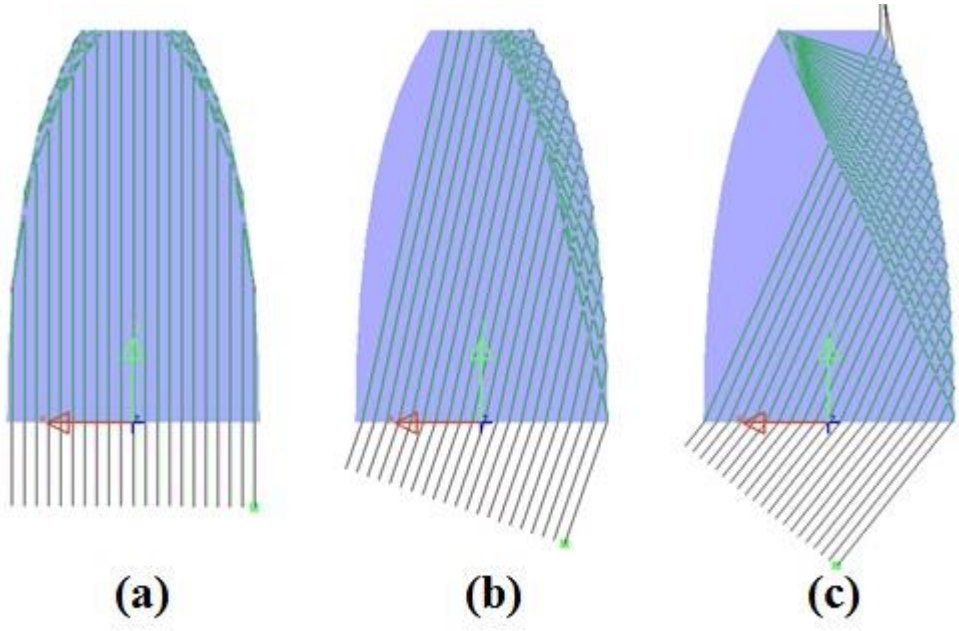

Figure 3.9: Preliminary ray-trace showing rays with (a) 0° incidence angle; (b) 19° incidence angle; (c) 37.8° incidence angle.

Light rays reflected by 25% of the total number of flat facet mirrors have an incident angle at the receiver of greater than 26°, therefore there will be a loss of energy of maximum 2% of the total energy that is reflected by all the mirrors.

3.2.2 Secondary Concentrator Comprising of the CCPC Array

The secondary concentrator is comprised of the CCPC lenses arranged into rows and columns to form the 2-D array as shown in Figure 3.10. Primary focused image size of 22.6 × 22.6 cm produced by the NIDC can be obtained from the simulated result as plotted in Figure 3.11. The entrance aperture was placed at the focal plane of the NIDC for collecting the concentrated sunlight from the NIDC and each of the CCPC lens further focused the sunlight onto their respective CPV cell. An array of 8 × 8 dielectric filled CCPC lenses was arranged closely with a gap of 0.5 mm between two adjacent lenses to form a secondary concentrator so that the total surface area of 19.55 × 19.55 cm of the entrance aperture matched with the primary focused image of the NIDC. The entrance aperture of the secondary concentrator was purposely designed to be slightly smaller in size than that of the primary focused image. Due to the solar disc effect, the peripheral region of the primary focused image with a much lower solar concentration ratio as compared to that of the central region was omitted. This was done to avoid imbalance in current generation by those CPV cells located in the peripheral region as compared to that of the central

region and to subsequently cause current mismatch problem affecting the overall conversion efficiency of the whole module.

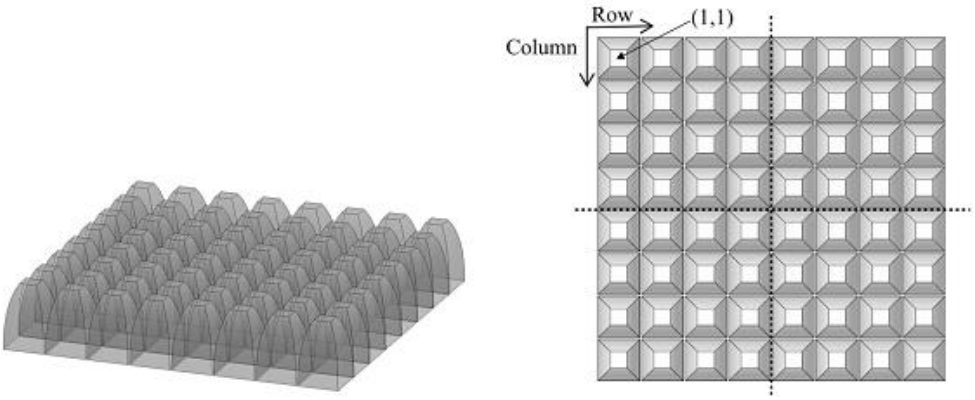

Figure 3.10: An array of 8 × 8 dielectric filled CCPCs was arranged closely with a gap of 0.5 mm between two adjacent lenses to form a secondary concentrator so that the total surface area of 19.55 × 19.55 cm of the entrance aperture matched with the primary focused image of the NIDC. The lenses were divided into four symmetrical quadrants.

3.3 Optical Performance Study with Ray-trace Simulation

3.3.1 Methodology

The optical performance was carefully evaluated using a commercial ray-tracing software, LightTools. The optical system consisted of two major elements: the primary concentrator, which is the NIDC and a secondary concentrator, which is an array of CCPC lenses with the specifications as listed in Table 3.2 and the 3-D optical layout design is illustrated in Figure 3.1.

In our numerical modelling using LightTools, a light source with a dimension slightly larger than the dimension of the NIDC was generated to generate parallel cone rays with a solar disc half angle of 4.65 mrad. The slightly larger light source is important to guarantee that the ray-tracing of sunrays has covered the entire facet mirrors of the NIDC in the simulation. In the setting of the simulation program, all the flat facet mirrors involved in the ray-tracing program were made of 3 mm thick dielectric glass with a back-coated reflective surface. The properties of the dielectric filled CCPC were set according to the specifications given by the B270 super white datasheet with a refractive index of 1.5 and transmittance of 87.5% (Schott Desag, 2000).

A receiver plane was fixed at the focal plane of the NIDC to study the solar flux distribution before the sunrays are further concentrated by the CCPC lenses to their respective exit apertures. Moreover, each exit aperture of the CCPC was also assigned with a receiver plane to study the concentrated flux distribution. The ratio of flux density at the receiver plane to flux density at the light source is defined as the Solar Concentration Ratio (SCR). In each simulation, 12 million rays were traced to obtain the simulated result, and the simulated flux distribution patterns are plotted as shown in Figures 3.11 and 3.12.

A study had been made to evaluate the performance of the CCPC under the effect of off-tracking. For the case of off-tracking, the light source was rotated around the *X*-axis, *Y*-axis, and both *X* and *Y* axes with a pointing error ranging from 0° to 0.4° with an increment step of 0.1°. The choice of

range for the pointing error takes into consideration the practical tracking accuracy as a 12-bits optical encoder was employed as a feedback sensor in the tracking algorithm (Chong et al., 2009a, 2009b). After setting all the parameters for the primary concentrator, secondary concentrator, and receiver planes, the ray-tracing program was initiated to plot the flux distribution pattern on the receiver planes for both the NIDC and exit apertures of the CCPC lenses.

3.3.2 Results and Discussion

Figure 3.11(a) depicts the simulated results of the primary focused image formed by the NIDC without a pointing error. The simulated solar flux distribution consisted of a flat top region with a maximum SCR of 88 suns located in the central region covering the area of 18.2 × 18.2 cm and was surrounded by a steep decrease of 88 suns to 0 within 2 cm near the edge, to form a total primary focused image size of 22.6 × 22.6 cm. The percentage of energy within the uniform illumination area was 79%. With such uniformity, it can minimize the current mismatch problem, which has made it suitable for dense array concentrator photovoltaic (DACPV) application.

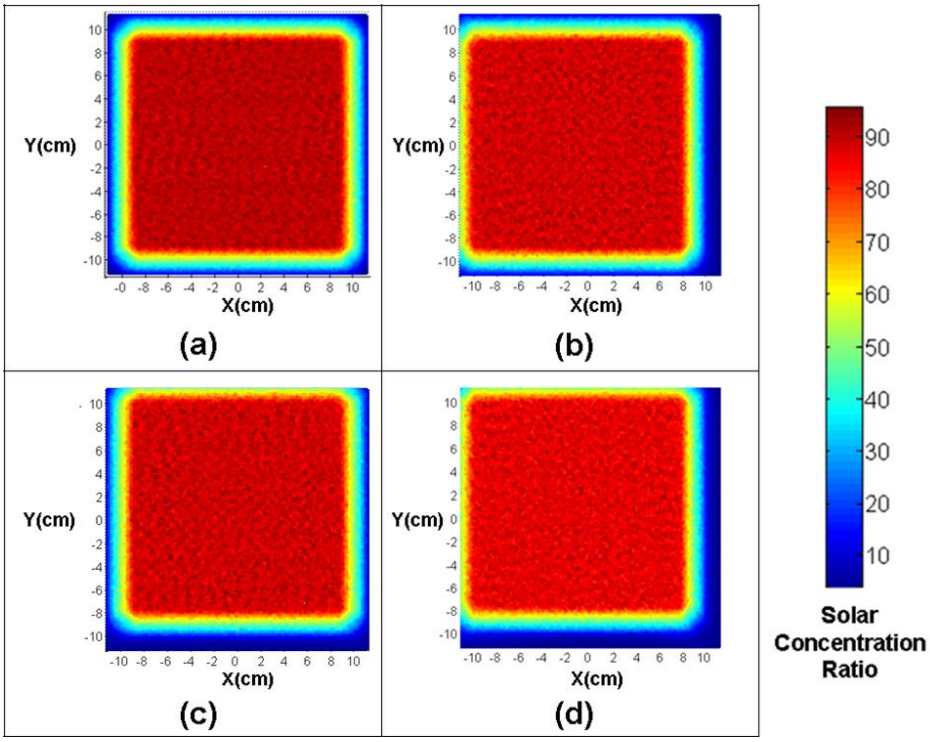

Figure 3.11: Solar flux distribution of primary focused image by NIDC: (a) no pointing error; (b) pointing error of 0.3° counter-clockwise rotation about *Y*-axis; (c) pointing error of 0.3° counter-clockwise rotation about *X*-axis; (d) pointing error of 0.3° counter-clockwise rotation about both *X*-axis and *Y*-axis.

Pointing error is caused by the inaccurate sun-tracking system and incident sunrays relative to the NIDC should be parallel with the *Z*-axis (optical axis of NICD) if no pointing error exists. To study the effect of the inaccurate sun-tracking towards the electrical performance of the CPV system, we simulated the cases of pointing error by rotating the light source from 0° to 0.4° with a 0.1° increment in the counter-clockwise direction about *X*-axis, *Y*-axis, and both *X* and *Y* axes concurrently. For a pointing error of 0.3° counter-clockwise about *Y*-axis as shown in Figure 3.11(b), the primary focused image had shifted to the negative direction of the *X*-axis without any obvious distortion in both the flux distribution pattern and image dimension. For a

pointing error of 0.3° counter-clockwise about *X*-axis as shown in Figure 3.11(c), the primary focused image had shifted to the positive direction of *Y*-axis without any obvious effect to both the flux distribution pattern and image dimension. Finally, the study also included the case of off tracking in both axes, $X = 0.3°$ counter-clockwise and $Y = 0.3°$ counter-clockwise, simultaneously. From the simulated results as shown in Figure 3.11(d), the whole image had shifted in both the *X* and *Y* directions without affecting the distribution pattern and dimension. According to the simulated results, the image had shifted about 6 mm towards the corresponding direction for each 0.1° of pointing error.

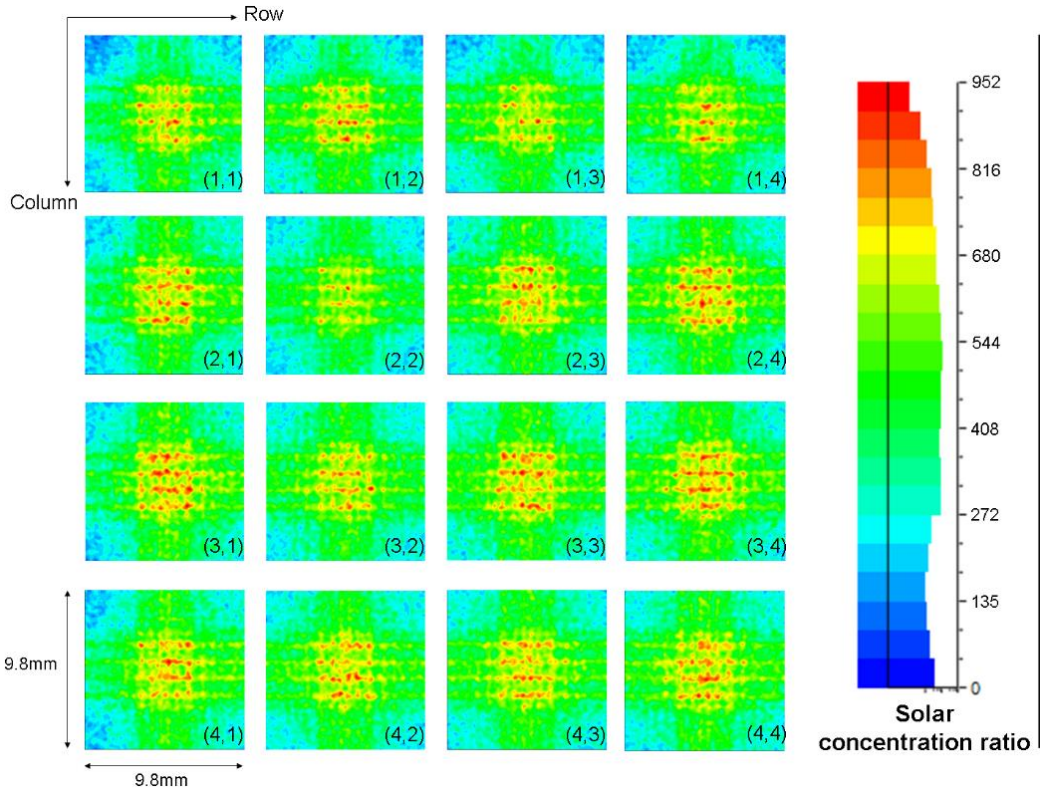

Figure 3.12: Solar flux distribution at the exit aperture of the top left quadrant (first 4 rows and first 4 columns) of the CCPC array for the case of without pointing errors during sun-tracking.

Figure 3.12 shows the simulated solar flux distribution on the receiver planes at the exit apertures of the CCPC lenses located in the top-left quadrant of the full array. The flux distribution patterns and solar concentration ratios of the other three quadrants were similar to the simulated results in which their relationship were mirror symmetry to each other.

Among all the concentrated flux at exit apertures, SCR for the exit aperture of CCPC at the four corners of the complete array was the lowest when it is compared to the SCR for other CCPC lenses. It was reflected by the flux distribution pattern of the primary focused image with the lowest average SCR at the corner. The total average of the SCR at the CCPC position (4, 4) or the central region of the secondary concentrator was 416 suns whilst the SCR was lower for those CCPC lenses located in the outermost ring with the lowest SCR at four corners. The overall uniformity of the solar flux distribution pattern is acceptable, in which the value of the peak to average ratio (PAR) of the all exit apertures ranged from 2.08 to 2.35 as listed in Table 3.3. For the solar flux distribution in the full CCPV array, the average SCR for the 6 × 6 array of the CCPC located in the central region of the receiver was 416 suns, but the average SCR ranged from 346 to 381 suns for CCPCs located at the four edges of the 8 × 8 array.

Table 3.3: The positions of the crossed compound parabolic concentrator (CCPC) lens in the top left quadrant of the full array and its corresponding peak-to-average ratios (PAR).

CCPC position	PAR	CCPC position	PAR
(1,1)	2.35	(3,1)	2.14
(1,2)	2.26	(3,2)	2.22
(1,3)	2.35	(3,3)	2.09
(1,4)	2.33	(3,4)	2.08
(2,1)	2.21	(4,1)	2.20
(2,2)	2.16	(4,2)	2.17
(2,3)	2.14	(4,3)	2.14
(2,4)	2.11	(4,4)	2.11

Herrero et al. (2012) and Baig et al. (2013) had done extensive studies on the non-uniform illumination in both concentrating solar cell and module. According to Baig et al. (2013), the non-uniform incident flux illuminated on the solar cell would affect the fill factor (FF) of the solar cell, which can reduce the maximum power output. In fact, it is very difficult to obtain uniform illumination as there are many factors that can cause non-uniformity such as the imperfection of optical geometry, aberration, geometrical error of the concentrator profile caused by manufacturing defect, inaccurate sun-tracking, optical misalignment of the solar concentrator, and mechanical failures. To quantify the different profiles of non-uniformity, Herrero et al. (2012) had introduced a parameter called peak-to-average ratio (PAR). They had characterized the non-uniform light patterns produced by the optical systems and reproduced them on CPV cells in experiments to obtain the fill factor under different profiles of non-uniformity; the percent variation of the fill factor (FF) versus the PAR of a multi-junction (MJ) solar cell is provided in Figure 3.13 (Herrero et al., 2012). Considering the CCPC located at (4, 4)

with a peak SCR of 952 suns and average SCR of 416 suns, the peak-to-average ratio (PAR) is only 952 ÷ 416 = 2.29. The PAR of illumination at the exit apertures of the CCPC lenses ranged from 2.08 to 2.35 in our study. As shown in Figure 3.13, the non-uniformity with a PAR below 2.5 will not significantly affect the fill factor of the CPV cell.

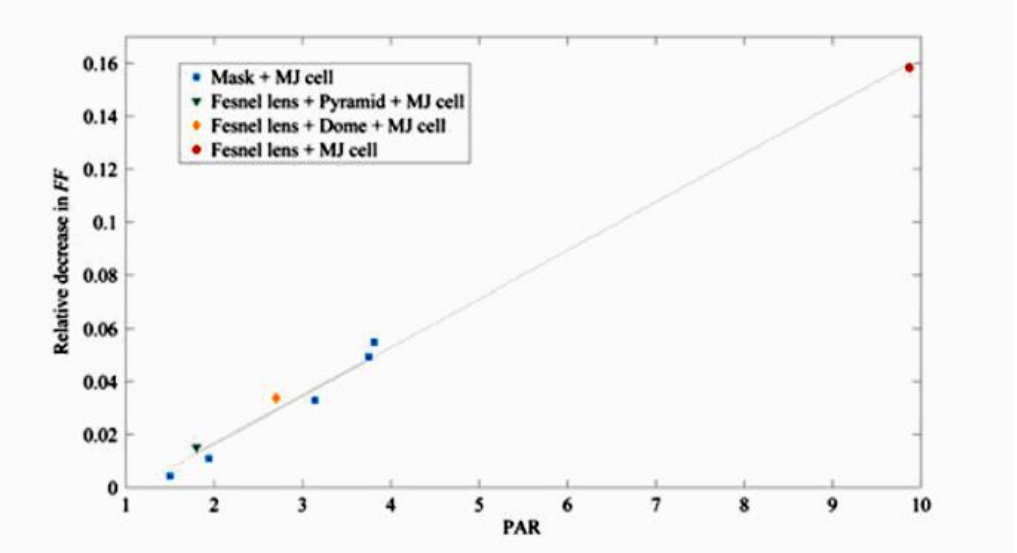

Figure 3.13: Percent variation of the fill factor (FF) versus the peak-to-average ratio (PAR) of a multi-junction (MJ) solar cell. (Herrero et al., 2012).

3.4 CCPC Lens Optical Efficiency Evaluation

The optical efficiency of the CCPC lens were evaluated with the CCPC + CPV assembly set. The short circuit current generated by a CCPC + CPV assembly set were compared to the short circuit current generated by the CPV module, which is the same type as the module used in a CCPC + CPV assembly set. Almost all the solar light flux that was focused on the receiver of

the NIDC were direct components from the sun. Therefore, knowing the relationship between the CPV module short circuit current and direct normal irradiance (DNI) is important to study the solar concentrator system's performance. A calibration work had been carried out to find out the short circuit output current from the CPV module that responds to DNI. When both the CPV module and the CCPC + CPV assembly set were facing the sun, they received energy from direct and diffuse sunlight. The acceptance angle of the CPV module was much larger than the CCPC + CPV assembly set as it had been limited by the CCPC lens. Therefore, there is a need to develop a way to measure the short circuit current generated by both the CPV module and the CCPC + CPV assembly set that responds to DNI only.

In order to limit the acceptance angle of the CCPC + CPV assembly set, we rolled a rough sand paper into the shape of a tube with the rough surface of the sand paper as the inner surface of the tube. The sand paper tube must have a certain length so that the sunlight that reached the entrance aperture of the CCPC is within an incident angle of 5°, which is similar to the acceptance angle of the pyrheliometer that is used to measure DNI. The sand paper tube was placed above the CCPC + CPV assembly set during the measurement of the short circuit current that responds to DNI, I_{sc}^{CCPC}.

For the CPV module, a way to calculate the short circuit current of the CPV module that responds to DNI was found during the calibration process. The finding eased the measurement as the acceptance angle of the CPV module does not have to be limited for every measurement. The short circuit

current of the CPV module that responds to the DNI, I_{sc}^{DNI}, was calculated using the following equation:

$$I_{sc}^{DNI} = I_{sc}^{measured} \frac{DNI}{GSI} \tag{3.9}$$

where $I_{sc}^{measured}$ is the measured short circuit current of the CPV module (mA) that responds to GSI; DNI is the direct normal solar irradiance reading from the pyrheliometer (Wm^{-2}); and global solar irradiance (GSI) is the global solar irradiance reading from the pyranometer (Wm^{-2}).

After both I_{sc}^{DNI} and I_{sc}^{CCPC} were measured, the measured solar concentration of the CCPC lens, $CR_{measured}$, was calculated using the following equation:

$$CR_{measured} = \frac{I_{sc}^{CCPC}}{I_{sc}^{DNI}} \tag{3.10}$$

Figure 3.14 shows a simple setup to measure $CR_{measured}$ of a CCPC + CPV assembly set. The sand paper tube was placed above CCPC + CPV assembly set during measurement.

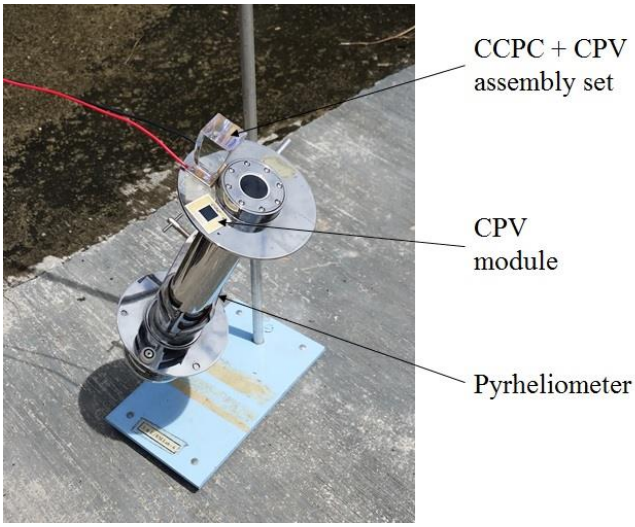

Figure 3.14: Calibration setup for optical efficiency evaluation. CCPC + CPV assembly set and a CPV module were mounted on the pyrheliometer to ensure that their surface are normal to the incident sunlight.

3.4.1 Results and Discussion

Table 3.4 shows the values of $CR_{measured}$ of a few CCPC + CPV assembly sets that were selected from the 8 × 8 array of dielectric filled CCPCs. During each measurement, I_{sc}^{CCPC}, $I_{sc}^{measured}$, DNI, and GSI were taken concurrently as the DNI and GSI might vary due to weather condition.

Table 3.4: Summary of $CR_{measured}$ of CCPC + CPV assembly sets with their respective position in the secondary concentrator.

CCPC position		I_{sc}^{CCPC} (mA)	$I_{sc}^{measured}$ (mA)	DNI (W/m^2)	GSI (W/m^2)	I_{sc}^{DNI} (mA)	$CR_{measured}$
Row	Column						
3	3	55.3	15.80	937	1046	13.96	3.96
	4	57.2	15.83	949	1058	14.01	4.08
	5	56.5	16.20	949	1071	14.17	3.98
	6	57.6	16.20	949	1071	14.17	4.06
4	3	56.0	15.92	949	1058	14.09	3.97
	4	57.7	15.87	949	1058	14.04	4.10
	5	57.5	16.35	937	1058	14.28	4.02
	6	59.2	16.34	937	1058	14.27	4.14
5	3	58.9	16.05	949	1071	14.04	4.19
	4	56.0	16.05	949	1071	14.04	3.98
	5	56.3	15.80	937	1058	13.80	4.07
	6	56.6	15.95	937	1058	13.93	4.06
6	3	56.9	16.22	949	1083	14.03	4.05
	4	58.0	16.05	949	1071	14.04	4.12
	5	58.8	15.90	949	1071	13.91	4.22
	6	57.0	15.80	937	1071	13.64	4.17
1	8	56.0	16.95	937	1131	13.85	4.04

From our measurement, $CR_{measured}$ of selected CCPC + CPV assembly sets ranged from 3.96–4.22. The small variation of the $CR_{measured}$ can be due to the alignment of the CCPC lens and CPV cell being not exactly same, and the output current from each CPV cell might have had a slight difference. The average $CR_{measured}$ was found to be 4.07. The value is only 67.9% of the theoretical geometrical concentration ratio. The loss was mainly due to a few reasons: the absorption of the dielectric material of the CCPC lens, Fresnel loss incurred when sunrays travelled from air into the glass medium and also from glass into the encapsulant medium. Some light rays with an incident angle larger than 26° that escaped through the side wall also contributed to the loss as discussed in section 3.2.1.

CHAPTER 4

ELECTRICAL PERFORMANCE OPTIMIZATION OF DENSE-ARRAY CONCENTRATOR PHOTOVOLTAIC SYSTEM WITH SECONDARY OPTICS

4.1 Assembly of the CCPC + CPV Assembly Set

The Spectrolab CCA 100 CPV module is a ready-made module consisting of a CDO 100, C3MJ solar cell, and a 12A Schottky by-pass diode attached to a direct bond copper (DBC) with Au/Ni surface plating (front and back surfaces) on an Al_2O_3 substrate. Figure 4.1 shows the CPV cell attached on the Au/Ni plated copper layer and the high current carrying interconnectors connecting the bus bar of the solar cell to the Au/Ni plated copper layer using Spectrolab's proprietary welding process. The Al_2O_3 substrate offers excellent thermal conductivity and a compatible coefficient of thermal expansion with the solar cell.

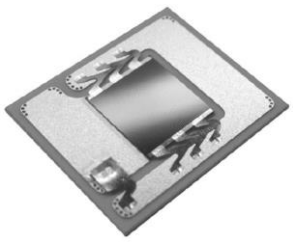

Figure 4.1: CPV module with a C3MJ solar cell and 12A Schottky by-pass diode attached to a direct bond copper (DBC) ceramic substrate.

The table below shows the summary of the specifications of the Spectrolab CCA 100 CPV module and the CDO 100 C3MJ solar cell.

Table 4.1: Specifications of CPV cell assembly and CPV cell.

CPV cell assembly (Spectrolab product: CCA 100 C3MJ Concentrator Cell Assembly)	
Dimensions of the CPV cell assembly	25 × 21 mm (note: original size is 25.5 × 21.0 mm as provided in the specification, but we trimmed it to 25 × 21 mm)
Typical performance efficiency	38.5%
Ceramic carrier	Direct bonded copper with Au/Ni surface plating (front and back surfaces) on an Al_2O_3 substrate
By-pass diode	12A Schottky
CPV cell (Spectrolab product: CDO 100 C3MJ)	
Typical performance efficiency	38.5%
Dimension of the cell aperture (active area)	9.85 × 9.89 mm (98.9 mm^2)
Mechanical dimension of the cell (including bus bar, etc.)	11 × 10 mm
VOC (1,000 W/m^2 irradiance)	2.77 V
ISC (1,000 W/m^2 irradiance)	14 mA
Operating temperature of the CPV cell	−40°C to 100°C

However, the module did not come with external connectors or wires. Therefore, before attaching the CCPC lens onto the CPV cell, two external wires with low resistance and high current capacity were soldered to each terminal of the module for external connection as shown in Figure 4.2. In order to solder the wire, the soldering iron rod needs to be heated to around 400°C−450°C instead of around the usual 300°C if working on a typical PCB board, as the DBC substrate of the CPV module dissipates the heat and causes the temperature to drop immediately. After soldering, a thin layer of DOW

CORNING SE 9120 clear sealant was applied on the CPV cell. DOW CORNING SE 9120 is a one-part translucent sealant which has moisture cure RTV, good flow, fast tack-free, and controlled volatility material. It is used as an encapsulant of the CPV cell and an adhesive between the CCPC lens and CPV cell. It can also act as a medium to replace the air-glass interface, which will cause total internal reflection when light travels from the CCPC lens towards the CPV cell.

As the DOW CORNING SE 9120 clear sealant is not designed for high concentration solar application, the durability of the material under high irradiance and temperature is unknown. The sample unit was installed at the receiver of the NIDC to study the behaviour of the sealant. We observed it for more than 20 hours under the sun and found no obvious degradation that could cause the output of the CPV cell to decrease.

The exit aperture of the CCPC lens was placed right on top of the CPV cell immediately after the sealant was applied on the CPV cell. The CCPC lenses were held with a jig so that it maintains a 100 nm of distance between the CPV cell and the exit aperture of the CCPC lens. After curing, a layer of 100 nm sealant was formed. When placing the CCPC lens, it must be ensured that no air bubbles are trapped in the sealant as it will create an air-glass interface and cause high air pressure in the bubble when the CCPC + CPV assembly set are put under high concentration. Figure 4.2 shows the procedure of attaching the CCPC lens onto the CPV module.

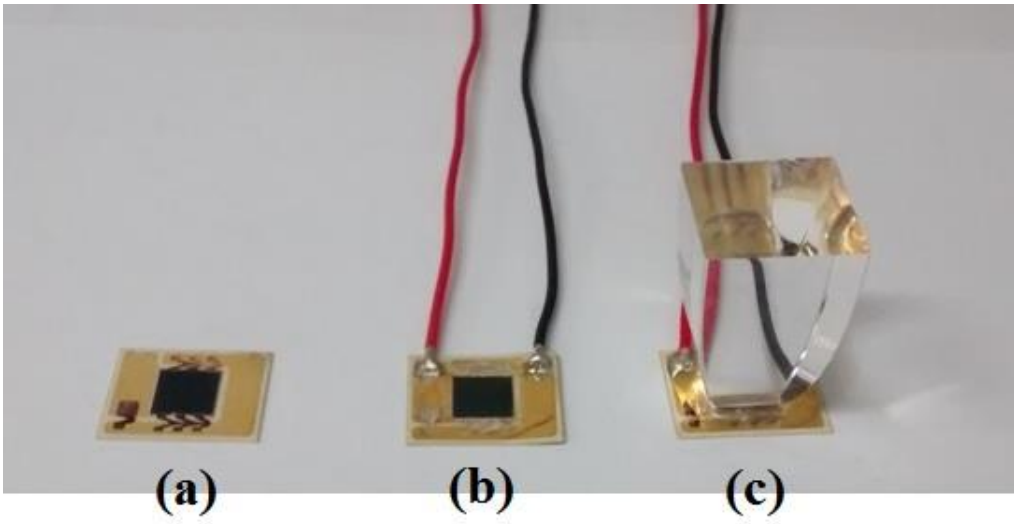

Figure 4.2: (a) Spectrolab CCA 100 CPV module; (b) two wires were soldered to the terminal of the module; (c) CCPC lens are attached on the CPV cell with DOW CORNING SE 9120 clear sealant.

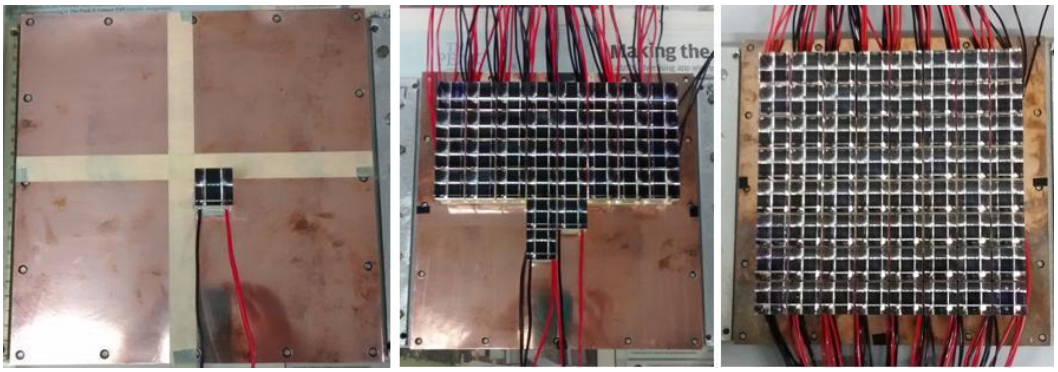

Figure 4.3: The process of attaching the CCPC + CPV assembly set to a copper block heat sink starting with a single assembly set until completing the 8 × 8 array.

After the assembly, 64 CCPC + CPV assembly sets were arranged into 8 × 8 arrays and attached to a copper block heat sink with Arctic Silver Thermal Adhesive. Arctic Silver Thermal Adhesive is a two-part permanent adhesive for thermal joints in minimum bond line applications. The adhesive

is made with 99.8% pure micronized silver and has 62% to 65% silver content by weight that exhibits superior thermal performance. Figure 4.3 shows the process of attaching the CCPC + CPV assembly set to a copper block heat sink starting with a single assembly set until completing the 8 × 8 array.

4.2 Electrical Performance Study with Simulation

4.2.1 Methodology

We have adopted the numerical modelling method using Simulink to analyse the electrical performance of two different electrical layout designs of the CPV cells: (1) dense array concentrator photovoltaic (DACPV) module based on solar flux distribution of primary focused image; and (2) array of integrated CPV cells and CCPC lenses (CPV + CCPC) assembly module based on solar flux distribution at CCPC exit apertures. As proposed by Siaw et al. (2014), a circuit with three current sources connected in series was applied in our study to represent a comprehensive equivalent circuit model for a triple-junction CPV cell. The triple-junction CPV cell circuit model was then simplified into a two-diode model, which is equivalent to a CPV cell block in SimElectronics, which is the function block in Simulink.

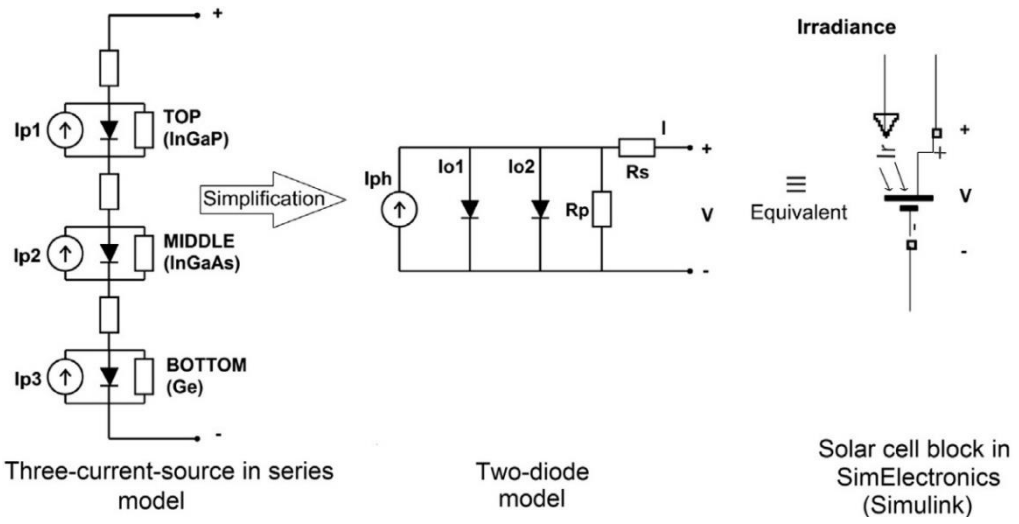

Figure 4.4: A schematic diagram to show the representation of a triple-junction solar cell, which is simplified from a three-current-source in the series model to the two-diode model, which is equivalent to a solar cell block in SimElectronics. (Siaw et al., 2014).

The CPV cell block represented by a single CPV cell as the current source with one exponential diode, a parallel resistor of resistance (R_P), and a serial resistor of resistance (R_S) were arranged into subsystems in the Simulink to form an array. The five-parameter model was chosen as it is good enough to perform a sensibly accurate analysis and it was successfully verified in the field test conducted by Siaw et al. (2014). The way to compute both the *I-V* and *P-V* curves is summarized in the block diagram for computational modelling under the Simulink environment and are shown in Figure 4.5 where the "CPV" block contains the subsystems of the CPV cell block. This model is ready for simulation with a selected simulation time that will affect the resolution of the *I-V* and *P-V* curves. Results generated from the simulation, such as the current, voltage, and output power values are stored in the MATLAB workspace and can be exported to Excel for further analysis.

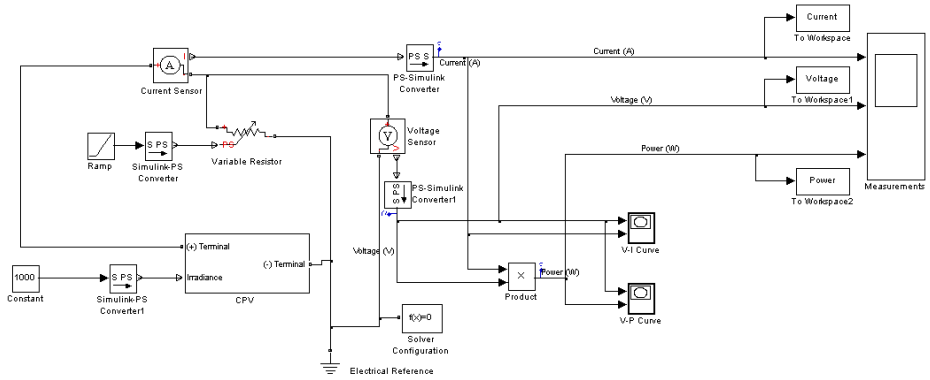

Figure 4.5: Overall Simulink implementation of both the DACPV and CPV + CCPC assembly modules simulation with block diagram.

The short circuit current of the CPV cell under one sun, I_{SC}^{1} and the open-circuit voltage under one sun, V_{OC}^{1} can be determined from the Spectrolab datasheet for the CPV cell (Spectrolab, 2010). The formulas of the short-circuit current, I_{SC}, and open-circuit voltage, V_{OC}, of the CPV cell are expressed in Eqs. (4.1) and (4.2), respectively (Siaw and Chong, 2013 and Siaw et al., 2014). Solar irradiance at a solar concentration ratio of one sun is equivalent to 1,000 W/m^2. For this study, the ideality factor of the CPV cell and the series resistance were assumed to be $N = 3$ and $R_S = 0\ \Omega$, respectively. The default temperature for the modelling was 25°C and the solar concentration ratio (SCR) is represented by C_R.

$$I_{SC} \cong I_{SC}^{1} \times C_R \tag{4.1}$$

$$V_{OC} \cong V_{OC}^{1} + N(kT/q) \ln C_R \tag{4.2}$$

The efficiency data of the CPV cell provided by the datasheet of Spectrolab is only limited to SCRs ranging from 350 to 900 suns (Spectrolab,

2010). For SCRs below 350 suns, the maximum power efficiency can be simulated using Simulink and is based on five parameters extracted from the Spectrolab datasheet, i.e. $I_{SC}^{1} = 14.0$ mA, V_{OC}^{1}=2.77V, 1 sun = 1,000 W/m^2, N = 3, and R_S = 0 Ω at 25°C.

For the completeness of the electrical performance study, we modelled and plotted the graph of the maximum power efficiency against the solar concentration ratio ranging from 1 to 1,000 suns for the single CPV cell as shown in Figure 4.6.

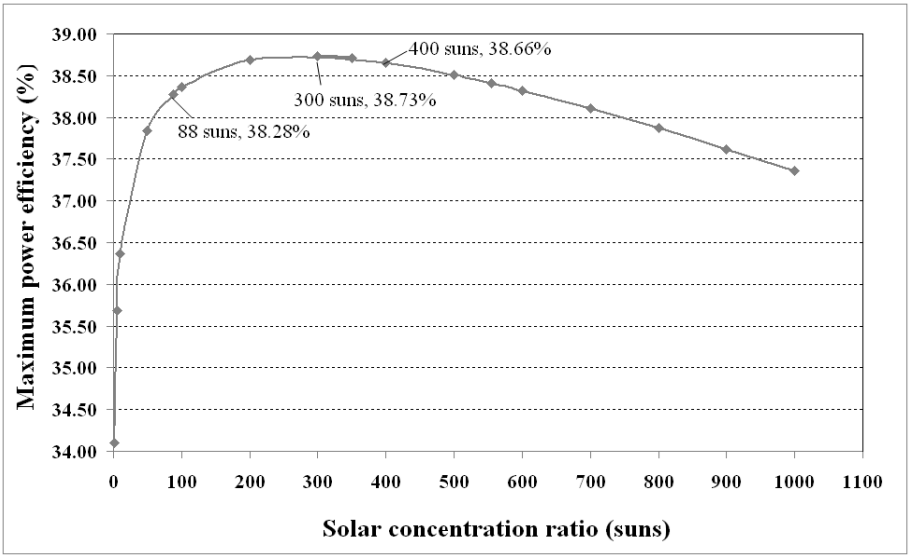

Figure 4.6: Maximum power efficiency of the CPV cell obtained from the numerical modelling using Simulink and five parameters extracted from the Spectrolab datasheet ($I_{SC}^{1} = 14.0$ mA, V_{OC}^{1}=2.77V, 1 sun = 1,000 W/m^2, N = 3, R_S = 0 Ω at 25°C). Note: The maximum power efficiency with SCRs of 350–900 suns obtained from our simulation is very close to that of the datasheet provided by Spectrolab as shown in Table 4.2.

The simulated maximum power efficiencies from the Simulink modelling were also verified with the data given in the Spectrolab datasheet with acceptable deviation between both results ranging from –0.15% to 0.81% for SCRs of 350–900 suns; the details are listed in Table 4.2.

Table 4.2: Comparison of the maximum power efficiency between the numerical modelling and the Spectrolab datasheet for the Spectrolab CPV cell.

Solar concentration ratio	Maximum power efficiency of the Spectrolab CPV cell (%)		Difference (%)
	Spectrolab datasheet	Numerical modelling	
350	38.56	38.71	−0.15
555	38.51	38.41	0.10
700	38.51	38.10	0.41
900	38.48	37.62	0.86

The maximum power efficiency of the CPV cell was calculated using the following equation:

$$\text{Maximum power efficiency} = \frac{\text{Maximum output power}}{\text{Active area of CPV cell} \times C_R \times 1000\ \text{W m}^{-2}} \times 100\% \quad (4.3)$$

4.2.2. Interconnection Optimization for the DACPV and the CPV + CCPC Assembly Modules

Before the optimization process was begun, the sizes of both the modules were set to be the same, which are 20 × 20 cm based on the size of a single flat facet mirror in the NIDC. It also provided a fair comparison for both the DACPV and CPV + CCPC assembly modules by using the same area of primary focused image for the electrical performance analyses. One major concern in the comparison for both the DACPV and CPV + CCPC assembly modules is that the electrical conversion efficiency is an SCR dependent parameter in which the SCR for the DACPV is in the range of 88 suns whilst the SCR for the CPV + CCPC is in the range of 400 suns. In reference to Figure 4.6, the conversion efficiencies for 88 suns and 400 suns are 38.2% and 38.7%, respectively, with a difference of only 0.5% and hence, it is still acceptable for an academic study to understand the advantage of inserting secondary optics into the system. The primary focused image size formed by the NIDC was 22.6 × 22.6 cm, which is slightly larger than the size of the module that we set. The external region beyond the boundary of the 20 × 20 cm of the primary focused image was ignored in our electrical simulation as the SCR was less than half of the highest SCR in the central region.

Figure 4.7 shows a detailed algorithm for optimizing the electrical layout for both the DACPV and CPV + CCPC assembly modules. From the optical simulation results presented in the previous section, the values

of I_{SC} and V_{OC} of every CPV cell or CPV + CCPC assembly set were calculated according to the solar concentration ratio mapped to them. All the SCR values were extracted from the results of the optical simulation discussed in Chapter 3.

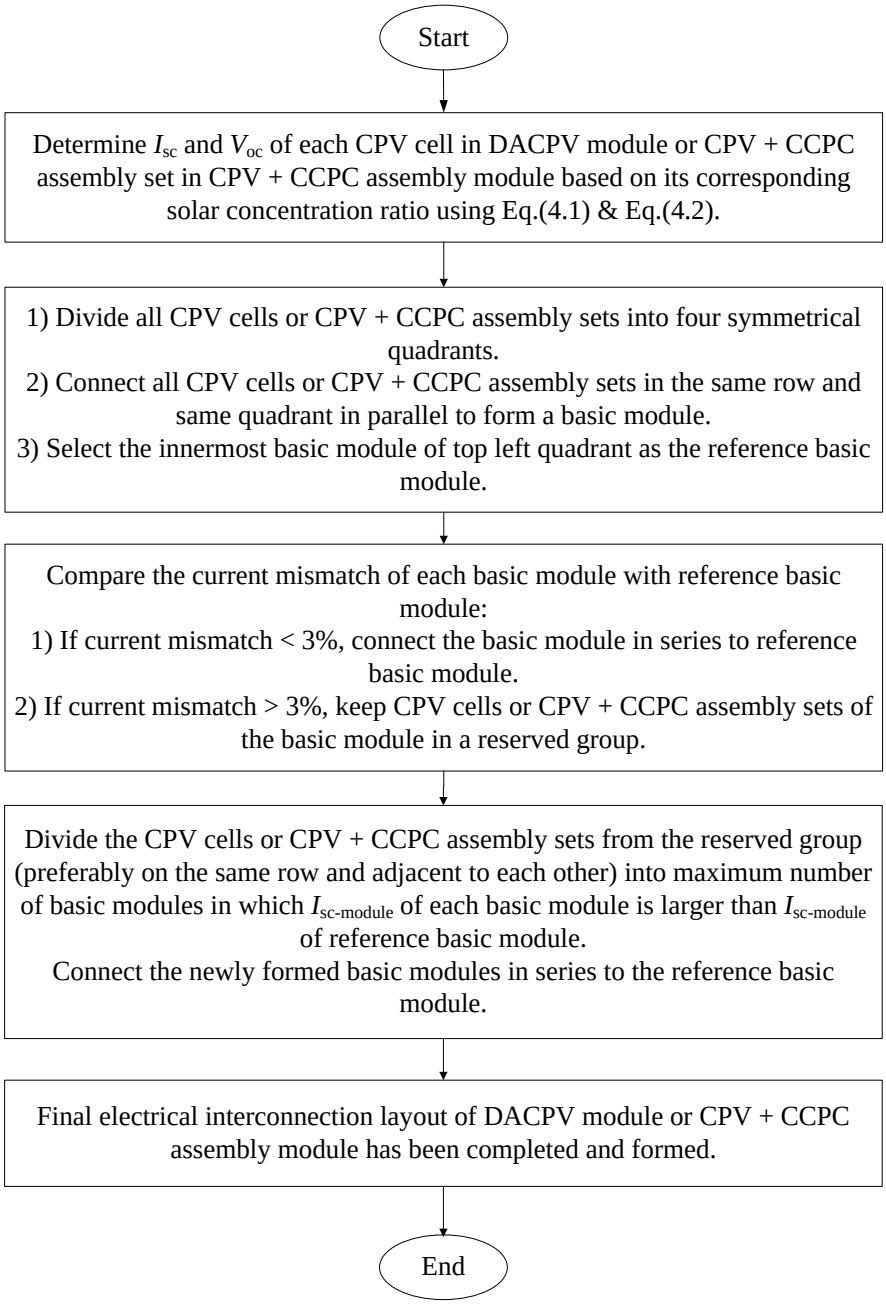

Figure 4.7: Flow chart to show an algorithm for optimizing the electrical layout for both the DACPV and CPV + CCPC assembly modules.

In the process of optimizing the electrical layout, the CPV cells or the CPV + CCPC assembly sets were divided into four symmetrical quadrants. All the CPV cells or CPV + CCPC assembly sets of the same row and quadrant were connected in parallel to form a basic module at first. In our study, there were 32 basic modules to form a complete DACPV module and 16 basic modules to form a complete CPV + CCPC assembly module. The innermost basic module of the top-left quadrant was selected as the reference basic module to form the complete DACPV or CPV + CCPC assembly modules. The short circuit current of the basic module, $I_{SC\text{-}module}$, is defined as the sum of the short circuit currents of all the CPV cells or all the CPV + CCPC assembly sets in the same basic module. Then, the $I_{SC\text{-}module}$ of all other basic modules were compared to the $I_{SC\text{-}module}$ of the reference basic module to determine the amount of current mismatch. If the amount of the current mismatch was less than 3%, the basic module will be connected in series with the reference basic module. Otherwise, the CPV cells or CPV + CCPC assembly sets of the basic module will be kept in a reserved group. After the first optimizing process was completed, the CPV cells or the CPV + CCPC assembly sets in the reserved group were divided into a maximum possible number of basic modules in which the $I_{SC\text{-}module}$ of each basic module must be larger than that of the reference basic module. The selection criterion for the CPV cells or the CPV + CCPC assembly sets in the reserved group to form a basic module is that those cells or assembly sets must be immediately adjacent to each other for a convenient and practical assembling process. Last but not least, all the basic modules from the reserved group were connected in series to the

reference basic module to form a complete DACPV or CPV + CCPC assembly modules as shown in Figures 4.8 and 4.9.

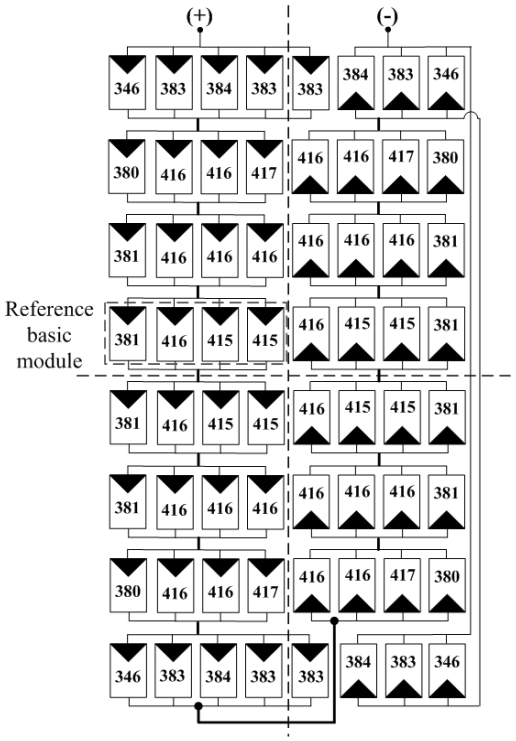

Figure 4.8: Optimized electrical layout design with an average solar concentration ratio assigned to each CPV cell for the CPV + CCPC assembly module under perfect sun-tracking conditions.

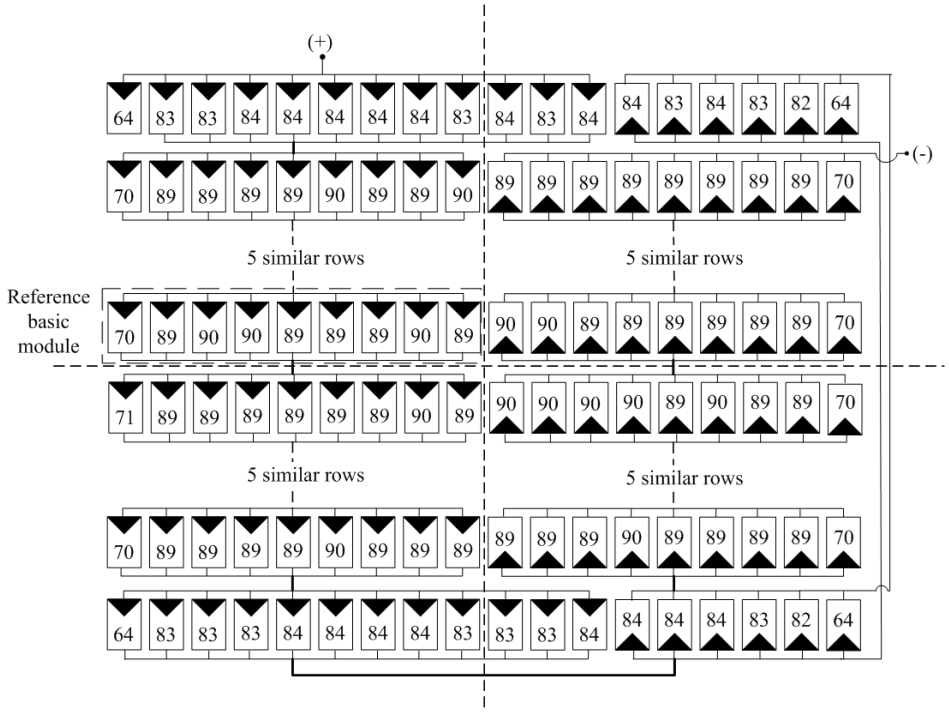

Figure 4.9: Optimized electrical layout design with an average solar concentration ratio assigned to each CPV cell for the DACPV module under perfect sun-tracking conditions.

Figure 4.8 and Figure 4.9 show the optimized electrical layout for the CPV + CCPC assembly and DACPV modules, respectively. In the design of the electrical interconnection layout for the DACPV module, two criteria must be fulfilled to include the practical consideration of the physical assembling process for the module. The first criterion is that the CPV cells from the same row of the array must be connected in parallel except those cells from the rows in both ends. The second criterion is that each basic module must contain at least one CPV cell located at the outermost ring of the array to allow each basic module to be connected to a by-pass diode to protect the cells from reverse bias voltage breakdown. The mechanical dimension of the CPV cell used in this study is 11 × 10 mm. Considering the requirements of preparing more space for both the die attachment of solar cells on the direct bond copper

(DBC) substrate and the interconnection between cells via the ribbon bonding process, gap between the adjacent CPV cells are 1 mm along the row direction and 2 mm along the column direction.

4.2.3 Results and Discussion

The optimized electrical layouts of the CPV + CCPC assembly module and the DACPV module used for the electrical performance study using Simulink are shown in Figures 4.8 and 4.9, respectively. Figure 4.10 illustrates the flow chart of the modelling process using Simulink to obtain the electrical performance results of the CPV module by plotting the *I*–*V* and *P*–*V* curves.

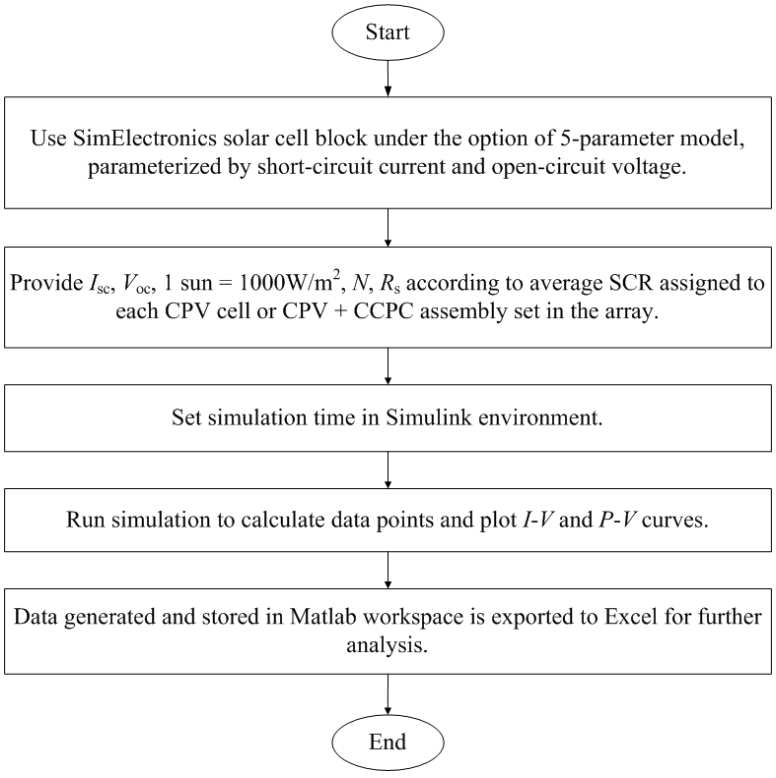

Figure 4.10: Flow chart to show the Simulink algorithm for the electrical performance modelling of the CPV module.

Figure 4.11 shows the simulated *I-V* and *P-V* curves of the CPV + CCPC assembly module without pointing errors and the maximum power output, P_{mp}, can be extracted from the *P-V* curve. Similarly, *I-V* and *P-V* curves for both the CPV + CCPC assembly module and the DACPV module were also plotted under different conditions, which includes pointing error 0, 0.1°, 0.2°, 0.3°, and 0.4° in the cases of *X*-axis, *Y*-axis, and *X* and *Y* axes concurrently. Maximum output power (kW) and system efficiency (%) were extracted from the aforementioned simulated results to plot against pointing error.

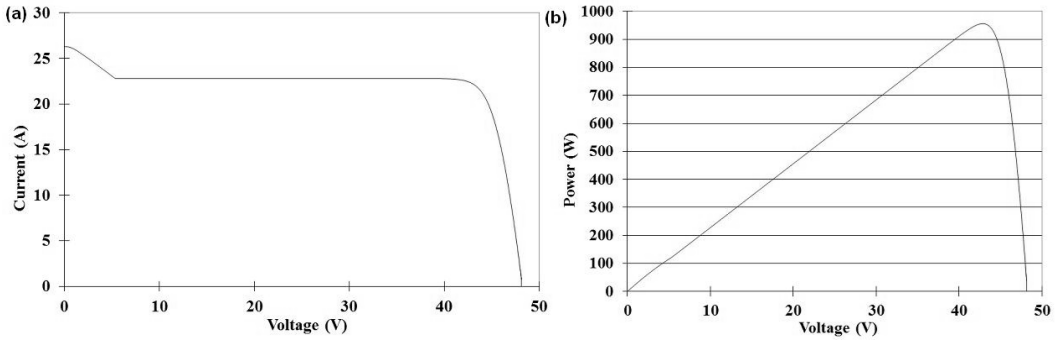

Figure 4.11: (a) *I–V* curve; (b) *P–V* curve of the CPV + CCPC assembly module without pointing errors.

System efficiency of the DACPV module and the CPV + CCPC assembly were calculated using the equation below.

$$\text{System efficiency} = \frac{\text{Maximum output power of DACPV module or CPV + CCPC assembly module}}{\text{Total projection area of NIDC} \times 1000\ \text{W m}^{-2}} \qquad (4.4)$$

Figure 4.12 depicts a comparison of maximum output power and system efficiency between the DACPV and the CPV + CCPC assembly modules for different pointing errors ranging from 0° to 0.4° by rotating the light source along the *X*-axis, *Y*-axis, and both the *X* and *Y* axes concurrently. Overall, the maximum output power of the CPV + CCPC assembly module was better than that of the DACPV module for all angles of pointing error about any axis, even though the absorption loss of the dielectric filled secondary concentrator as high as 12.5% was introduced.

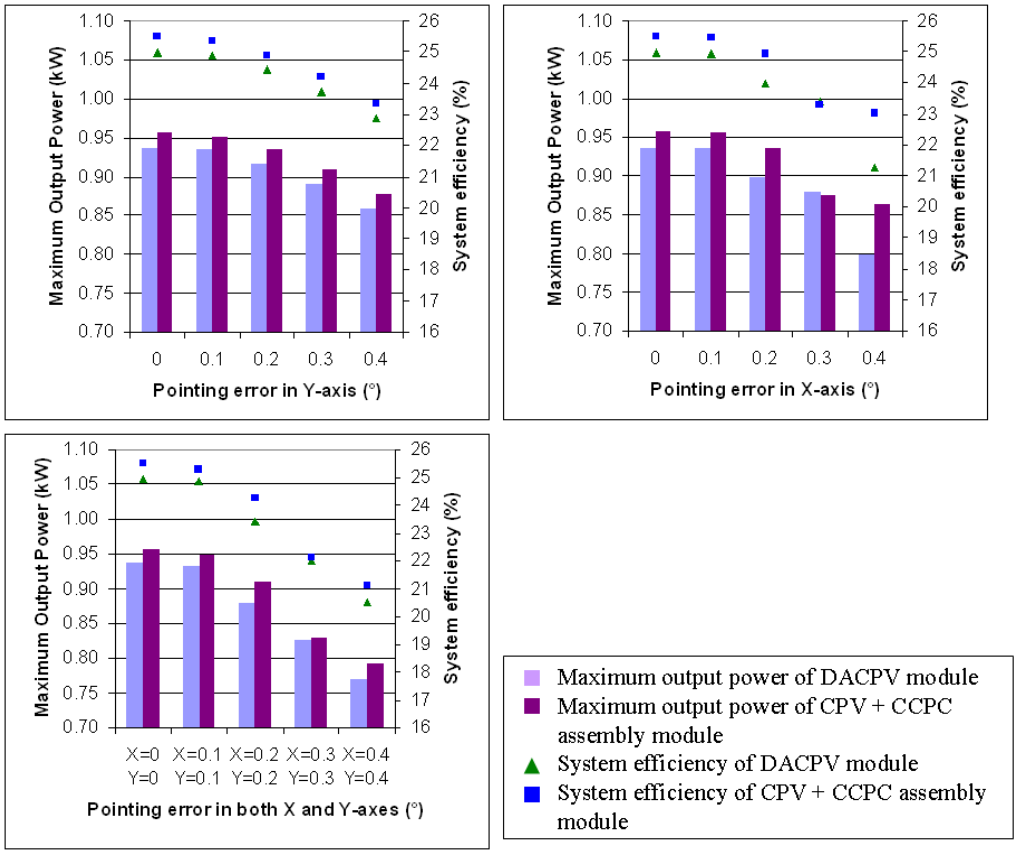

Figure 4.12: Comparison of the maximum output power (kW) and system efficiency (%) for the DACPV and CPV + CCPC modules with pointing errors ranging from 0° to 0.4° caused by rotating the light source about *Y*-axis (top left), *X*-axis (top right), and both *X* and *Y* axes (bottom).

By increasing the pointing error about *X*-axis, the primary focused image will gradually shift along the *Y*-direction and it will cause a drastic drop in the maximum output power when the pointing error has reached 0.3° because the outermost basic module is no longer illuminated and the current mismatch becomes more severe owing to the serial connection of all the basic modules in the *Y*-direction. According to Figure 4.12, there is indeed a drastic drop in the maximum power output of the CPV + CCPC assembly module when the pointing error about the *X*-axis increased from 0.2° to 0.3°. It is also revealed in the percentage of the current mismatch between the outermost basic module and the reference basic module in which the current mismatch was only 5% when the pointing error was 0.2°, but it increased steeply to 20% when the pointing error was 0.3°. For the DACPV module, a steep increase in the current mismatch between the outermost basic module and the reference basic module only happened when the pointing error about the X-axis increased from 0.3° to 0.4° in which the percentage of the current mismatch at pointing errors 0.3° and 0.4° are 23% and 55%, respectively. Consequently, the decrease in the maximum power output for the DACPV module at pointing error 0.3° about the X-axis was less than that of the CPV + CCPC assembly module. In this case, the maximum power output of the DACPV module is 5 W more than the CPV + CCPC assembly module.

The CPV + CCPC assembly module can reduce the usage of CPV cells by 77% in which a total of 282 CPV cells were employed in the DACPV module but only 64 CPV cells were utilized in the CPV + CCPC assembly module. The packing factor of the DACPV was only 0.7 and hence 30% of the

solar energy was concentrated on the non-active area of the receiver without being converted to electricity. The major causes of the low packing factor in the DACPV module are: the two stripes of bus bar with the width of 0.5 mm each on the surface of the CPV cell, the adjacent CPV cells cannot be arranged too close to each other to avoid short circuit current and a 1 mm of gap was introduced for the sake of the die attachment process of the CPV cells on the DBC, the limitation of the DBC substrate where the size of the alumina layer is always larger than the size of copper layer to create a 2 mm gap when the DBCs are attached onto a heat sink.

4.3 Experimental Study of Electrical Performance

4.3.1 Methodology

A secondary concentrator comprising of 8 × 8 arrays of CPV + CCPC assembly sets were installed at the receiver of the NIDC with a focal distance of 210 cm. Figure 4.13 shows the solar concentrator system setup in University Tunku Abdul Rahman, Setapak, Kuala Lumpur Campus (now shifted to Sungai Long, Selangor).

(a) (b)

Figure 4.13: (a) dense-array concentrator photovoltaic system with secondary optics; (b) secondary concentrator comprised of 8 × 8 arrays of CPV + CCPC assembly sets installed at the receiver of the NIDC with a focal length of 210 cm.

The university is yet to have an *I-V* tracer with a high power and current range which can measure power of more than 100 W and current of more than 10 A. Therefore, a procedure had been designed to predict the *I-V* and *P-V* curves of the system to estimate its maximum power and to evaluate the efficiency of the system.

The procedure started with acquiring the short circuit current, $I_{sc\text{-}module}$, and the open circuit voltage, $V_{oc\text{-}module}$, for each of the 15 basic modules and at the same time the short circuit current of the CPV module that responded to the DNI under one sun, $I_{sc}^{DNI\text{-}1\ sun}$, was also measured. The $I_{sc}^{DNI\text{-}1\ sun}$ was used

to calculate the solar concentration ratio of the basic module, SCR_{module}, of each basic module using the equation below:

$$SCR_{module} = \frac{I_{SC\text{-}module}}{I_{sc}^{DNI\text{-}1\ sun}} \tag{4.5}$$

The SCR_{module} obtained was used to calculate the $I_{sc\text{-}module}$ according to the DNI when measuring the output current and output voltage of the CCPC + CPV assembly module connected to load. This step is essential as the DNI when the $I_{sc\text{-}module}$ and $V_{oc\text{-}module}$ are measured and the DNI when measuring the output current and output voltage of the CCPC + CPV assembly module connected to load are different. This is feasible as the $I_{sc\text{-}module}$ responds linearly to the DNI and solar concentration ratio.

The values were then inserted into the Simulink modelling circuit to plot the *I-V* and *P-V* curves to get the maximum output power of the system. The *I-V* and *P-V* curves obtained were then verified by matching the curves with 10 different operating points, including the short circuit of the CCPC + CPV assembly module under the sun. The load was made up by 11 units of the same 22 Ohm, 100 W wirewound resistor with aluminium housing. When all resistors were connected in parallel, it produced effective resistance of 2 Ohm. The resistors were then disconnected one by one from the 11 resistors to produce different operating points which were 2.20 Ω, 2.44 Ω, 2.75 Ω, 3.14 Ω, 3.67 Ω, 4.40 Ω, 5.50 Ω, 7.33 Ω, and 11.00 Ω. For each operating point, output current and output voltage of the CCPC + CPV assembly module were measured together with the value of the DNI. The measurement was done

during the period of stable DNI to ensure that the operating condition of the CCPC + CPV assembly module is the same.

4.3.1.1 Current Measurement Circuit

A current measurement circuit was designed and fabricated to measure the short circuit current of the multiple basic module simultaneously. The circuit consisted of two boards: signal acquisition board and transducer board. The transducer board consisted of 13 units of Allegro ACS713 DC current sensors that sense current using the Hall Effect. Applied current that flows through the copper conduction path generates a magnetic field which is sensed by the integrated Hall IC and is converted into a proportional voltage. The range of sensing is 0−30 A and its output sensitivity is 185 mV/A. The output voltage of the current sensor is then acquired by the signal acquisition board which consist of a Microchip PIC18F4550 40-pin USB Microcontrollers with 13 channels of 10-bit Analog-to-Digital Converter (ADC) module. The microcontrollers communicate with the computer to carry out data acquisition from the transducer board. A command is sent from the computer to start the reading and conversion of the analogue voltage from the output of the current sensor. The data will be temporally stored in the memory of the microcontroller and finally sent to the computer and saved in an Excel sheet. Figure 4.14(a) shows the signal acquisition board that communicated with the computer through USB. Figure 4.14(b) shows the top view of the transducer

board and Figure 4.14(c) shows the bottom view of the transducer board with 13 units of Allegro ACS713 DC current sensor IC.

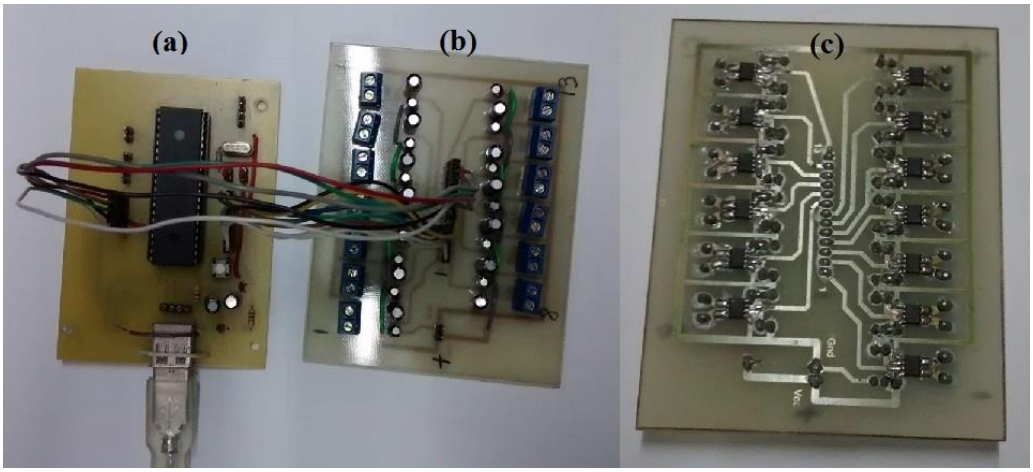

Figure 4.14: (a) signal acquisition board consisting of a Microchip PIC18F4550 40-pin USB Microcontrollers with 13 channels of 10-bit Analog-to-Digital Converter (ADC) module; (b) top view of the transducer board; (c) bottom view of the transducer board with 13 units of Allegro ACS713 DC current sensor IC.

4.3.2 Results and Discussion

The measurement results of the SCR_{module} and $V_{oc\text{-}module}$ of each basic modules are listed in Table 4.3. Since the solar concentration ratio is above 300 suns, therefore the open circuit voltage is the same for all basic modules as the voltage will not increase significantly as the solar concentration ratio increases.

Table 4.3: SCR_{module} and $V_{oc\text{-}module}$ of each basic module according to their location. The location of the basic module can be referred from Figure 4.8. The measurement was taken when the DNI was 826 W/m^2 and GSI was 985 W/m^2. Shaded cells indicate that the rows of the module were connected in parallel.

1408 suns, 3.92 V	1136 suns, 3.92 V
1106 suns, 3.92 V	1105 suns, 3.92 V
1102 suns, 3.92 V	1110 suns, 3.92 V
1125 suns, 3.92 V	1111 suns, 3.92 V
1112 suns, 3.92 V	1110 suns, 3.92 V
1115 suns, 3.92 V	1117 suns, 3.92 V
1106 suns, 3.92 V	1105 suns, 3.92 V
1130 suns, 3.92 V	

With the measurement results, the values were inserted to the Simulink modelling circuit to simulate the *I-V* curve as shown in Figure 4.15 and *P-V* curve as shown in Figure 4.16. Both figures show that the measured operating point match correctly with the *I-V* and *P-V* curves acquired from the numerical simulation in Simulink.

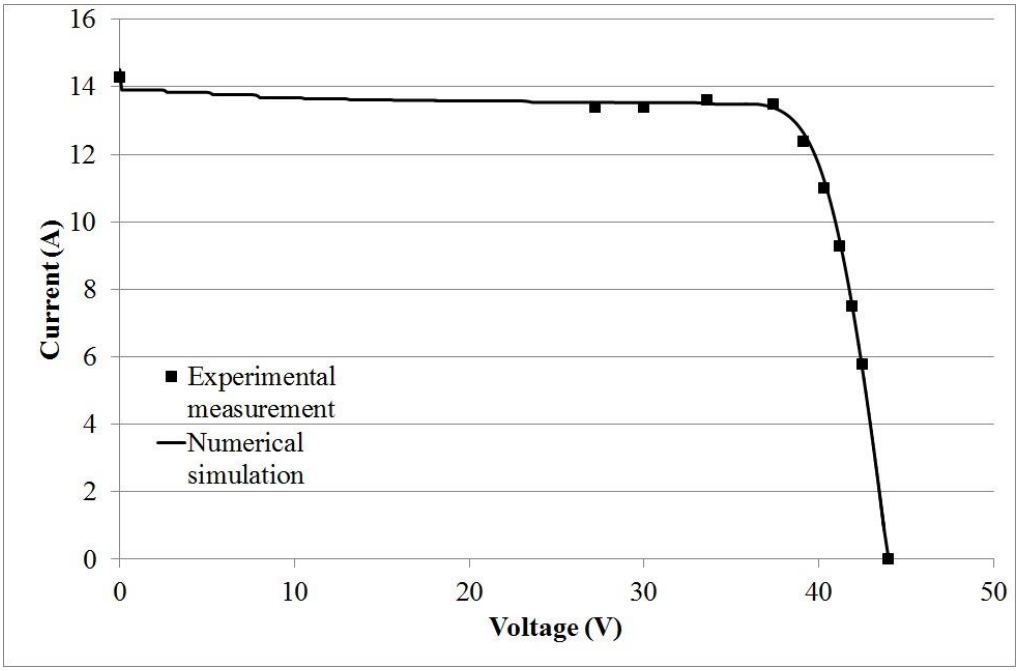

Figure 4.15: *I-V* curve from the numerical simulation matching the 11 operating points from the experimental measurement.

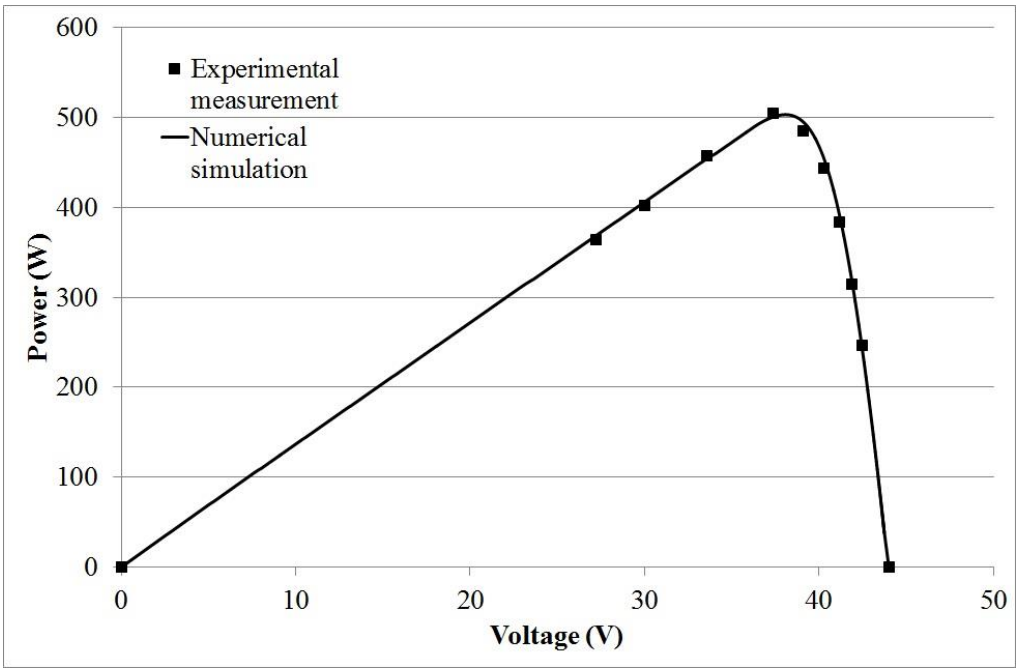

Figure 4.16: *P-V* curve matching the 11 operating points from the experimental measurement.

From Figure 4.16, the maximum power was 503 W when DNI was 789 W/m^2 and GSI was 973 W/m^2. The system efficiency of the dense-array concentrator photovoltaic system was calculated to be 17% using the equation below where the total projection area of the NIDC was 3.76 m^2.

$$\text{System efficiency} = \frac{\text{Maximum output power of CPV + CCPC assembly module}}{\text{Total projection area of NIDC} \times 1000 \text{ W m}^{-2}} \quad (4.6)$$

CHAPTER 5

CONCLUSION AND FUTURE WORK

5.1 Design and Optical Evaluation of Secondary Optics of the Dense-array Concentrator Photovoltaic System

The procedure of determining the suitable geometry and dimension of the secondary concentrator was discussed and the dielectric filled cross compound parabolic concentrator was found to be the most suitable candidate. The final design of the CCPC has an angular half acceptance angle, θ_i, of 37.77°; square entrance aperture size, $2a$, of 24 mm; square exit aperture size, $2a'$, of 9.8 mm; and the total length, L, of 37.78 mm. The optical characterization of the CCPC was carried out and the overall uniformity of the solar flux distribution pattern was found to be acceptable in which the value of the peak to average ratio (PAR) of the all exit apertures ranged from 2.08 to 2.35. The CCPC was also evaluated with an experiment under the sun to study its optical efficiency. It was found that the solar concentration ratio (SCR) of the CCPC ranged from 3.96−4.22. The SCR obtained from the experiment is lower than the theoretical ratio, which is 6 and this is due to the losses incurred during the air-glass transmission. The losses can be reduced by adding a single or multi-layer anti-reflective coating on the surface of the entrance and exit apertures of the CCPC.

5.2 Electrical Performance Optimization of the Dense-array Concentrator Photovoltaic System

Electrical analyses of the NIDC with an array of the CCPC lenses as the secondary concentrator for application in the DACPV system were presented. The modelling of the electrical performance has shown that overall, the maximum output power of the CPV + CCPC modules was better than that of the DACPV module, despite an absorption loss of 12.5% in the CCPC lens. In addition to that, the CPV + CCPC module can reduce the usage of the CPV cells by 77% as compared to the DACPV module. The use of the CCPC lenses as the secondary concentrator can provide more space to ease the electrical interconnection among the CPV cells and to allow the by-pass diode to be connected to each CPV cell as compared to the DACPV module, which has very limited electrical connection. Furthermore, any damage or faulty CPV cell assembly in the CPV + CCPC module is easily replaceable without affecting others unlike the DACPV module whereby any faulty cell can cause unrecovered damaged to the whole module. Experimental study of the electrical performance had found that the maximum power of the DACPV system was 503 W when the DNI was 789 W/m^2 and GSI was 973 W/m^2. The system efficiency of the dense-array concentrator photovoltaic system is calculated as 17%.

5.3 Concluding Remarks and Future Work

The aim of this research is to propose a method to improve the packing factor of the dense array CPV as the receiver of the NIDC. Dielectric filled CCPC was found to be the most suitable type of secondary concentrator to increase the packing factor by acting as a tunnel to guide the concentrated sunlight onto solar cells. The research also found that by adding a secondary concentrator to the receiver of the NIDC, the use of the solar cell had significantly reduced while still providing a similar output power.

However, the loss incurred by the additional secondary concentrator is still high as determined from our experimental findings. Future work can be done to find ways to reduce the loss caused and it will improve the overall efficiency of the dense-array CPV system.

REFERENCES

Andreev, V.M., Grilikhes, V.A., Khvostikov, V.P., Khvostikova, O.A., Rumyantsev, V.D., Sadchikov, N.A. et al., 2004. Concentrator PV modules and solar cells for TPV systems. *Solar Energy & Solar Cells*, 84, pp. 3–17.

Arqueros, F., Jiménez, A., Valverde, A., 2003. A novel procedure for the optical characterization of solar concentrators. *Solar Energy*, 75, pp. 135–142.

Baig, H., Heasman, K.C., Mallick, T.K., 2012. Non-uniform illumination in concentrating solar cells. *Renew. Sustain. Energy Rev*., 16 (8), pp. 5890–5909.

Baig, H., Sarmah, N., Heasman, K.C., Mallick, T.K., 2013. Numerical modelling and experimental validation of a low concentrating photovoltaic system. *Sol. Energy Mater. Sol. Cells*, 113, pp. 201–219.

Baig, H., Sellami, N., Chemisana, D., Rosell, J., Mallick, T.K., 2014. Performance analysis of a dielectric based 3D building integrated concentrating photovoltaic system. *Sol. Energy*, 103, pp. 525–540.

Benitez, P., Cvetkovi,c A., Winston, R., Reed, L., 2006. New high-concentration mirror-based Kohler integrating optical design for multijunction solar cells. *Optical Society of America 2006*; paper TuD3.

Boes, E.C., 1990. Photovoltaic concentrator technology development. *Photovoltaic Specialists Conference, 1990., Conference Record of the Twenty First IEEE*, Kissimmee, FL, pp. 944-951 vol.2.

Buchanan, M., 2015. Need Energy? Look to the Sun. http://www.bloombergview.com/articles/2015-09-28/only-solar-power-can-meet-human-needs-in-long-term.

Chemisana, D., Ibanez, M., Rosell, J.I., 2011. Characterization of a photovoltaic-thermal module for Fresnel linear concentrator. *Energy Conversion and Management*, 52, pp. 3234–3240.

Chen, Leon L.C., 2003. Stationary photovoltaic array module design for solar electric power generation systems. US Patent 6,653,551.

Chen, Leon L.C., 2004. Photovoltaic array module design for solar electric power generator systems. US Patent 6,717,045.

Chong K.K., Lau, S.L., Yew, T.K., Philip Tan, C.L., 2013. Design and development in optics of concentrator photovoltaic system. *Renew. Sustain. Energy Rev.*, 19, pp. 598–612.

Chong K.K., Wong, C.W., Siaw, F.L., Yew, T.K., 2010. Optical characterization of non-imaging planar concentrator for the application in concentrator photovoltaic system. *Journal of Solar Energy Engineering*, 132 , p. 011011 (9 pages).

Chong K.K., Wong, C.W., Yew, T.K., Tan, M.H., 2012. Solar concentrator assembly. Malaysian Patent; 2012: No. PI 2012002439 (pending) filed on 31st May 2012.

Chong, K.K., Siaw, F.L., Wong, C.W., Wong, G.S., 2009. Design and construction of non-imaging planar concentrator for concentrator photovoltaic system. *Renewable Energy*, 34 , pp. 1364–1370.

Chong, K.K., Wong, C.W., Siaw, F.L., Yew, T.K., Ng, S.S., Liang, M.S., Lim, Y.S., Lau, S.L., 2009a. Integration of an on-axis general sun-tracking formula in the algorithm of an open-loop sun-tracking system. *Sensors*, 9 (10), pp. 7849–7865.

Chong, K.K., Wong, C.W., Yew, T.K., Tan, M.H., 2013a. Solar Concentrator Assembly. US Patent, Application No.: 13/901,519 (pending) filed on 23rd May 2013.

Chong, K.K., Yew, T.K., Tan, M.H., 2014a. Dense-Array Concentrator Photovoltaic System Utilising Non-Imaging Dish Concentrator and Array of Crossed Compound Parabolic Concentrators. Malaysian Patent, No. PI 2014000210 (pending) filed on 23rd January 2014.

Chong, K.K., Yew, T.K., Tan, M.H., 2014b. Dense-Array Concentrator Photovoltaic System Utilising Non-Imaging Dish Concentrator and Array of Crossed Compound Parabolic Concentrators. US Patent, Application No.: 14/462,891 (pending) filed on 19th August 2014.

Chong, K.K., Yew, T.K., Tan, M.H., 2014c. Dense-Array Concentrator Photovoltaic System. China Patent. Application No./Patent No.: 201410529913.2 Date of Filing: October 9, 2014.

Clemens, D.D., 1997. Photovoltaic concentrator system. US Patent 5,660,644.

Coventry, J.S., 2005. Performance of a concentrating photovoltaic/thermal solar collector. *Solar Energy*, 78, pp. 211–222.

Davies, P.A., 1993. Design of single-surface spherical lenses as secondary concentrators for photovoltaic cells. *Pure and Applied Optics*, 2, pp. 315–324.

Eli, S., 2008. Solar energy utilization unit and solar energy utilization system. US Patent 7,435,898.

Feuermann, D., Gordon, J.M., 2001. High-concentration photovoltaic designs based on miniature parabolic dishes. *Solar Energy*, 70, pp. 423–430.

Fork, D.K., Horne, S.J., 2007. Laminated solar concentrating photovoltaic device. US Patent application publication; p. US2007/0256726.

Fork, D.K., Maeda, P.Y., 2006. Concentrating solar collector with solid optical element. US Patent application publication; p. US2006/0231133.

Fraunhofer ISE, 2009. World record: 41.1% efficiency reached for multi-junction solar cells at Fraunhofer ISE. *Fraunhofer-Institute for Solar Energies systems*.

Gordon, J.M., 1996. A 100-sun linear photovoltaic solar concentrator design from inexpensive commercial components. *Solar Energy*, 57, pp. 301–305.

Gordon, J.M., Concentractor optics. In: Luque, A., Andreev, V., editors., 2007. Concentrator photovoltaics. *New York:Springer*, p.113–132.

Green, M. A., Emery, K., Hishikawa, Y., Warta, W., & Dunlop, E. D., 2015. Solar cell efficiency tables (version 46). *Prog. Photovolt: Res. Appl. Progress in Photovoltaics: Research and Applications, 23*(7), 805-812.

Hein, M., Dimroth, F., Siefer, G., Belt, A.W., 2003. Characterisation of a 300× photovoltaic concentrator system with one-axis tracking. *Solar Energy Materials & Solar Cells*, 75, pp. 277–283.

Herrero, R., Victoria, M., Domínguez, C., Askins, S., Antón, I., Sala, G., 2012. Concentration photovoltaic optical system irradiance distribution measurements and its effect on multi-junction solar cells, *Prog. Photovoltaics Res. Appl*., 20, pp. 423–430.

Ittner III, W.B., 1980. An array of directable mirrors as a photovoltaic solar concentrator. *Solar Energy*, 24, pp. 221–234.

Jebens, R.W., 1989. Fresnel lens concentrator. US Patent 4,799,778.

Jorgensen, G., Wendelin, T., 1992. Uniform Flux Dish Concentrators for Photovoltaic Application. *National renewable energy laboratory*.

Joseph, O.M., 2000. Stretched Fresnel lens solar concentrator for space power. US Patent 6,075,200.

Kenji, A., Taizo, Y., Hisafumi, U., 2008. Concentrator solar photovoltaic power generating apparatus. US Patent application publication; p.US2008/0087323.

King, R., Bhusari, D., Larrabee, D., Liu, X., Rehder, E., Edmondson, K., Cotal, H., Jones, R., Ermer, J., Fetzer, C., Law, D., Karam, N., 2012. Solar cell generations over 40% efficiency. *Prog. Photovoltaics Res. Appl*., 20 (6), pp. 801–815.

Kreske, K., 2002. Optical design of a solar flux homogenizer for concentrator photovoltaics. *Applied Optics*, 41, pp. 2053–2058.

Law D.C., King, R.R., Yoon, H., Archer, M.J., Boca, A., Fetzer, C.M. et al., 2010. Future technology pathways of terrestrial III–V mulitjunction solar cells for concentrator photovoltaic systems. *Solar Energy Materials and Solar Cells*, 94, pp. 1314–1318.

Leutz, R., Suzuki, A., Akisawa, A., Kashiwagi, T., 1999. Design of a non-imaging Fresnel lens for solar concentractors. *Solar Energy*, 65 , pp. 379–387.

Lichy, J.I., 2006. Asymetric three dimensional, non-imaging, light concentrator. US Patent application publication; p. US2006/0072222.

Maeda, P.Y., 2007. Beam integration for concentrating solar collector. US Patent application publication; p. US2007/0251568.

Mallick, T.K., Eames, P.C., Hyde, T.J., Norton, B., 2004. The design and experimental characterisation of an asymmetric compound parabolic

photovoltaic concentrator for building facade integration in the UK. *Sol. Energy*, 77, pp. 319–327.

Mammo, E.D., Sellami, N., Mallick, T.K., 2012. Performance analysis of a reflective 3D crossed compound parabolic concentrating photovoltaic system for building façade integration. *Prog. Photovoltaics Res. Appl*., 21, pp. 1095–1103.

Micheli, L., Sarmah, N., Fernandez, E.F., Reddy, K.S., Mallick, T.K., 2014. Technical issues and challenges in the fabrication of a 144-Cell 500× concentrating photovoltaic receiver. In: *Photovoltaic Specialist Conference (PVSC), 2014 IEEE 40th*, pp. 2921, 2925.

Miller, D.C., Kurtz, S.R., 2011. Durability of Fresnel lenses: a review specific to concentrating photovoltaic application. *Solar Energy Materials and Solar Cells*, 95, pp. 2037–2068.

Neubauer, J.B., Gibson, G.M., 2007. Solar electric power generator. US Patent application publication; p. US2007/0181173.

Oommen, R. and Jayaraman, S., 2002. Development and performance analysis of compound parabolic solar concentrators with reduced gap losses—'V' groove reflector. *Renew. Energy*, 27, pp. 259–275.

Ota, Y. and Nishioka, K., 2012. Three-dimensional simulating of concentrator photovoltaic modules using ray trace and equivalent circuit simulators. *Solar Energy*, 86, pp. 476–481.

Pihl, E., 2009. Concentrating solar power. *Report prepared for the energy committee of the Royal Swedish Academy of Science, Chalmers University*.

Ries, H., Gordon, J.M., Lasken, M., 1997. High-flux photovoltaic solar concentrators with kaleidoscope-based optical designs. *Solar Energy*, 60, pp. 11–16.

Rumyantsev. V.D., Terrestial concentrator PV systems. Luque, A., Andreev, V., (Eds.), 2007.*Concentrator Photovoltaics*, Springer, New York, pp. 151–174.

Ryu, K., Rhee, J.G., Park, K.M., Kim, J. 2006. Concept and design of modular Fresnel lenses for concentration solar PV system. *Solar Energy*, 80, pp. 1580–1587.

Sala, G., Arboiro, J.C., Luque, A., Minano, J.C., Miňano, J.C., Dramsch, C. et. al, 1996. The EUCLIDES prototype: an efficient parabolic trough for PV concentration. *25th PVSC* May13–17 1996, Washington D.C.

Schott Desag, 2000. Specification: Physical and Chemical Properties B270 Superwite. Datasheet. Date Release: 02 May 2000. 04.00, 14 pages.

Scott, F., 2001. Double reflecting solar concentrator. US Patent application publication; p. US2001/0045212.

Segal, A., Epstein, M., Yogev, A., 2004. Hybrid concentrated photovoltaic and thermal power conversion at different spectral bands. *Solar Energy*, 76, pp. 591–601.

Sellami, N., Mallick, T.K., 2013. Optical efficiency study of PV crossed compound parabolic concentrator. *Appl. Energy*, 102, pp. 868–876.

Sellami, N., Mallick, T.K., McNeil, D.A., 2010. Optical performance modeling of a typical 3-D cross compound parabolic photovoltaic concentrator using ray trace technique. *Paper Presented at 6th Photovoltaic Science, Applications and Technology Conference, Southampton, United Kingdom*, 24/03/10–26/03/10.

Shifma, E., 2008. Solar energy utilization unit and solar energy utilization system. US Patent 7,435,898.

Siaw, F.L., Chong, K.K., 2013. A systematic method of interconnection optimization for dense-array concentrator photovoltaic system. *Sci. World J.* Article ID 275169, 11 pages.

Siaw, F.L., Chong, K.K., Wong, C.W., 2014. A comprehensive study of dense-array concentrator photovoltaic system using non-imaging planar concentrator. *Renew. Energy*, 62, pp. 542–555.

Singh, P., Liburdy, J.A., 1993. A solar concentrator design for uniform flux on a flat receiver. *Energy Conversion and Management*, 34, pp. 533–543.

Sonneveld, P.J., Swinkels, G.L.A.M., van Tuijl, B.A.J., Janssen, H.J.J., Campen, J., Bot, G.P.A., 2011. Performance of a concentrated photovoltaic energy system with static linear Fresnel lenses. *Sol. Energy*, 85, pp. 432–442.

Spectrolab Inc., 2010. CCA 100 C3MJ Concentrator Cell Assembly. Datasheet. <www.spectrolab.com>.

Straka, C.W., 2006. Reflecting photonic concentrator. US Patent application publication; p. US2006/0249143.

Tan, M.H., Chong, K.K., Wong, C.W., 2014. Optical characterization of nonimaging dish concentrator for the application of dense-array concentrator photovoltaic system. *Appl. Opt*., 53 (3), pp. 475–486.

Terao, A. and Krippendorf, R., 2007. Compact micro-concentrator for photovoltaiccells. U.S. Patent 7,297,865.

Terao, A., Mulligan, P., Daroczi, S.G., Pujol, O.C., Richard, P.J., Swanson, R.M., 2000. A mirror-less design for micro-concentrator modules. *Photovoltaic Specialists Conference, 2000. Conference Record of the Twenty-Eighth IEEE*, Anchorage, AK, pp. 1416-1419.

Tsadka, S., Segev, R., Migalovich, P., Levin, O., Tarazi, E., Whelan, R., 2009. Solar electricity generation system. US Patent application publication; p. US2009/0065045.

Vasylyev, S., 2005. Non-imaging reflective lens concentrator, *presented at international conf. on solar concentractors for generation of electricity or hydrogen*, May 1–5, 2005, Scottsdale, AZ.

Vasylyev, S.V., Vasylyev, V.P., 2003. Non-imaging system for radiant energy flux transformation. U.S. Patent 6,620,995.

Verlinden, P.J., Lewandowski, A., Bingham, C., Kinsey, G.S., Sherif, R.A., Lasich, J.B., 2006. Performance and reliability of multijunction III–V modules for concentrator dish and central receiver applications. *2006 IEEE 4th World Conference on Photovoltaic Energy Conference*, Waikoloa, HI, pp. 592-597.

Vivar, M., Herrero, R., Anton, I., Martinez-Moreno, F., Moreton, R., Sala, G., et al., 2010. Effect of soiling in CPV systems. *Solar Energy*, 84, pp. 1327–1335.

Vladimir, D., 2009. Solar concentrator and solar concentrator array. US Patent application publication; p. US2009/0056789.

Walter, L., John, L., 1994. Multiple reflector concentrator solar electric power system. US Patent 5,374,317.

Welford, W.T. and Winston, R., 1978. Optics of Nonimaging Concentrators. Light and Solar Energy. *Academic Press Incorporated*, New York, United States.

Whitfield, G.R., Bentley, R.W., Weatherby, C.K., Hunt, A.C., Mohring, H.D., Klotz, F.H., et al., 1999. The development and testing of small concentrating PV system. *Solar Energy*, 67, pp. 23–34.

Winston, R., Miñano, J.C., Benítez, P., 2005. Nonimaging Optics. *Elsevier Academic Press*, Burlington, Mass. pp. 50–57.

Winston, R., Ritschel, A., 2008. Concentrating photovoltaic system using a Fresnel lens and non-imaging secondary optics. US Patent application publication, p.US2008/0245401.

Zalman, S., 2008. Solar concentrator device for photovoltaic energy generation. US Patent application publication, p.US2008/0041441.

Zubi, G., Bernal-Agustin, J.L., Fracastoro, G.V., 2009. High concentration photovoltaic systems applying III–V cells. *Renew. Sustain. Energy Rev.*, 13, pp. 2645–2652.

APPENDIX A

Renewable and Sustainable Energy Reviews 19 (2013) 598–612

Contents lists available at SciVerse ScienceDirect

Renewable and Sustainable Energy Reviews

journal homepage: www.elsevier.com/locate/rser

Design and development in optics of concentrator photovoltaic system

Kok-Keong Chong [a,*], Sing-Liong Lau [a], Tiong-Keat Yew [a], Philip Chee-Lin Tan [b]

[a] Faculty of Engineering and Science, Universiti Tunku Abdul Rahman, Off Jalan Genting Kelang, Setapak, 53300 Kuala Lumpur, Malaysia
[b] Board of commissioners, Energy Commission Malaysia, No. 12, Jalan Tun Hussein, Presint 2, 62100, Putrajaya, Malaysia

ARTICLE INFO

Article history:
Received 4 June 2011
Received in revised form
31 October 2012
Accepted 1 November 2012

Keywords:
Optical design
Solar concentrator
Solar energy
Concentrator photovoltaic
High solar concentration

ABSTRACT

Due to the dramatic advances in commercial multi-junction solar cells with 40% conversion efficiency, solar concentrator capable of delivering flux levels of hundreds to thousands of suns at high collective efficiency is the key factor for the success of novel Concentrator Photovoltaic (CPV) system. This paper would review and survey the progress in the last 30 years including the optical design and development in the optics of solar concentrators for the CPV system. The detailed architectural design and optical principle of solar concentrators are presented to show various innovative and creative ideas of harnessing solar energy.

Contents

1. Introduction

In the past few years, we have witnessed a paradigm shift in photovoltaic power generation [1]. It stems from the confluence of dramatic advances in commercial high-efficiency multi-junction solar cells capable of 40% conversion efficiency, and optical design in solar concentrators capable of delivering flux levels of hundreds to thousands of suns at high collective efficiency. In the high concentration systems, even with cells that are two orders of magnitude more expensive on an area basis than conventional photovoltaic (PV), the cost contributed by the cell becomes attractively low. The burden then shift to the optical design to provide a cost-effective and practical system. The focus is on the new classes of high-flux, ultra-compact, practical optics, traced from initial concepts through commercial realization. Concentrator Photovoltaic (CPV) system can be built with high photonic-to-electric efficiencies [2]. The most advanced solar cell actually performs better in focused sunlight than with ordinary sunlight. State-of-the-art triple-junction cells have been developed with 40–41% efficiency at 100–900 times concentration, the world record presently being 41.1% at 454 times concentration [3]. Law et al. from Boeing-Spectrolab Inc (2010) have discussed on future terrestrial concentrator cells that will likely feature four or more junctions. The better division of the solar spectrum and the lower current densities in these new multi-junction cells reduce the resistive power loss and provide a significant advantage in

* Corresponding author. Tel.: +603 41079802; fax: +603 41079803.
E-mail addresses: chongkk@utar.edu.my, kokkeong_c@yahoo.com (K.-K. Chong).

1364-0321/$ - see front matter © 2012 Elsevier Ltd. All rights reserved.
http://dx.doi.org/10.1016/j.rser.2012.11.005

achieving higher efficiencies of 45–50% [4]. Interest in CPV grew substantially after promoting in practice that higher-efficiency multi-cascade solar cells demonstrated a perspective to achieve photovoltaic conversion efficiencies as high as 40–50% [5].

Boes summarizes the progress that has been made in 1990 in the area of photovoltaic concentrator technology development [6]. A brief description of the status of two photovoltaic concentrator power systems is given: the 300 kW ENTECH-3M-Austin system and the single-pedestal Alpha Solarco system. The paper emphasizes those module development activities that have resulted in significantly higher conversion efficiencies or new module design concepts. Whitfield et al. compared some 90 possible small PV concentrator designs that might be suitable for use at remote sites [7]. They had apertures of about 2 m^2, used BP solar LBG cells, and employed small aperture module to reduce heat sinking and construction costs. The designs included fixed V-troughs and Compound Parabolic Concentrators (CPCs), single axis tracked cylindrical lens and mirror systems, and two axis tracked spherical-symmetry system. Performance and volume production costs were estimated. Several designs of small concentrator systems can be significantly cheaper than conventional planar arrays, reducing cost/watt and cost/kWh by a factor of 2 or 3. To achieve such reduced costs, the concentrators should be designed to use minimum amount of material, and be manufactured in such a way, and in sufficient quantity, as to keep down the manufacturing cost. In addition, CPV systems have a number of unique attributes that could shortcut the development process of producing hydrogen [8]. The development of efficient, renewable methods of producing hydrogen is essential for the success of the hydrogen economy. The development of a hydrogen economy can have many benefits for the environment. It can play a role in reducing global warming and air quality problems in and around major cities.

Durability and reliability of CPV system are the major concerns due to the effects of ageing and soiling especially on the optical material that cause significant reduction in electrical output. Miller and Kurtz have carried out literature review on the durability of Fresnel lenses specific to the concentrating photovoltaic application [9]. The review includes the topic of optical durability, discoloration, soiling and accumulation of particulate matter etc. Vivar et al. has studied the effect of soiling in CPV systems [10]. The effect of soiling in flat PV modules has been already studied causing a reduction of the electrical output of 4% on average. For CPV, as far as soiling produces light scattering at the optical collector surface, the scattered rays should be definitely lost because they cannot be focused onto the receiver again. Some experiments have been conducted by Vivar et al. at the IES-UPM and CSES-ANU sites, consisting in linear reflective concentration systems, a point focus refractive concentrator and a flat module. In general, CPV systems are more sensitive to soiling than flat panels, accumulating losses in short-circuit current of about 14% on average. Appropriate design of optical system to minimize dust particle trapping and cleaning implemented at an economically optimized frequency are important to improve the electrical production.

2. Types of solar concentrator and optical design

Solar concentrator system employs either lenses or reflectors or a combination of both types associated with tracking system to concentrate a large area of sunlight onto a small beam. Some concentrator system also employs secondary concentrator or even tertiary concentrator to enhance the solar concentration ratio as well as to homogenize the distribution of solar flux on the receiver. CPV panel is more sensitive than a heat receiver to the distribution of focused sunlight and therefore it requires a proper optical design of concentrator that is capable of spreading the focused sunlight evenly over the receiver surface. Although there are wide ranges of concentrating technologies exist in worldwide, all these optical technologies can be fundamentally categorized into five major groups based on their primary focusing method: linear focusing lens, two-dimensional focusing lens, linear focusing reflector, two dimensional focusing reflector and central receiver system. The architectural designs and optical principles for various solar concentrators specially tailored for the CPV systems are depicted and presented in the following section.

2.1. Linear focusing lens

Leutz et al. designed an optimum convex shaped non-imaging Fresnel lens according to the edge ray principle [11]. If a secondary concentrator and a diffuser are provided, non-tracking operation is possible and the irradiance should be well distributed over the photovoltaic panel. The schematic diagram is given in Fig. 1 where the flux concentration in such a system is around 15–20 times. The proposed truncated non-imaging Fresnel lens offers the advantage of requiring only passive tracking and seasonal tilt. Chemisana et al. proposed a photovoltaic-thermal module for Fresnel linear concentrator by combining a domed linear Fresnel lens as primary concentrator (5 ×), a compound parabolic reflector as secondary concentrator (2 ×) and a photovoltaic-thermal module [12].

O'Neill patented a high efficiency, extremely light-weight, and robust stretched Fresnel lens solar concentrator coupled to photovoltaic concentrator array for generating power in space [13]. The stretched Fresnel lens solar concentrator consists of a flexible Fresnel lens attached to end supports to maintain its proper position and shape as shown in Fig. 2.

2.2. Two-dimensional focusing lens

Jebens and Skillman patented Fresnel lens concentrator that is formed by a specially designed Fresnel lens and a solar cell located on the axis of the lens at its focal plane as depicted in Fig. 3 [14]. The lens is designed so that its central facets project the light from the sun towards the outer periphery of the cell and facets progressively toward the periphery of the lens project light progressively toward the center of the cell to obtain a uniform distribution of light on the cell. Adjacent groups of facets of the lens project the light alternatively in front and beyond the cell to maintain a constant light intensity for a certain depth of focus of the lens.

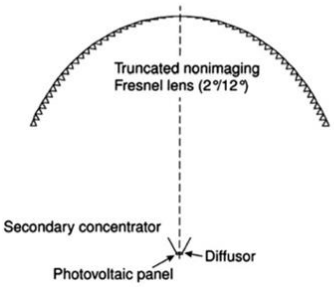

Fig. 1. Schematic of truncated non-imaging Fresnel lens with secondary concentrator for application in photovoltaic systems.

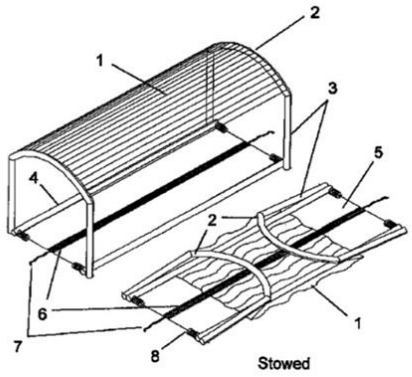

Fig. 2. A perspective view of a deployable embodiment of stretched Fresnel lens solar concentrator for space power.

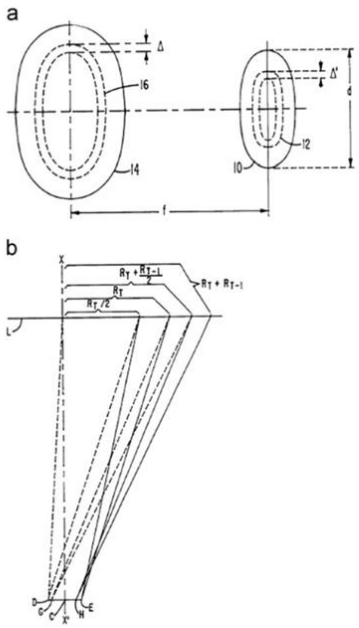

Fig. 3. (a) Schematic view of Fresnel lens with an intermediate facet and a circular target with an intermediate ring, (b) Diagrammatic view of the direction of some light beams going from the lens to the target.

Davies studied the design of single-surface spherical lens as secondary concentrator in the two-stage concentrator with Fresnel lens as primary stage [15]. Fig. 4 shows a cross section view of a two-stage, axially-symmetric concentrator with Fresnel lens as primary whose first surface is flat and single-surface spherical

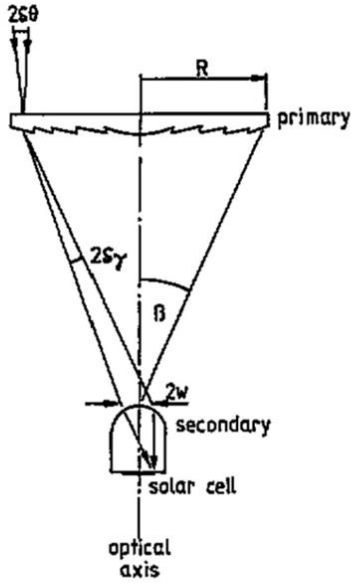

Fig. 4. Sketch showing a cross section through a two-stage, axially-symmetric concentrator with Fresnel lens as primary and single-surface spherical lens as secondary.

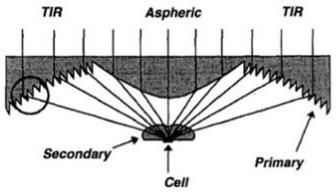

Fig. 5. TIR-R concentrator with detail of TIR lens.

lens as secondary in the form of a domed pillar glued to the cell. In this design, Fresnel lens with maximum concentration of about 100 times at *f*/1.37 has been improved in the two-stage concentrator system to maximum concentration of 530 times at optimal *f*-number of *f*/2.84.

Terao et al. proposed a non-imaging optics design for a flat-plate CPV system [16]. In Fig. 5, the design consists of a conventional primary/secondary lens combination, but uses aspheric and total internal reflection lens components in the primary to reduce the focal length and hence the thickness of the whole module. Ray-tracing simulations indicates that an acceptance angle in excess of $\pm 2.6^{\circ}$ can be achieved, which makes the design suitable for light-weight, low-cost tracking systems.

Chen patented a stationary solar photovoltaic array module design, which constitutes three or four steps of optical concentrations of photovoltaic power generation system [17,18]. The concentrator can have either one layer (2004) or two layers (2003) of Fresnel lens concentrating sunrays. A compound

parabolic concentrator (CPC) is mounted under a first or second Fresnel lenses to further concentrate the intensity of sunlight with twenty times more. Then, the concentrated sunlight is homogenized as it passes through a third or fourth optical concentrator glass lens with anti-reflection coating on the top surface just before incident on the multi-junction solar cell. Fig. 6 shows the combination of multi-stage Fresnel lenses and optical reflectors which can concentrate solar intensity 300 to 1000 times within a six-inch distance.

Andreev et al. proposed a modified structure of the high concentration all glass PV modules for a solar-powered Thermo-Photovoltaic (TPV) system with III–V solar cells [19]. Main structural features of the concentrator modules under development are the following: small aperture area and short focal length Fresnel lenses as the primary concentrators; lens panels with a composite (glass–silicone) structure; "all-glass" module design, which implies that all the main parts of a module cabinet are made of conventional silicate glass. In the all glass module design, the secondary lenses arranged in an intermediate composite (glass–silicone) panel is inserted between a panel of the primary composite Fresnel lens concentrators and a panel of the solar cells as shown in Fig. 7.

Ryu et al. proposed a new configuration of solar concentration optics utilizing modularly faceted Fresnel lenses to achieve a uniform intensity on the receiver plane with moderate concentration ratio [20]. Fig. 8 reveals that the uniform illumination is obtained by the superposition of flux distribution resulted from modularly faceted Fresnel lenses. The flux distribution at the cell plane are estimated to be uniform within ~20% with transmission efficiency larger than 65% for 3×3, 5×5 and 7×7 arrays of Fresnel lenses. With $f/1.2$, the intensity levels of various concentration ratios are 7 suns for the 3×3 array, 19 suns for the 5×5 array, 31 suns for the 7×7 array, 47 suns for the 9×9 array, and 60 suns for the 11×11 array, respectively.

Winston and Ritschel patented an optical device that consists of a primary Fresnel lens and secondary non-imaging optics to provide high solar flux onto a multi-junction solar cell for producing efficient

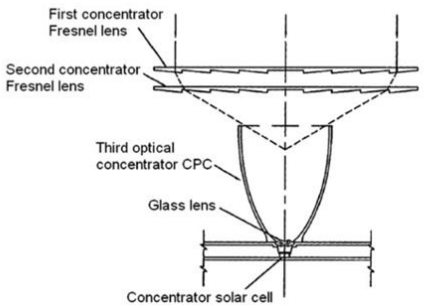

Fig. 6. Stationary photovoltaic array module design with sequence from top to bottom: First concentrator Fresnel lens for focusing sunrays five to ten times, second concentrator Fresnel lens, third optical concentrator CPC, fourth optical concentrator: a specially shaped glass lens, and concentrator solar cell with a 45% conversion efficiency.

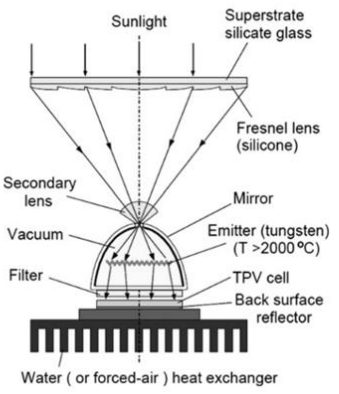

Fig. 7. Optical design concept of a modified structure of the high concentration all glass PV modules for solar-powered TPV system with high temperature ($T>2000$ °C) vacuum bulb emitter.

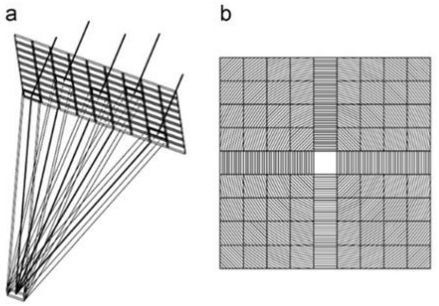

Fig. 8. Optical design concept of modular Fresnel lenses for solar flux concentration: (a) 3-D of concentration optics (b) facet directions of modularly faceted Fresnel lenses.

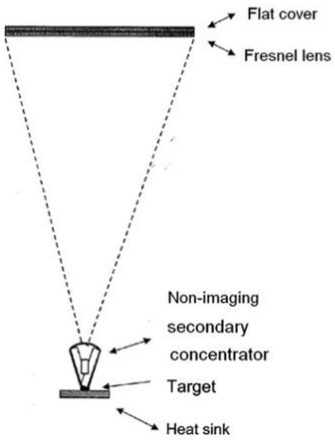

Fig. 9. Concentrating photovoltaic system using Fresnel lens and non-imaging secondary optics.

electrical output as illustrated in Fig. 9 [21]. The primary Fresnel lens with an *f*-number of greater than 1 (e.g., between 1 and 4 or greater) is configured to focus light from a distant source onto the entry aperture of the secondary concentrator. The solar cell is located at the exit aperture of the secondary concentrator. The optical device has an optical acceptance angle of about $\pm 5^{\circ}$ or greater with an optical efficiency of about 80–85%. It can be configured with a 125 mm × 125 mm entry aperture and a depth of about 230 mm to provide a geometric concentration of about 500× for 5.5 mm × 5.5 mm multi-junction cell and 150× for 10 mm × 10 mm Si cell.

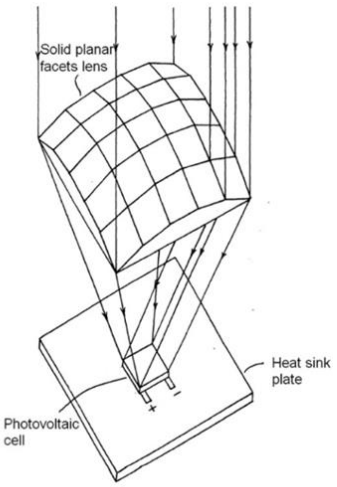

Fig. 10. Perspective view showing a solid lens with 25 planar facets on the top side facing the sun and a planar surface on the bottom side facing the photovoltaic cell mounted on a heat sink plate.

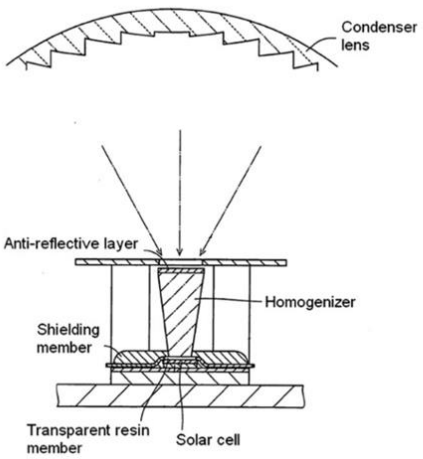

Fig. 11. A generation module of a concentrator solar photovoltaic apparatus which comprises of a plurality of generation modules disposed within in an enlarged cross sectional view.

Schwartzman designed a solar energy concentrator lens formed by a prism array [22]. Fig. 10 shows how each prism of 25 planar facets is designed to deflect the incident solar rays and fully illuminate a rectangular photovoltaic cell with uniform intensity. The combination of multiple prisms uniformly illuminating a common target area yields concentrated uniform illumination across the target area.

Araki et al. patented a concentrator solar photovoltaic apparatus including a primary optics for concentrating sunlight, a columnar optical member, and a transparent resin member and the solar cell (refer to Fig. 11) [23]. A columnar optical member or homogenizer acting as secondary optics is used for guiding the sunlight, which is concentrated by the primary optics to the solar cell.

Ota and Nishioka proposed a 3-D simulation for concentrator photovoltaic module using triple-junction solar cell by connecting ray-trace simulation for an optics model and 3-D equivalent circuit simulation for a triple junction solar cell. It has been used to study a typical flat Fresnel lens (110 mm × 110 mm in entry aperture area and focal length 150 mm) and homogenizer (9 mm × 9 mm in entry aperture area, 4.5 mm × 4.5 mm in exit aperture area, and 35 mm in height) was set in the vicinity of the focal length of the Fresnel lens to have the effective geometrical concentration ratio of 597 times [24].

2.3. Linear focusing reflector

Singh and Liburdy presented a reflective concentrator capable of concentrating a collimated beam of light onto a flat receiver to

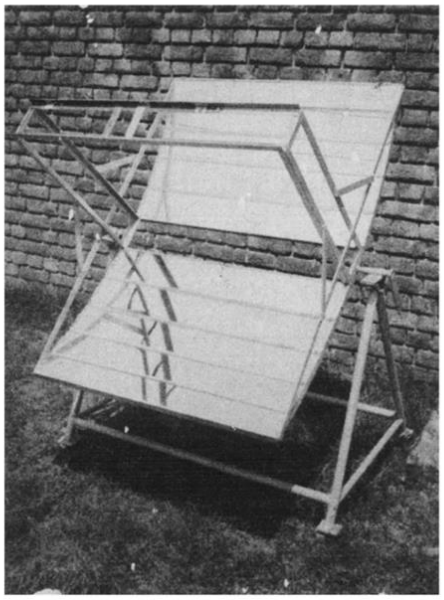

Fig. 12. Picture of the experimental solar concentrator consists of a series of flat panels of different sizes.

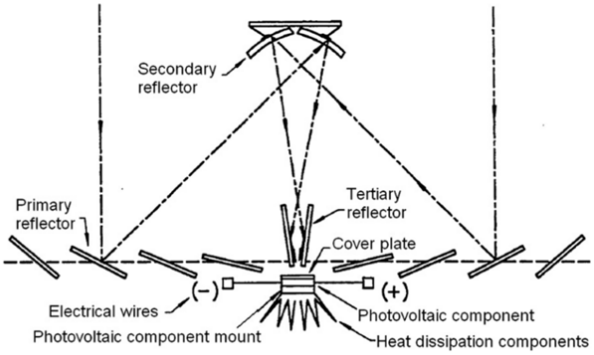

Fig. 13. A cross sectional schematic of multiple-reflector-concentrator module where the secondary reflector being placed at the focal line of primary reflector.

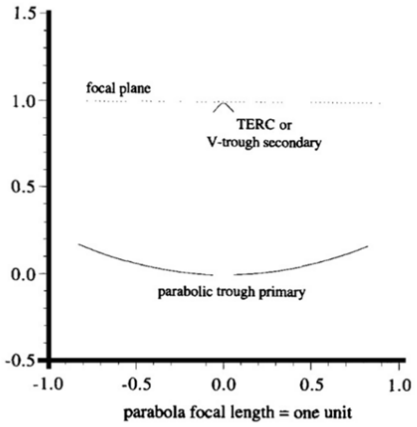

Fig. 14. Scale drawing of parabolic trough primary, TERC (or V-trough) secondary, and photovoltaic absorber. Parabola focal plane is also shown (above absorber).

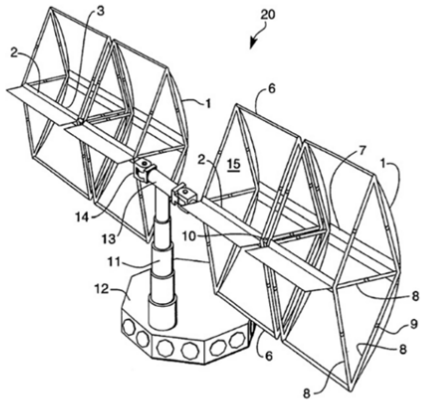

Fig. 15. Photovoltaic concentrator (20) with foldable struts (8) extended forming triangular frame section (15): End arms (6) are connected at the top and bottom of the triangular frame section (15) and are used to attach a reflective concentrator (1) to the structure. The reflective concentrator is an inflatable concentrator made of silvered Kapton film.

obtain a uniform flux distribution with the maximum theoretical concentration ratio of 22.79[25]. The main advantage of this design is that the reflector consists of a series of flat panels of different sizes enabling the use of commercially available plane mirror as shown in Fig. 12. Measurement of the flux on its receiver indicates a quite uniform flux distribution in about 80% of the receiver area.

Lamb and Lawrence patented multiple-reflector concentrator to concentrate sunlight onto a panel of photovoltaic cell in a solar electric power system as shown in Fig. 13 [26]. The power system, consisting of multiple reflectors, mounted PV cells and a heat dissipation component, is mounted on a tracker that keeps the system directed to the sun. The system can operate on either a single or dual axis tracker with active or passive tracking.

Gordon presented the optical design for a high-efficiency linear photovoltaic solar concentrator assembled from readily-available inexpensive components as shown in Fig. 14 [27]. Accounting for all geometric and material-related optical losses, he found that it should easily produce flux levels of 50–100 suns with homogeneous irradiance of the absorber. The specification of the system components are as follow: parabolic focal length is 1.49 m and the parabola entrance aperture width is 2.47 m; the solar cell width is 0.033 m; the secondary V-trough has a depth of 0.072 m and an entrance width of 0.176 m.

For the project EUCLIDES (EUropean Concentration Light Intensity Development of Energy Sources), Sala et al. developed a one axis horizontal tracking, North/South oriented parabolic trough reflector for CPV system [28]. The geometric concentration ratio is 32 and the overall efficiencies of 14 series connected receiving modules are 15% at the temperature of 25 °C. Such modules consist of 12 BP solar SATURN concentrator cells fully encapsulated.

Clemens disclosed a light weight photovoltaic concentrator having a foldable, easily deployed structure for concentrating sunrays on solar cells for generating electricity [29]. The concentrator can be inflated to a shape of parabolic trough for focusing sunlight onto the solar cell at the ratio of 20 suns. The inflatable

concentrator is inflated by gas stored in the central arm which supports one end of the concentrator. The concentrator is inflated until the epicenters of the front and rear surfaces reach a specified distance and the concentrator is thereafter maintained at this position as shown in Fig. 15.

Frazier patented a double reflecting solar concentrator utilizing a primary reflective surface (parabolic mirror) which reflects incident light toward a secondary surface (directrix plane) [30]. The incident light reflects off the secondary surface away from the primary surface's natural focus point toward a secondary focal point positioned on or substantially near the surface of the primary reflective surface. The invention provides an exemplary double reflecting style of parabolic trough structure that is substantially more rigid than a simple parabolic surface where the photovoltaic cell can be placed along focal line as shown in Fig. 16.

Hein et al. achieved a high geometrical concentration ratio of 300 suns using a parabolic trough mirror and a three-dimensional second stage consisting of compound parabolic concentrators (CPC) [31]. In the design, the geometrical concentration of the first stage concentrator and the CPC are 39.7 and 7.7 times, respectively leading to the concentration ratio of more than 300 times. Fig. 17 shows the prototype of this concentrator system built at Fraunhofer Institute for Solar Energy (ISE).

Coventry published the performance of a prototype parabolic trough photovoltaic/thermal collector with a geometric concentration of 37 suns constructed at the Australian National University [32]. Measured results under typical operating conditions show thermal efficiency of around 51% and electrical efficiency around of 11% to result a combined efficiency of 69%. The measured illumination flux profile along the length shows significant variation with the peak flux intensities shown to be around 100 suns, despite the mirror shape error less than 1 mm for most of the mirror area. The impacts of the illumination non-uniformities due to shape error, receiver support post shading and gaps between the mirrors are shown to have a significant effect on the overall electrical performance.

Straka patented a non-imaging reflective trough that receives spectral energy and linearly reflects that energy onto a smaller area on one side of the device with geometric concentration of seven suns (see Fig. 18) [33]. The linearly reflecting trough

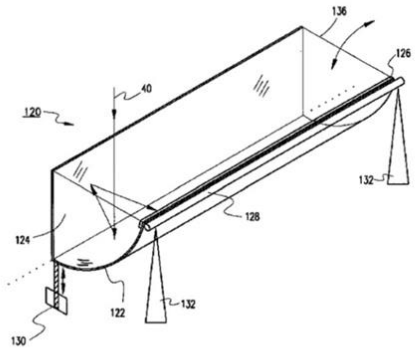

Fig. 16. A three-dimensional view of double reflecting solar concentrator (1 2 0) mounted on a support structure (1 3 2) and connected to hydraulic driving system (1 3 0): Incident light (40) reflects off the primary reflective surface (1 2 2) toward the secondary reflective surface (1 2 4) and then toward a solar collector or photovoltaic (1 2 6) located at the focal line.

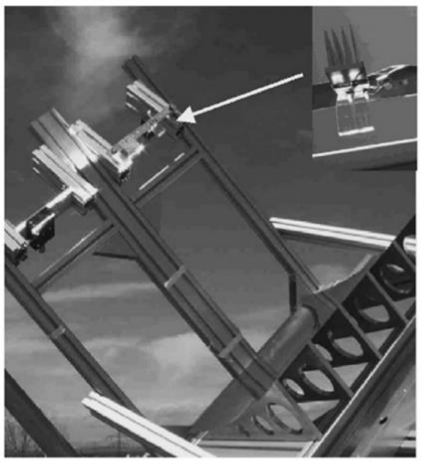

Fig. 17. Picture of a prototype of the concentrator module on a tracker. Two GaAs cells with CPCs have been mounted on heat sinks and installed in the focal line.

concentrator has the geometry of a single slope-relief interval in a Fresnel lens, and in preferred embodiment comprises an array of plane facet reflectors connected continuously to form the base of the trough, a non-imaging focal point where a photovoltaic receiver is located, and a relief surface to connect the mirrors array to the receiver location. The concentrator comprises of array of plane mirrors oriented according to the negative profile of two interleaved linear Fresnel lens, where the slope of one is the relief of the other.

2.4. Two-dimensional focusing reflector

Jorgensen and Wendelin designed a multi-step-molded-dish concentrator capable of producing a uniform flux profile on a flat target plane [34]. Concentration levels of 100–200 suns, which are uniform over an area of several square inches, can be directly achieved for collection apertures of a reasonable size of approximately 1.5 m in diameter. For the arrangement as shown in Fig. 19, five concentric annular regions were arranged so that each annulus represents one fifth of the total aperture area. Each step section was offset along the optical axis and specified to be a spherical element whose curvature $1/2f$.

Ries et al. proposed and analyzed sample designs for a high flux photovoltaic concentrator comprised of a large-aperture paraboloidal-dish primary concentrator, and a second-stage kaleidoscope flux homogenizer [35]. Referring to Fig. 20, the design satisfied highly uniform irradiance on the solar cell absorber, high collective efficiency and not exceeding the prescribed target flux of 500 suns. The solution is to move the absorber out of the nominal focal plane, away from the dish, to a plane where the average concentration is 500 suns.

Feuermann and Gordon proposed a high concentration photovoltaic design based on miniature paraboloidal dish and kaleidoscope to achieve 1000 suns [36]. The collection unit is a miniature parabolic dish with a diameter of the order of 10 cm that concentrates sunlight into a short glass rod called kaleidoscope. The flux distribution of the transported light is homogenized in a miniature glass kaleidoscope that is optically coupled to a small,

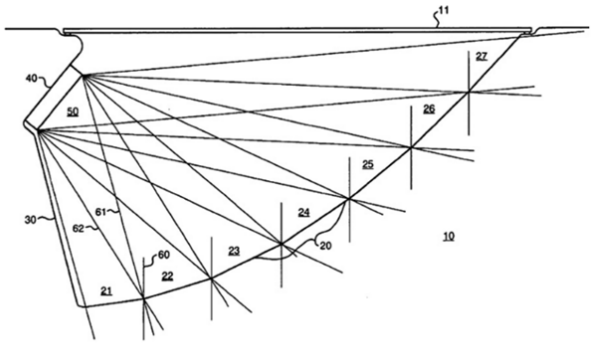

Fig. 18. Spectral energy (60) enters the aperture of the concentrator reflector (10) at an incident angle 90° to the horizontal plane. For seven plane facet mirrors (21–27) that are connected to form non-imaging reflective array, spectral energy is redirected onto solar receiver (50) for obtaining geometry concentration ratio of seven suns.

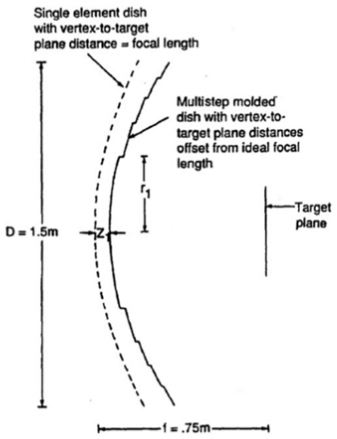

Fig. 19. Cross sectional geometry of 5-element molded dish.

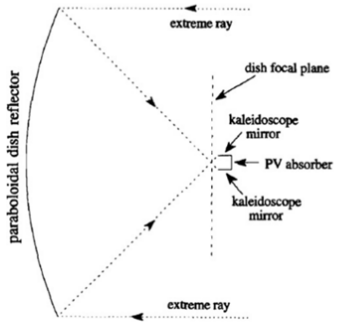

Fig. 20. Side view of the paraboloidal dish, its focal plane and the recessed kaleidoscope. The extreme rays from the dish cut the smallest waist in the focal plane, which defines its average concentration (e.g., 10,000). The kaleidoscope is recessed to a plane where the area delimited by the extreme rays corresponds to the prescribed concentration ratio (e.g., 500).

high-efficiency solar cell as illustrated in Fig. 21. The cell resides behind the dish and can be cooled adequately with a passive heat sink.

Kreske developed an optical solution for the redistribution of the light reflected from a 400 m^2 paraboloidal solar concentrating dish as uniform as possible over an approximately 1 m^2 plane as shown in Fig. 22 [37]. It is proposed that the solar cell will be mounted at the output of a rectangular receiver box with reflective sidewalls (i.e., a kaleidoscope or solar flux homogenizer) which will redistribute the light. From ray analysis, it is theoretically possible to achieve flux uniformity within the limits necessary for photovoltaic applications with a concentration ratio in the range of 500 suns.

Vasylyev et al. patented a non-imaging energy flux transformation system that includes a concentrator incorporating a set of nested, ring-like, concave reflective elements and a receiver as shown in Fig. 23 [38]. The system efficiently concentrates sunlight by means of focusing the energy striking the entrance aperture of concentrator to the receiver located on the side of concentrator's exit aperture. The mirror surface of the reflective elements having appropriate individual non-imaging profiles represented by curved or straight lines are positioned so that the energy portions reflected from individual surfaces are directed, focused and superimposed on one another to cooperatively form a common focal region on the receiver. The receiver can be an energy absorbing device (e.g., photovoltaic array), a secondary energy concentrating transformer or a flux homogenizer. Vasylyev then published the prototype of non-imaging reflective lens concentrators which provide solar concentration ratio of 1000 suns and flux uniformity on the rear of concentrator [39].

Terao and Krippendorf patented a compact micro-concentrator for photovoltaic cells that comprises of partial parabolic reflectors arranged in rows and columns with each reflector directing radiation to a photovoltaic cell [40]. In a compact photovoltaic cell arrangement, each cell is shielded from direct radiation by the adjacent reflector as depicted in Fig. 24. A secondary optical element, either reflective or refractive, can be provided with each cell receiver to further concentrate the reflected radiation to a photovoltaic cell at a more accessible location in the array.

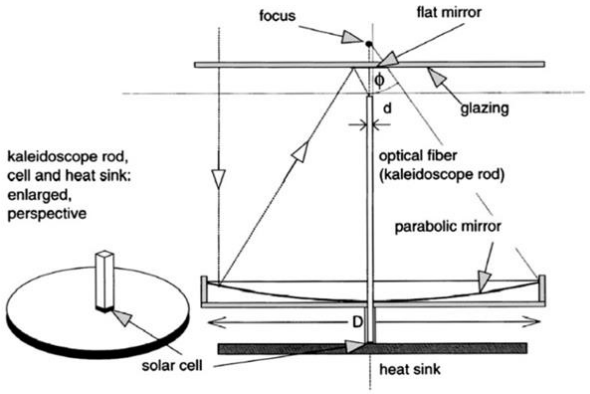

Fig. 21. Schematic illustration of a solar mini-dish photovoltaic concentrator: The parabolic mini-dish sits in an opaque encasement, except for the protective glazing. A small mirror deposited on the glazing redirects rays reflected from the mini-dish to the fibre's proximate tip, which is sited at a prescribed recession below the focal plane. A square cross section kaleidoscope optically couples the distal end of the fiber and the solar cell.

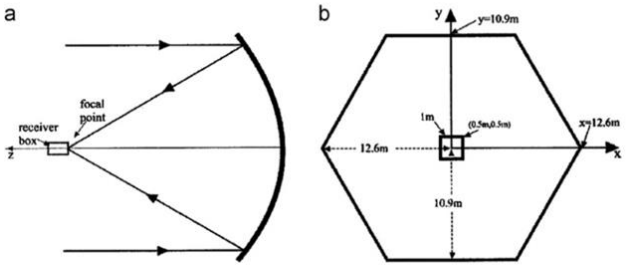

Fig. 22. Schematic view of the paraboloidal concentrator and its associated receiver box: (a) cross-section including the optical axis, (b) projection of the receiver box on the hexagonal periphery of the paraboloid.

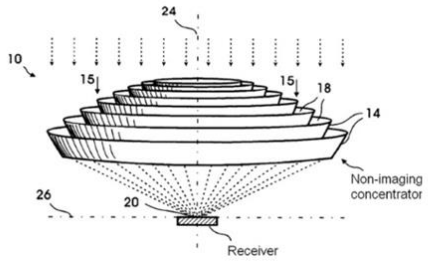

Fig. 23. Schematic view of the non-imaging system (10) includes a non-imaging concentrator comprising a plurality of coaxial ring-like elements (14) having inner reflective surface (18) and a receiver. Surfaces (18) receive incident sunlight (15) on the entrance aperture of concentrator and form a concentrated energy spot (20) on the target plane (26).

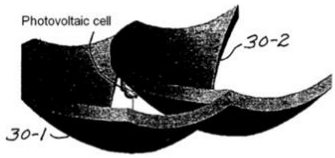

Fig. 24. Perspective view of two adjacent parabolic reflectors (30–1 & 30–2) with a photovoltaic cell.

Benitez et al. developed a two-mirror high concentration non-imaging optics that shares the advantage of present two-mirror imaging concentrators but also overcomes their main limitation like their trade-off between acceptance angle and irradiance uniformity [41]. From Fig. 25, the design is capable to work with an acceptance of 15 mrad half-angle and an average concentration over 800 suns (local concentration below 2000 suns).

As illustrated in Fig. 26, Lichy patented asymmetric, three dimensional, non-imaging, light concentrator adapted for use with a CPV cell [42]. The proposed solar concentrator has a hollow first stage formed by two pairs of facing reflective sides curved to different parabolas to form compound parabolic concentrator (CPC). The first stage CPC is optically coupled to a second stage solid CPC with two pairs of facing reflective sides curved to different parabolas. The second stage solid CPC with reflective index from 1.48 to 1.52 is optically coupled to a solid

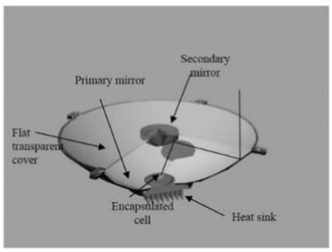

Fig. 25. CAD modal of the prototype design (a quarter of the primary, secondary and cover have been removed).

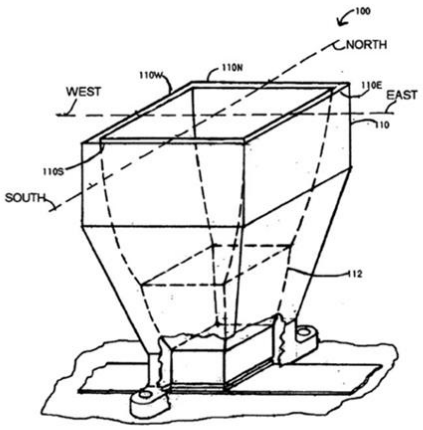

Fig. 26. Schematic illustration of an asymmetric, three-dimensional, non-imaging, compound parabolic concentrator (1 0 0): The hollow reflector (1 1 0) partially encloses and contains a solid reflector (1 1 2).

light diffuser. The solid light diffuser is optically coupled to the photovoltaic cell with a clear encapsulant. The whole concentrator is mounted on a metal substrate for thermal management. The proposed concentrator can operate efficiently with only single axis tracking of the sun in part because the reflective sides form orthogonal acceptance angles corresponding to the annual and daily apparent passage of the sun on Earth.

Fork and Maeda patented a Cassegrain-type concentrating solar collector cell including primary and secondary mirrors disposed on opposing convex and concave surfaces of a light-transparent optical element [43]. As shown in Fig. 27, light enters an aperture surrounding the secondary mirror toward the primary mirror, and is reflected by the primary mirror toward the secondary mirror, which re-reflects the light onto a photovoltaic cell mounted on a central region surrounded by the convex surface.

Neubauer and Gibson patented a solar concentrator consisted of a first reflective surface formed parabolic along a first axis and a second reflective surface formed parabolic along a second axis which is perpendicular to the first axis [44]. The focal length of the second reflective surface is shorter than the focal length of the first reflective surface for crossing the focal lines of the first and

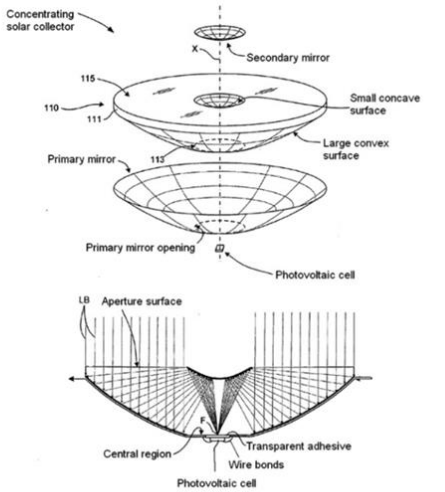

Fig. 27. An exploded perspective view showing an internal mirror, Cassegrain-type concentrating solar collector consisted of an optical elements (1 1 0), a photovoltaic cell located at central region (1 1 3), a primary mirror with an opening and a secondary mirror. Optical element is a solid, dish-like, light-transparent structure including an upper layer (1 1 1), a relatively large convex surface protruding from a lower side of upper layer, a substantially flat aperture surface (1 1 5) disposed on an upper side of upper layer and a relatively small concave surface defined in aperture surfaces.

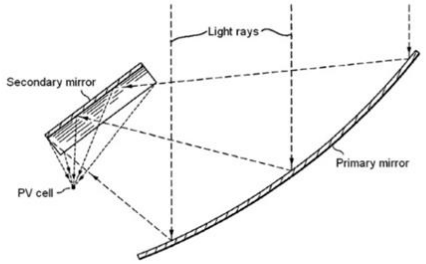

Fig. 28. A ray diagram illustrate an optical path for concentrated sunlight: Parallel rays are shown striking a primary mirror and reflecting towards reflective surface which serves as a secondary mirror and then to a focal point where PV cell is placed.

second reflective surfaces at a point as shown in Fig. 28. In other words, the whole concentrator consists of two parabolic troughs that are aligned along an optical axis. Hence, each parabolic trough can take parallel sunrays and focus them to a line. The parabolic axis of the first parabolic trough is oriented perpendicular to the parabolic axis of the second parabolic trough to focus the light from a line to a point.

Maeda patented beam integration for concentrating solar collector to concentrate sunlight onto a PV cell. Fig. 29 shows the whole system wherein an array of first optical elements that divide the sunlight into separate beams and a secondary optical system that integrates the separate beams in a defocused state at the image plane in order to form a uniform light distribution

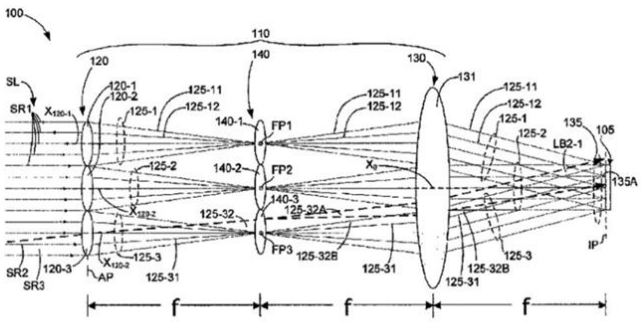

Fig. 29. A layout view showing a concentrating solar collector (1 0 0) that includes a CPV cell (1 0 5) supported in an image plane IP and a solar collector optical system (1 1 0). Solar collector optical system (1 1 0) includes a first array (1 2 0) with several first optical elements (120–1 to 120–3) that arranged in an aperture plane AP, a secondary optical system (1 3 0) with at least one secondary optical element (1 3 1), and an optical elements (140–1 to 140–3) disposed between first optical elements and secondary optical element.

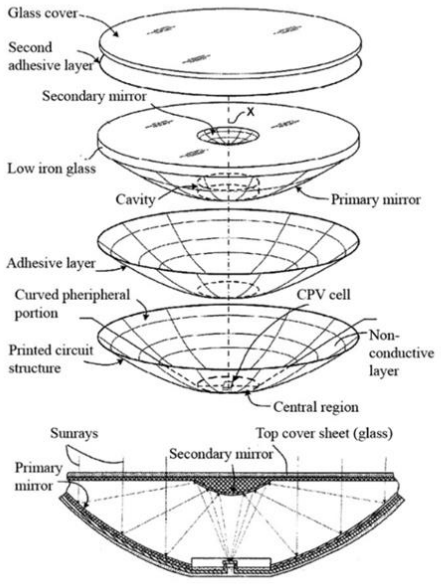

Fig. 30. An exploded perspective view (upper diagram) and a cross-sectional side-view (lower diagram) showing a laminated solar concentrating photovoltaic device.

pattern on the CPV cell [45]. The secondary optical system is positioned at a distance from the aperture plane, whereby the rays of each separate beam leaving the secondary optical element are parallel. The image plane (CPV cell) is located at the back focal point of the second imaging system, whereby all of the separate beams are superimposed on the PV cell in a defocused state.

Fork and Horne patented a laminated solar concentrating photovoltaic device as exploded in Fig. 30 in which concentrator elements (optics, CPV cells, and wiring) are laminated to form a composite, substantially planar structure [46]. Primary mirror and secondary mirror are disposed on convex and concave surfaces, respectively. Both primary and secondary mirrors are arranged such that, as shown in Fig. 30, sunrays traveling perpendicular to aperture surface. Sunrays entering optical element through a specific region of aperture surface is reflected by a corresponding region of primary mirror to an associated region of secondary mirror and from the secondary mirror to CPV cell. Top coversheet serves to protect secondary mirror from the harsh outdoor environment by providing a thin, optically transparent layer (glass) over aperture surface and secondary mirror.

Shifman patented a solar energy utilization system to be comprised of a Cassegrain-type concentrator and two solar radiation receiver components [47]. As depicted in Fig. 31, the first receiver component is designed to convert first part of the solar spectral energy into electrical energy, and the second receiver component is designed to convert second part of the solar spectral energy into electrical energy. The solar radiation concentrating optics comprises of a concave primary reflector and a convex secondary reflector. The secondary reflector is adapted to reflect solar radiation in the first part of the solar spectrum into the first receiver component and to transmit radiation in the second part of the solar spectrum into the second receiver component.

Draganov patented a solar concentrator with folded beam optical configuration allowing for compact, lightweight construction [48]. Reflective optics is employed, including dichroic mirror and antireflection coating, to remove unwanted infrared radiation from reaching the solar cell. In Fig. 32, the solar concentrator comprises of three reflecting surfaces. The primary mirror (concave surface) reflects solar radiation upward to the second reflecting surface (plane reflector) that is optically coupled to the primary mirror for reflecting the solar radiation downward to the tertiary mirror (concave surface). The tertiary mirror is configured to reflect the solar radiation upward again to the second reflecting surface in such a way that the solar radiation is then reflected from the second reflecting surface towards focal plane where photovoltaic cell is located.

Chong et al. proposed a non-imaging planar concentrator consisted of numerous square flat mirrors, capable of producing uniform sunlight and reasonably high concentration ratio [49,50]. The uniform concentrated light is formed from the superposition

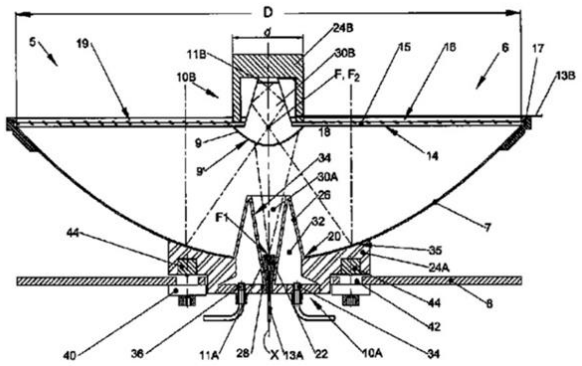

Fig. 31. Solar energy utilization unit (5) comprises of a solar radiation concentrating optics (6) including a concave primary reflector (7) and a concave secondary reflector (9) and a solar receiver designed to convert the radiation concentrated by the optics (6) into electrical energy. The solar receiver components (10A and 10B), each associated with either primary reflector (7) or secondary reflector (9) where (11A and 11B) may be a singular plate cell or an array of cells with different sensitivity wavebands.

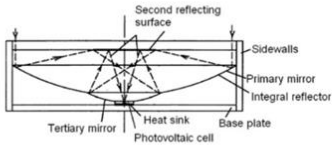

Fig. 32. The primary mirror and tertiary mirror form the integral reflector also called unitary reflector. The second reflecting surface 6 is a planar surface and is disposed between the primary mirror and the focal plane of the primary mirror. The PV cell is mounted on a heat sink with the base plate. On top of the solar concentrator, a piece of flat glass is spaced apart from the double curved reflector with sidewalls.

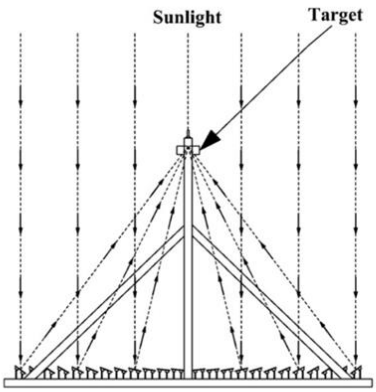

Fig. 33. Conceptual layout design of the non-imaging planar concentrator: Cross-sectional view of the planar concentrator to show how the individual mirror directs the solar rays to the target.

of the flat mirror images into one as illustrated in Fig. 33. The prototype consisted of 360 flat mirrors, each with a dimension of

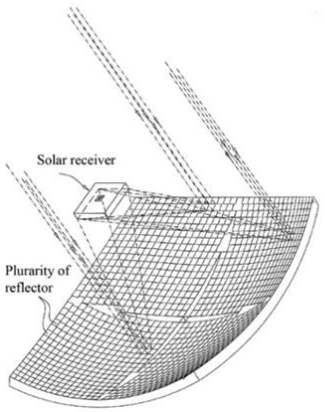

Fig. 34. Solar concentrator by Tsadka et al.: a simplified pictorial illustration of beam paths from some of the mirrors of the reflector portion to the receiver portion of the solar energy converter assembly.

4.0 cm × 4.0 cm, to achieve the solar concentration ratio of 298 suns at focal distance of 78 cm.

Tsadka et al. patented the optical design of new concentrator with plurality of reflectors to reflect sunrays directly onto the solar receiver or CPV panel for electricity and heat generation as shown in Fig. 34 [51]. Plurality of reflectors arranged on support surface and each reflector is configured as well as aligned to reflect solar radiation with high degree of uniformity onto the solar receiver.

Chong et al. has filed the patent for non-imaging dish concentrator that provides uniform solar flux, match the square or rectangular solar images to the square or rectangular dimension of the photovoltaic receiver and produce high solar concentration ratio [52]. The non-imaging dish concentrator consists of plurality of optical assembly sets (see Fig. 35(a)) and each optical assembly

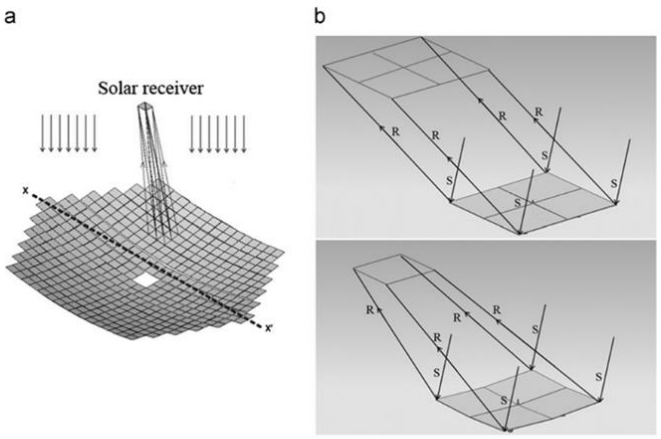

Fig. 35. (a) Non-imaging dish concentrator by Chong et al. consists of optical assembly set in which the solar concentration ratio is dependent on the applications by simply increasing or decreasing the total number of optical assembly sets, (b) The superposition of all the images of four flat component mirrors of each optical assembly set into one by inclining them relative to the pivot at the centre. Four flat mirrors are placed together to form one optical assembly set and they share one common pivot point at the meeting point. The shape of each mirror is either rectangular or square dependent on the solar cells arrangement at the photovoltaic receiver. The mechanism of inclining the four flat mirrors arrangement with a reference to the common pivot point at the centre results in the solar images of four component mirrors to superpose or overlap into one.

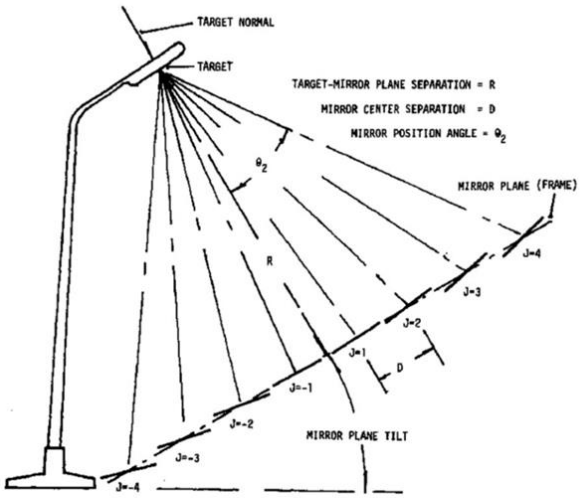

Fig. 36. Cross section, target-mirror geometries. Centers of mirrors lie in mirror frame plane. Mirrors may be moved individually (or in groups) to direct sun's image. In addition, target-mirror plane structure could be rotated and tilted to track sun.

set comprises of four flat mirrors placed together sharing one common pivot point at the centre (see Fig. 35(b)). Referring to Fig. 35(b), flat facet mirrors are used to ensure rectangular and uniform solar flux in which the superposition of all the images of four facet mirrors of each optical assembly set into one by inclining them relative to the pivot at the centre.

2.5. Central receiver system

Ittner proposed an array of directable mirrors as a photovoltaic concentrator [53]. The mirror field consists of a two dimensional matrix of mirrors which may be plane or focused. For simplicity, it is assumed that the centers of the mirrors all lie in a plane which

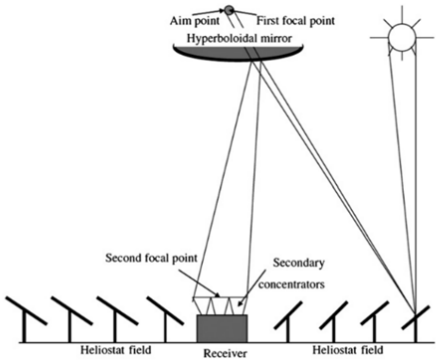

Fig. 37. The principle of tower reflector optics.

is centered on the photovoltaic target normal and is parallel to the plane of the target. The photovoltaic target normal thus defines the target mirror frame axis that may either be fixed in direction or arranged to track the sun in one or two dimensions (for instance, by rotating the arrangement as shown in the east-west direction about a vertical axis and by tilting the target-heliostat axis relative to the plane of the horizon). Independently, the individual mirrors may be moved so that they direct the sun's rays onto the plane of the target. Mirrors are positioned in two dimensions within the plane as shown in cross section in Fig. 36.

As illustrated in Fig. 37, Segal et al. presented the option to use the beam down optics of a solar tower system for large-scale and grid-connected CPV cells [54]. Two optical approaches for a large scale hybrid CPV and thermal power conversion at different spectral bands are proposed. In the first approach, the hyperboloid-shaped tower reflector is used as the spectrum splitter. Its mirrors can be made of transparent fused silica glass, coated with a dielectric layer, functioning as a band-pass filter. The transmitted band reaches the upper focal zone, where an array of PV modules is placed. The location of these modules and their interconnections depend on the desirable concentration level and the uniformity of the flux distribution. The reflected band is directed to the second focal zone near the ground, where a compound parabolic concentrator is required to recover and enhance the concentration to a level depending on the operating temperature at this target. In the second approach, the total solar spectrum is reflected down by the tower reflector. Before reaching the lower focal plane, the spectrum is split and filtered. One band can be reflected and directed horizontally to a PV array and the rest of the spectrum is transmitted to the lower focal plane. The system intended to operate under concentrated solar radiation in the range of 200–800 suns. The study shows that 6.5 MW from the PV array and 11.1 MW from a combined cycle can be generated starting from solar heat input of 55.6 MW.

3. Conclusion

The technology of CPV can be viewed as a potential major energy source in the future. The future cost of energy from conventional sources is a main factor determining how much society may be willing to pay for the social and environmental benefits of solar energy. A great revolution in solar electricity generation is underway due to the progress in the CPV materials and creative optical designs. Commercial multi-junction CPV technologies have already demonstrated solar cell efficiencies of about 40% under high concentrated solar irradiation of hundreds to thousands of suns [55]. On the other hand, dense array CPV receiver for 500 suns reflective dish has been successfully deployed with the efficiency ranging from 30% to 36% at six different locations in Australia, counting for more than 1 MWp of installed peak power [56].

Under these high concentrated solar irradiations, the cost of CPV is greatly dependent on the optical system. In this article, we have reviewed various optical systems proposed and patented by the world renowned authors and inventors. Despite many optical designs have been presented, the ultimate goal is to provide cost-effective, rigid, easy-manufactured and high efficient solutions to the CPV system either in small or large scale.

Acknowledgements

The authors would like to express their gratitude to Ministry of Energy, Green Technology & Water (AAIBE Trust Fund) and Ministry of Science, Technology & Innovation (e-Science Fund) with project number 03–02–11-SF0143 for the financial support.

References

[1] Gordon JM. Concentractor optics. In: Luque A, Andreev V, editors. Concentrator photovoltaics. New York:Springer; 2007. p.113–132.
[2] Erik Pihl. Concentrating solar power. Report prepared for the energy committee of the Royal Swedish Academy of Science, Chalmers University.
[3] Fraunhofer ISE, World record: 41.1% efficiency reached for multi-junction solar cells at Fraunhofer ISE, 2009. Fraunhofer-Institute for Solar Energies systems, 2009.
[4] Law Daniel C, King RR, Yoon H, Archer MJ, Boca A, Fetzer CM, et al. Future technology pathways of terrestrial III–V mulitjunction solar cells for concentrator photovoltaic systems. Solar Energy Materials and Solar Cells 2010;94:1314–8.
[5] Rumyantsev VD. Terrestial concentrator PV systems. In: Luque A, Andreev V, editors. Concentrator Photovoltaics. New York: Springer; 2007. p. 151–74.
[6] Boes EC. Photovoltaic concentrator technology development. IEEE Xplore 1990.
[7] Whitfield GR, Bentley RW, Weatherby CK, Hunt AC, Mohring HD, Klotz FH, et al. The development and testing of small concentrating PV system. Solar Energy 1999;67:23–34.
[8] Arqueros F, Jiménez A, Valverde A. A novel procedure for the optical characterization of solar concentrators. Solar Energy 2003;75:135–42.
[9] Miller David C, Kurtz Sarah R. Durability of Fresnel lenses: a review specific to concentrating photovoltaic application. Solar Energy Materials and Solar Cells 2011;95:2037–68.
[10] Vivar M, Herrero R, Anton I, Martinez-Moreno F, Moreton R, Sala G, et al. Effect of soiling in CPV systems. Solar Energy 2010;84:1327–35.
[11] Leutz Ralf, Suzuki Akio, Akisawa Atsushi, Kashiwagi Takao. Design of a non-imaging Fresnel lens for solar concentractors. Solar Energy 1999;65:379–87.
[12] Chemisana D, Ibanez M, Rosell JI. Characterization of a photovoltaic-thermal module for Fresnel linear concentrator. Energy Conversion and Management 2011;52:3234–40.
[13] O'Neill Mark Joseph. Stretched Fresnel lens solar concentrator for space power. US Patent 6,075,200; 2000.
[14] Jebens Robert W. Fresnel lens concentrator. US Patent 4,799,778; 1989.
[15] Davies PA. Design of single-surface spherical lenses as secondary concentrators for photovoltaic cells. Pure and Applied Optics 1993;2:315–24.
[16] Terao Akira, Mulligan P, Daroczi Shandor G, Chao Pujol Oscar, Richard Pierre J, Swanson Richard M. A mirror-less design for micro-concentrator modules. IEEE 2000:1416–9.
[17] Chen Leon LC. Stationary photovoltaic array module design for solar electric power generation systems. US Patent 6,653,551; 2003.
[18] Chen Leon LC. Photovoltaic array module design for solar electric power generator systems. US Patent 6,717,045; 2004.
[19] Andrew VM, Grilikhes VA, Khvostikov VP, Khvostikova OA, Rumyantsev VD, Sadchikov NA, et al. Modules and solar cells for TPV systems. Solar Energy & Solar Cells 2004;84:3–17.
[20] Ryu Kwangsun, Rhee Jin-Geun, Park Kang-Min, Kim Jeong. Concept and design of modular Fresnel lenses for concentration solar PV system. Solar Energy 2006;80:1580–7.
[21] Winston Roland, Ritschel Alexander. Concentrating photovoltaic system using a Fresnel lens and non-imaging secondary optics. US Patent application publication; 2008. p.US2008/0245401.

[22] Schwartzman Zalman. Solar concentrator device for photovoltaic energy generation. US Patent application publication; 2008. p.US2008/0041441.
[23] Araki Kenji, Yano Taizo, Uozumi Hisafumi. Concentrator solar photovoltaic power generating apparatus. US Patent application publication; 2008. p.US2008/0087323.
[24] Ota Yasuyuki, Nishioka Kensuke. Three-dimensional simulating of concentrator photovoltaic modules using ray trace and equivalent circuit simulators. Solar Energy 2012;86:476–81.
[25] Singh P, Liburdy JA. A solar concentrator design for uniform flux on a flat receiver. Energy Conversion and Management 1993;34:533–43.
[26] Lamb Walter, Lawrence John. Multiple reflector concentractor solar electric power system. US Patent 5,374,317; 1994.
[27] Gordon JM. A 100-sun linear photovoltaic solar concentrator design from inexpensive commercial components. Solar Energy 1996;57:301–5.
[28] Sala G, Arboiro JC, Luque A, Minano JC, Miñano JC, Dramsch C et. al. The EUCLIDES prototype: an efficient parabolic trough for PV concentration. 25th PVSC May13–17 1996, Washington D.C.
[29] Clemens Donald D. Photovoltaic concentrator system. US Patent 5,660,644; 1997.
[30] Frazier Scott. Double reflecting solar concentrator. US Patent application publication; 2001. p. US2001/0045212.
[31] Hein M, Dimroth F, Siefer G, Belt AW. Characterisation of a 300× photovoltaic concentrator system with one-axis tracking. Solar Energy Materials & Solar Cells 2003;75:277–83.
[32] Joe S Coventry. Performance of a concentrating photovoltaic/thermal solar collector. Solar Energy 2005;78:211–22.
[33] Straka Christopher W, Reflecting photonic concentrator. US Patent application publication; 2006. p. US2006/0249143.
[34] Jorgensen G, Wendelin T. Uniform Flux Dish Concentrators for Photovoltaic Application. National renewable energy laboratory; 1992.
[35] Ries Harald, Gordon JM, Lasken Michelle. High-flux photovoltaic solar concentrators with kaleidoscope-based optical designs. Solar Energy 1997;60:11–6.
[36] Feuermann Daniel, Gordon Jeffrey M. High-concentration photovoltaic designs based on miniature parabolic dishes. Solar Energy 2001;70:423–30.
[37] Kreske Kathi. Optical design of a solar flux homogenizer for concentrztor photovoltaics. Applied Optics 2002;41:2053–8.
[38] Vasylyev Sergiy Victorovich, Vasylyev Viktor Petrovych. Non-imaging system for radiant energy flux transformation. U.S. Patent 6,620,995.; 2003.
[39] Vasylyev S. Non-imaging reflective lens concentrator, presented at international conf. on solar concentractors for generation of electricity or hydrogen, May 1–5, 2005, Scottsdale, AZ.
[40] Terao Akira, Krippendorf Ralph Compact micro-concentrator for photovoltaiccells. U.S. Patent 7,297,865; 2007.
[41] Benitez P, Cvetkovic A, Winston R, Reed L New high-concentration mirror-based Kohler integrating optical design for multijunction solar cells. Optical Society of America 2006; paper TuD3.
[42] Lichy Joseph I. Asymetric, three dimensional, non-imaging, light concentrator. US Patent application publication; 2006. p. US2006/0072222.
[43] Fork David K, Maeda Patrick Y. Concentrating solar collector with solid optical element. US Patent application publication; 2006. p. US2006/0231133.
[44] Neubauer Jeffrey B, Gibson Grant M. Solar electric power generator. US Patent application publication; 2007. p. US2007/0181173.
[45] Maeda Patrick Y. Beam integration for concentrating solar collector. US Patent application publication; 2007. p. US2007/0251568.
[46] Fork David K, Horne Stephen J. Laminated solar concentrating photovoltaic device. US Patent application publication; 2007. p. US2007/0256726.
[47] Shifman Eli. Solar energy utilization unit and solar energy utilization system. US Patent 7,435,898; 2008.
[48] Draganov Vladimir. Solar concentrator and solar concentrator array. US Patent application publication; 2009. p. US2009/0056789.
[49] Chong KK, Siaw FL, Wong CW, Wong GS. Design and construction of non-imaging planar concentrator for concentrator photovoltaic system. Renewable Energy 2009;34:1364–70.
[50] Chong KK, Wong CW, Siaw FL, Yew TK. Optical characterization of non-imaging planar concentrator for the application in concentrator photovoltaic system. Journal of Solar Energy Engineering 2010;132:011011 (9 pages).
[51] Tsadka S, Segev R, Migalovich P, Levin O, Tarazi E, Whelan R. Solar electricity generation system. US Patent application publication; 2009. p. US2009/0065045.
[52] Chong KK, Wong CW, Yew TK, Tan MH. Solar concentrator assembly. Malaysian Patent; 2012: No. PI 2012002439 (pending) filed on 31st May 2012.
[53] Ittner III WB. An array of directable mirrors as a photovoltaic solar concentrator. Solar Energy 1980;24:221–34.
[54] Segal Akiba, Epstein Michael, Yogev Amnon. Hybrid concentrated photovoltaic and thermal power conversion at different spectral bands. Solar Energy 2004;76:591–601.
[55] Jorgensen G, Wendelin T. Uniform Flux Dish Concentrators for Photovoltaic Application. National renewable energy laboratory; 1992.
[56] Verlinden Pierre J, Lewandowski Allan, Bingham Carl, Kinsey Geoffrey S, Sherif Raed A, Lasich John B. Performance and reliability of multijunction III–V modules for concentrator dish and central receiver applications. IEEE 2006:592–7.

APPENDIX B

US 20150207455A1

(19) **United States**

(12) **Patent Application Publication**

Chong et al.

(10) **Pub. No.: US 2015/0207455 A1**

(43) **Pub. Date: Jul. 23, 2015**

(54) **DENSE-ARRAY CONCENTRATOR PHOTOVOLTAIC SYSTEM UTILISING NON-IMAGING DISH CONCENTRATOR AND ARRAY OF CROSSED COMPOUND PARABOLIC CONCENTRATORS**

(71) Applicant: **Universiti Tunku Abdul Rahman**, Petaling Jaya (MY)

(72) Inventors: **Kok Keong Chong**, Kuala Lumpur (MY); **Tiong Keat Yew**, Jitra (MY); **Ming Hui Tan**, Penampang (MY)

(21) Appl. No.: **14/462,891**

(22) Filed: **Aug. 19, 2014**

(30) **Foreign Application Priority Data**

Jan. 23, 2014 (MY) PI2014000210

Publication Classification

(51) **Int. Cl.**
H02S 40/22 (2006.01)

(52) **U.S. Cl.**
CPC ***H02S 40/22*** (2014.12)

(57) **ABSTRACT**

Disclosed is a solar concentrator assembly (**100**) having a non-imaging dish concentrator (NIDC) (**110**) which consists of a plurality of flat facets mirrors (**160**) arranged in such a way that all the mirror images are superimposed to form reasonably uniform irradiance and either square or rectangular pattern of concentrated sunlight at a common receiver without sunlight blocking and shadowing on each other. The geometry of the NIDC (**110**) is determined using a special computational method. A plurality of secondary concentrators (**120**) formed by an array of crossed compound parabolic concentrators is used to further focus the concentrated sunlight by the NIDC (**110**) onto active area of solar cells (**230**) of the concentrator photovoltaic receiver (**170**). The invention maximizes the absorption of concentrated sunlight for the electric power generation system.

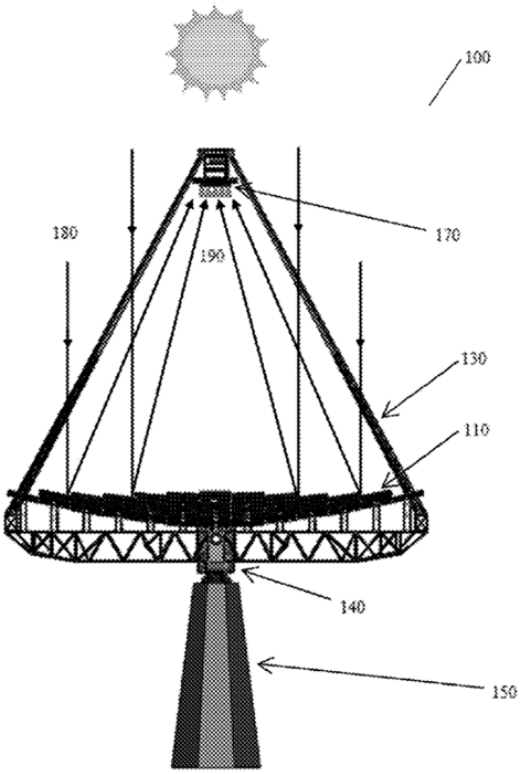

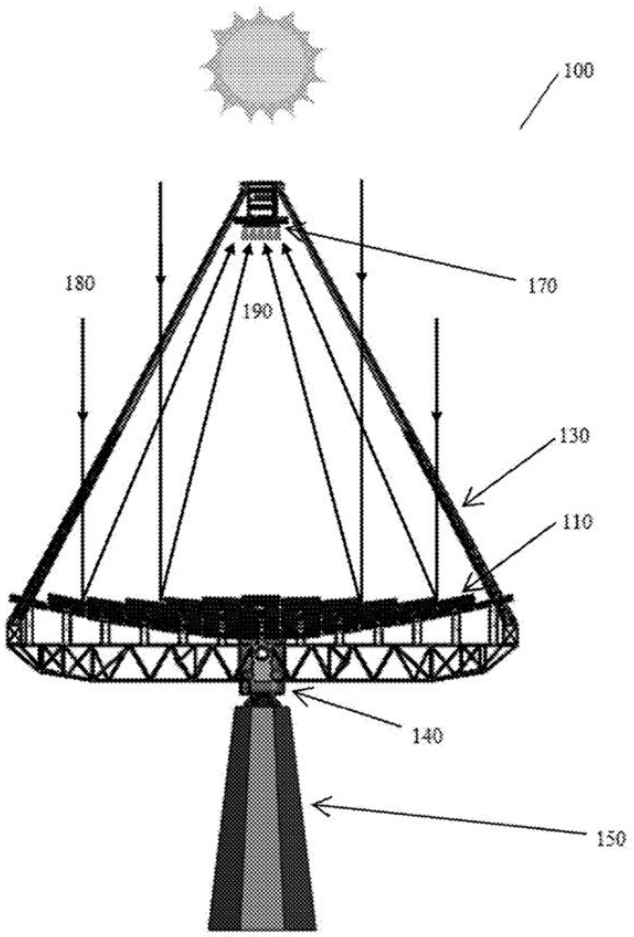

Figure 1

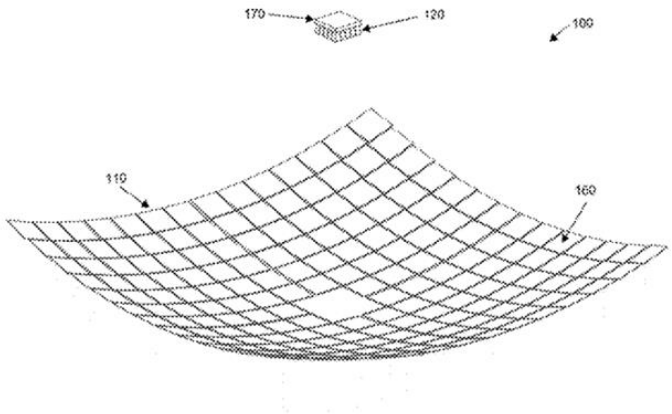

Figure 2

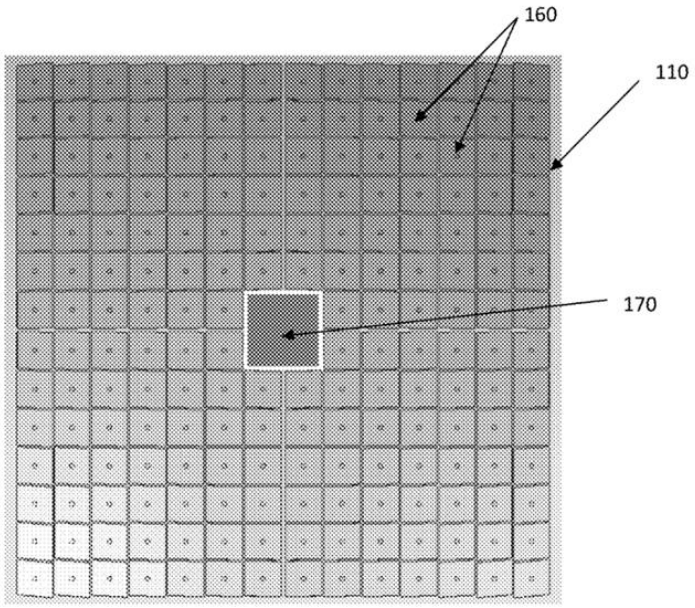

Figure 3

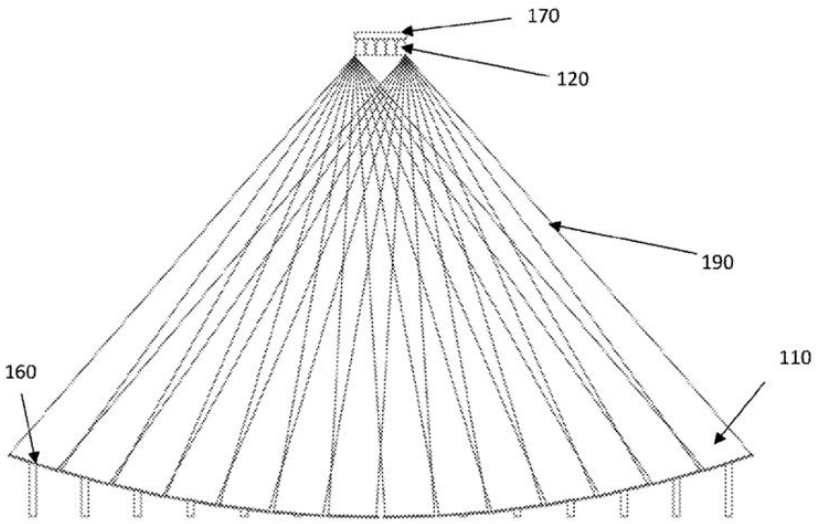

Figure 4

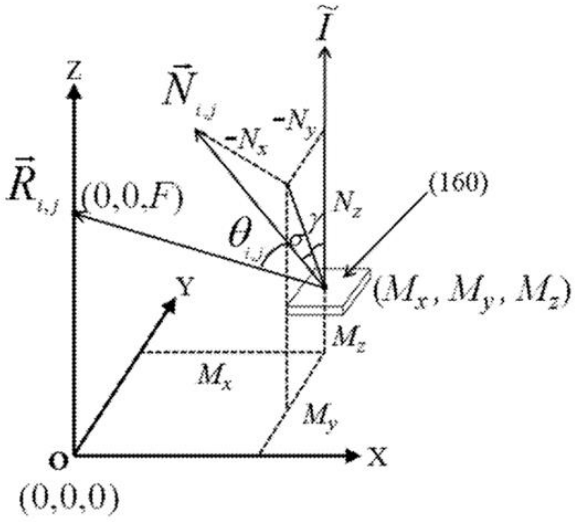

Figure 5(a)

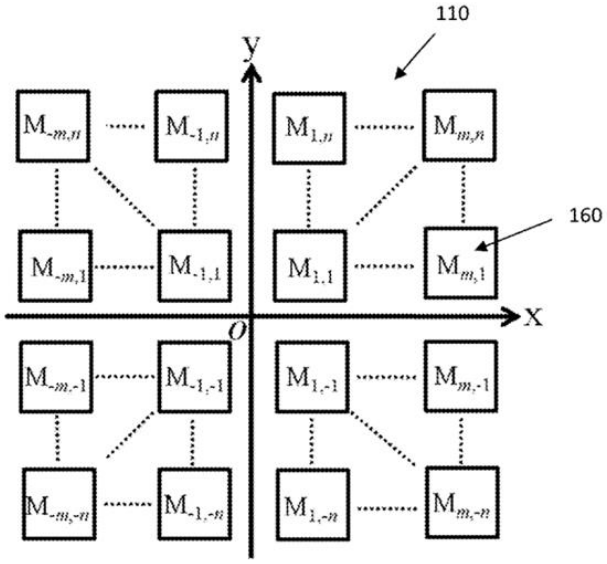

Figure 5(b)

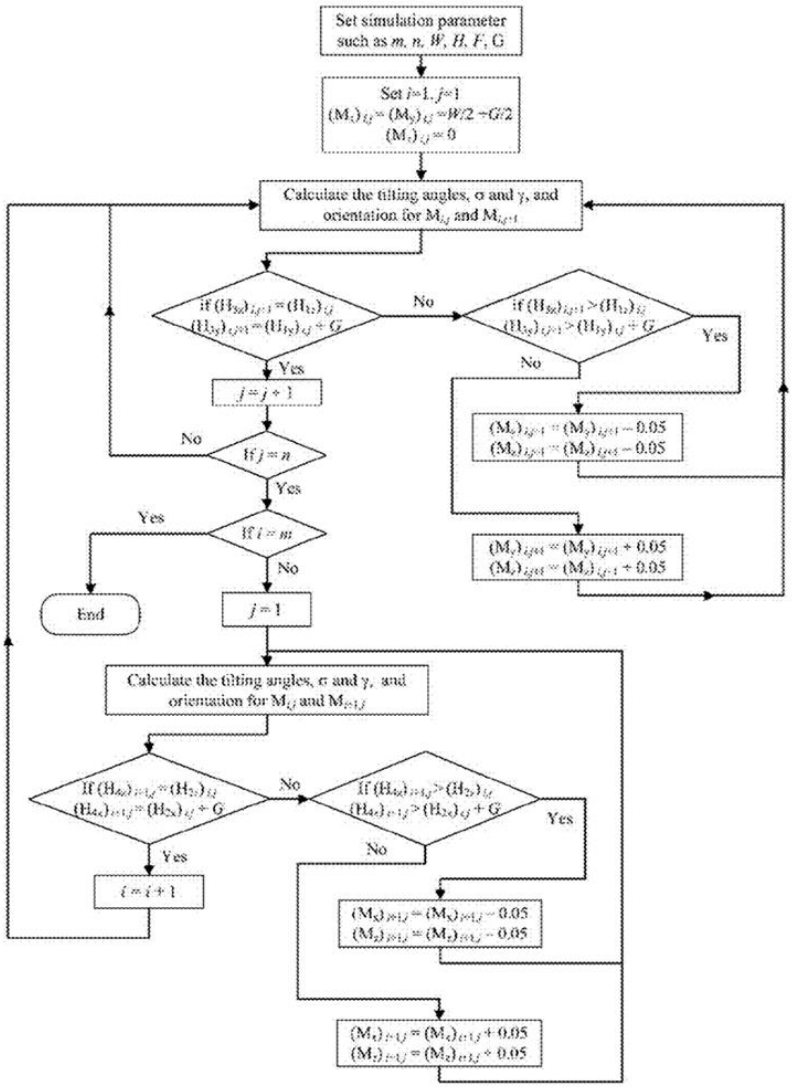
Set simulation parameter such as m, n, W, H, F, G
Set i=1, j=1
Calculate the tilting angles, σ and γ, and orientation for M_ij and M_i,j+1
No
Yes
j = j + 1
No
If j = n
Yes
Yes
If i = m
End
No
j = 1
Calculate the tilting angles, σ and γ, and orientation for M_ij and M_i+1,j
No
Yes
i = i + 1
No
Yes

Figure 6

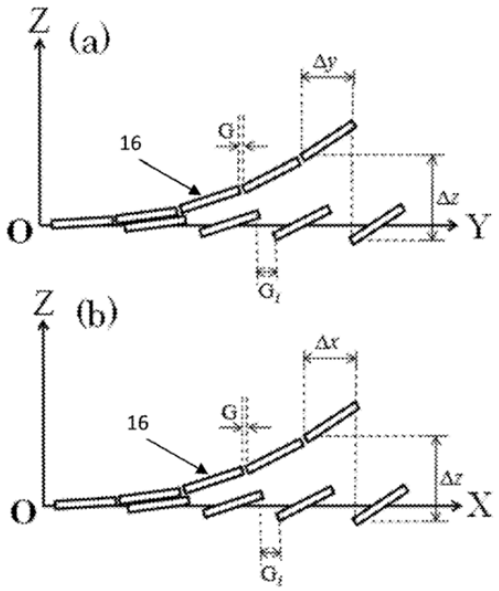

Figure 7

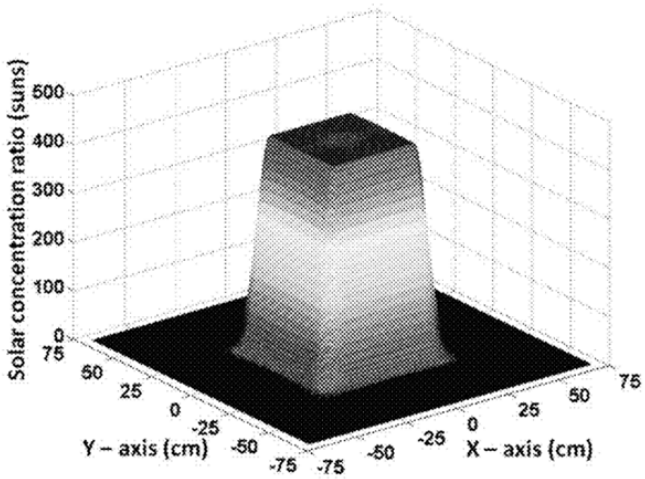

Figure 8

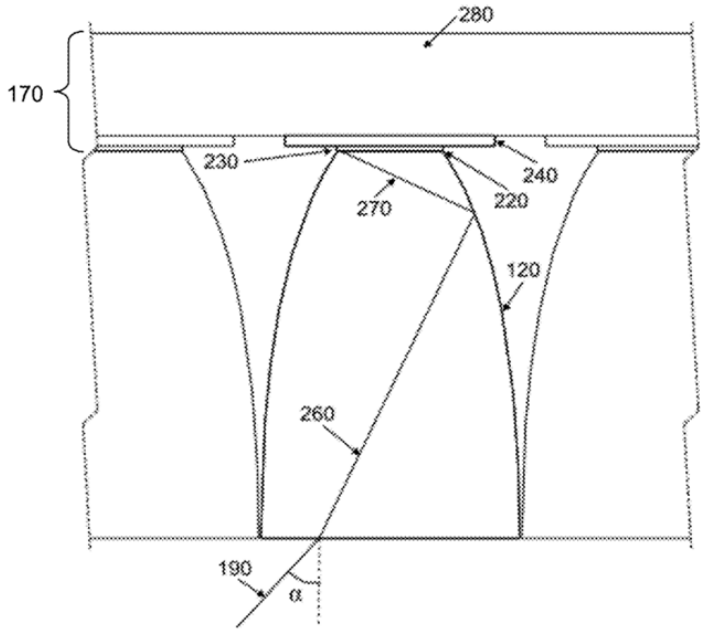

Figure 9

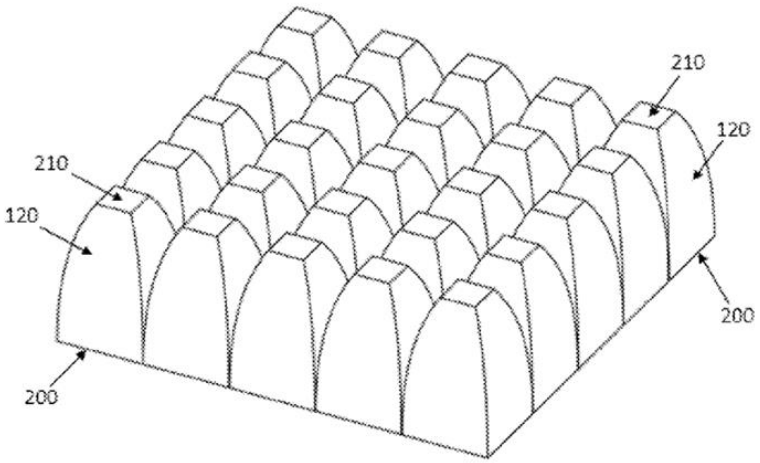

Figure 10(a)

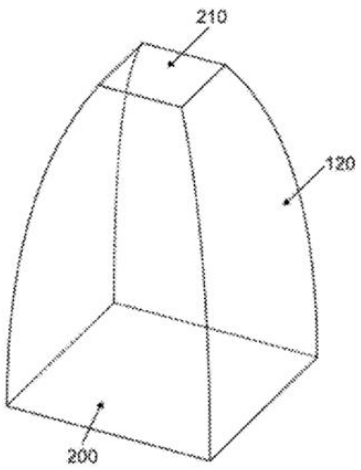

Figure 10(b)

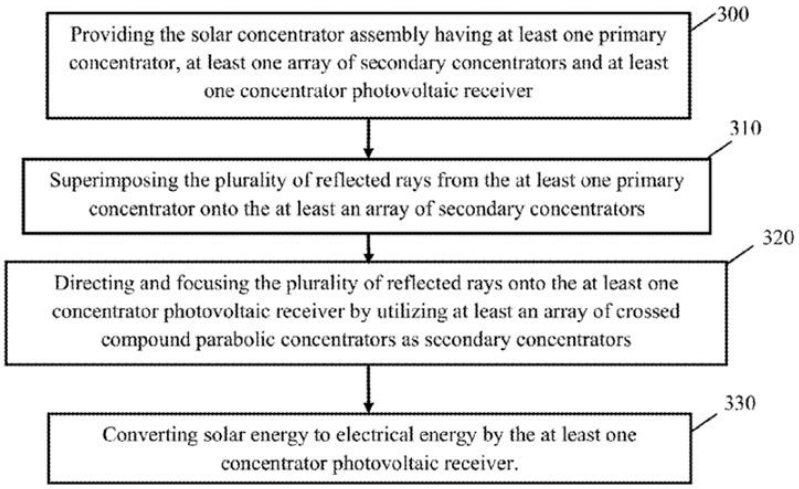
Providing the solar concentrator assembly having at least one primary concentrator, at least one array of secondary concentrators and at least one concentrator photovoltaic receiver
300
Superimposing the plurality of reflected rays from the at least one primary concentrator onto the at least an array of secondary concentrators
310
Directing and focusing the plurality of reflected rays onto the at least one concentrator photovoltaic receiver by utilizing at least an array of crossed compound parabolic concentrators as secondary concentrators
320
Converting solar energy to electrical energy by the at least one concentrator photovoltaic receiver.
330

Figure 11

DENSE-ARRAY CONCENTRATOR PHOTOVOLTAIC SYSTEM UTILISING NON-IMAGING DISH CONCENTRATOR AND ARRAY OF CROSSED COMPOUND PARABOLIC CONCENTRATORS

CROSS-REFERENCE TO RELATED APPLICATIONS

[0001] This application claims the benefit under 35 U.S.C. §119(a) of Malaysian Application No. PI 2014000210, filed on Jan. 23, 2014, and is hereby incorporated by reference in its entirety for all purposes.

FIELD OF INVENTION

[0002] The present invention relates to the field of solar electrical power generation system. More particularly, the present invention relates to dense-array concentrator photovoltaic (CPV) systems utilizing non-imaging dish concentrator and array of crossed compound parabolic concentrators (CCPC) to improve the overall energy conversion efficiency.

BACKGROUND OF THE INVENTION

[0003] Developing countries across the globe struggle in deriving or generating the basic necessities of life for themselves. Among the other necessities, energy supply such as electricity still remains one of the major requirements in the economies of developing nations which is unattained. Over the years, people have largely relied on fossil fuels to meet their energy demands. However, the indiscriminate uses of these non-renewable sources of energy have posed a threat of their depletion in the near future and hence the search for alternative sources of energy generation is sought. Owing to the need of the hour, tapping of renewable sources of energy such as solar energy to meet the growing demands has significantly increased.

[0004] Solar energy is available in plenty and it can be utilized by converting it to different energy forms such as thermal and electrical energy. Thus, the solar energy can be stored in different forms for use according to the need of the consumer. However, conventional flat plate solar energy converters are less efficient and having higher cost compared to fossil fuel. Alternatively, a more advanced energy conversion systems such as solar concentrating systems are proposed with the aim to improve the conversion efficiency of solar energy converter.

[0005] Photovoltaic cells are in use to convert solar energy into electrical energy. These cells can operate on the sunlight falling on it directly. However, since the photovoltaic cells are relatively expensive, it is judicious to concentrate the solar energy with the aid of concentrators which can then be targeted to the photovoltaic cells. A number of individual photovoltaic cells comprise a photovoltaic receiver that converts solar energy to electrical energy.

[0006] Various types of reflective and refractive solar concentrators have been devised for concentrating photovoltaic systems such as the parabolic dish, line-focus concentrator, Fresnel lens and point focus lens. With the different types of concentrators in use, the receiver of the concentrator can be configured in either individual cell receiver or dense-array of solar cells receiver dependent on the area of the focused sunlight. For individual cell configuration, the area of focused sunlight that is incident on the solar cell is about the same as the area of the single solar cell active area. For dense-array configuration, the area of the focused sunlight is much larger than the active area of one solar cell, therefore an array of solar cells that is connected in series or parallel to form a receiver with larger area is used to convert the sunlight into electricity. The solar cells need to be assembled closely to each other to avoid blank gap without active area of solar cell. In the assembly of dense-array module, packing factor is defined as percentage of active area of solar cells over the total module area and is useful in defining the efficiency of the solar electricity generation system. Practically, it is impossible to achieve 100% of packing factor due to the presence of physical connections between solar cells and physical constrain of the substrate of solar cells. Constrains mentioned above will create some blank gap without active area in the assembled module and the focused sunlight that drop at the blank gap will become losses to the system because it cannot be converted to electricity.

[0007] In existing dense-array CPV system such as parabolic dish and central receiver system, the secondary optics is not widely applied or fully explored for improving the overall performance of CPV receiver especially in reducing the energy losses due to lower packing factor of solar cells. The most common application of secondary optics is only limited to single cell CPV module coupled to Fresnel lens as the primary concentrator especially for improving uniformity of concentrated sunlight.

[0008] To reduce the losses mentioned above in dense array configuration system, an improved system would be needed to increase the sunlight falling on the active area of the solar cell. The needed system would introduce more improved concentrators by integrating an array of secondary concentrators that would guide the sunlight that drop outside the solar cell active area onto the active area and thereby increasing the electrical power output.

SUMMARY OF THE INVENTION

[0009] The present invention is an improved and efficient solar concentrator assembly of a solar electrical power generation system. The present invention utilizes a non-imaging dish concentrator integrated with an array of crossed compound parabolic concentrators (CCPC) in the application of dense-array concentrator photovoltaic (CPV) system.

[0010] The non-imaging dish concentrator (NIDC) consists of a plurality of flat facet mirrors arranged in such a way that all the mirror images are superimposed at the common receiver without sunlight blocking and shadowing on each other. The arc-shape or a new geometry of the NIDC according to the present invention is generated with a special computational algorithm, which is designed to determine the relative height and tilted angles of each flat facet so that all the facet images are well superimposed on the common receiver without sunlight blocking and shadowing among the facet mirrors. A plurality of secondary concentrators or secondary optics, which is an array of CCPC in the form of lenses, is used to direct the concentrated sunlight by the NIDC falling onto active area of CPV cells only. The secondary optics acts as optical funnel with larger area on the entrance surface and smaller area in exit surface, which allow more space for the inter-connection among the CPV cells located at exit surface in either series or parallel as to minimize current mismatch in the circuit without affecting the overall performance of CPV system.

[0011] The invention can reduce the losses in dense-array CPV cells caused by the difficulty to achieve high packing

factor due to the unavoidable spacing needed for cell interconnection and thus maximize the absorption of concentrated sunlight for the electrical power generation system. With the secondary optics, it also allows more flexibility of inter-connection among the cells for minimizing the current mismatch loss. In addition, the array of secondary concentrators can increase the acceptance angle of dense-array CPV system and hence allow higher tolerance to pointing error of sun-tracking system. Furthermore, the proposed primary NIDC can project a reasonably uniform irradiance and square or rectangular pattern of concentrated sunlight onto the secondary optics.

[0012] Other objects and advantages of the embodiments herein will become readily apparent from the following detailed description taken in conjunction with the accompanying drawings.

BRIEF DESCRIPTION OF THE DRAWINGS

[0013] Other objects, features, and advantages of the invention will be apparent from the following description when read with reference to the accompanying drawings. In the drawings, wherein like reference numerals denote corresponding parts throughout the several views:

[0014] FIG. **1** illustrates a perspective view of a solar concentrator assembly of a solar electrical power generation system according to an exemplary embodiment of the invention.

[0015] FIG. **2** illustrates a schematic diagram showing a non-imaging dish concentrator, a plurality of secondary concentrators arranged to form an array, and a concentrator photovoltaic receiver according to a preferred embodiment of the present invention.

[0016] FIG. **3** illustrates a top view of the non-imaging dish concentrator consisting of a plurality of flat facet mirrors and the concentrator photovoltaic receiver located at the center according to a preferred embodiment of the present invention.

[0017] FIG. **4** illustrates a schematic diagram showing how the sunrays are focused by the non-imaging dish concentrator towards the array of secondary concentrators and then towards the concentrator photovoltaic receiver in the cross-sectional view.

[0018] FIG. **5** illustrate:

[0019] (a) The Cartesian coordinate system in 3-D representing a coordinate (M_x, M_y, M_z), incident angle (θ_{ij}) and a pair of tilted angles (σ,γ) of a i,j-facet mirror where F is the focal distance of the NIDC and the origin 'O' is center of the concentrator frame. $\vec{I}$ is unit vector of the incident sunray, $\vec{N}_{i,j}$ is unit vector of the normal of i,j-facet mirror, $\vec{R}_{i,j}$ is unit vector of the reflected solar ray of i,j-facet mirror.

[0020] (b) The initial facet mirror's configuration of the non-imaging dish concentrator. The concentrator can be divided into four quadrants which are the top-right, top-left, bottom-right and bottom-left.

[0021] FIG. **6** is a flow chart to illustrate a special computational method or algorithm or computer program operational steps describing on how to compute geometry of a plurality of flat facet mirrors for non-imaging dish concentrator (NIDC), which defines initial orientations of all facet mirrors arranged in an array at the same height first and then obtains final orientations of facet mirrors one by one from central to peripheral region of the NIDC with gradually increased height so that all the images can remain superimposition at the common receiver without sunlight blocking and shadowing among adjacent mirrors.

[0022] FIG. **7** illustrates the conceptual drawing on how to obtain final positions and orientations of flat facet mirrors in non-imaging dish concentrator using the special computational method or algorithm or computer program operational steps as described in FIG. **6** according to an embodiment of the present invention. In this process, we define initial orientations of all facet mirrors arranged in an array at the same height first and then obtains final orientations of facet mirrors one by one from central to peripheral region of the NIDC with gradually increased height so that all the images can remain superimposition at the common receiver without sunlight blocking and shadowing among adjacent mirrors: (a) Side view in y-z direction (b) Side view in x-z direction.

[0023] FIG. **8** illustrates an example of simulated solar flux distribution with maximum solar concentration ratio of 435 suns focused by the non-imaging dish concentrator at the entrance surface of the array of secondary concentrators according to a preferred embodiment of the present invention. The simulated result of solar flux distribution is performed using ray-tracing technique for the case of 22×22 array of facet mirrors with each facet dimension of 49.8 cm×49.8 cm and focal distance of 10 m.

[0024] FIG. **9** illustrates a schematic diagram showing a cross-sectional view of the arrangement of array of the crossed compound parabolic concentrators and concentrator photovoltaic receiver that consists of concentrator photovoltaic cells, concentrator photovoltaic cell substrates and heat sink.

[0025] FIG. **10** illustrates schematic diagrams showing (a) a trimetric view for an array of crossed compound parabolic concentrators. It is just an example of an array with 5×5 pieces secondary concentrators but the real design is not limited to this number; and (b) a trimetric view for one of the crossed compound parabolic concentrators.

[0026] FIG. **11** is a flow chart to illustrate a method of operating the dense-array concentrator photovoltaic system utilizing non-imaging dish concentrator, array of crossed compound parabolic concentrators and concentrator photovoltaic receiver as the solar electrical power generation system for optimizing solar power generation efficiency.

DETAILED DESCRIPTION OF THE PREFERRED EMBODIMENTS

[0027] The present invention will now be described in detail with reference to the accompanying drawings. However, the description or the illustrations as disclosed herein should not be construed as the limitation of said invention.

[0028] The present invention relates to the field of solar electrical power generation system. More particularly, the present invention relates to a NIDC integrated with an array of crossed compound parabolic concentrators in the application of concentrator photovoltaic (CPV) system. The present invention is an improved and efficient solar concentrator assembly (**100**) of a solar electrical power generation system. The solar concentrator assembly (**100**) comprises at least one array of facet mirrors (**160**) arranged to form at least one primary concentrator (**110**), at least one concentrator photovoltaic receiver (**170**) and at least one array of secondary concentrators (**120**) for directing solar energy to the at least one concentrator photovoltaic receiver (**170**). A non-imaging dish concentrator (NIDC) is employed as the at least one primary concentrator (**110**). A plurality of crossed compound parabolic concentrators that is arranged in an array forms the array of secondary concentrators (**120**).

[0029] FIG. **1** illustrates a perspective view of a solar concentrator assembly (**100**) acting as a solar electrical power generation system according to a preferred embodiment of the invention. The NIDC (**110**) includes a plurality of flat facet mirrors arranged to form a large array to collect the sunlight incident over a large area. The NIDC (**110**) is supported on a truss member assembly. The truss member assembly forms a part of a structural supporting means (**130**) which provides mechanical support to the solar concentrator assembly (**100**). The truss member assembly is attached to at least one pedestal (**150**). The at least one pedestal (**150**) supports the entire solar concentrator assembly (**100**). The at least one NIDC (**110**) acts as the primary concentrator for reflecting the incident solar energy towards the at least one array of secondary concentrators (**120**) and then towards at least one concentrator photovoltaic receiver (**170**). The truss member assembly with the NIDC (**110**) is attached to the at least one pedestal (**150**) with the help of at least one gearbox (**140**). The at least one gearbox (**140**) is preferably fixed on the at least one pedestal (**150**). The truss member assembly with the NIDC (**110**) can be tilted by the rotational movement of the at least one gearbox (**140**). For effectively improving the efficiency in collecting the incident sunlight during daytime, the NIDC (**110**) is tilted by operating the at least one gearbox (**140**). The at least one gearbox (**140**) is operated to orient the NIDC (**110**) towards the direction of maximum sunlight during daytime for receiving maximum sunlight onto the NIDC (**110**).

[0030] The NIDC (**110**) includes a plurality of flat facet mirrors arranged to form an array. The plurality of flat facet mirrors are arranged to form an arc-shaped NIDC (**110**), in which the peripheral flat facet mirrors are positioned at a higher level than the centrally located flat facet mirrors. This type of configuration allows for avoiding sunlight blocking and shadowing among adjacent mirrors. The arc-shaped NIDC (**110**) is attached to the at least one gearbox (**140**) utilizing at least one rotational axial joint means. The concentrator photovoltaic receiver (**170**) and the array of secondary concentrators (**120**) are positioned at a predetermined height depending on the size and shape of the arc-shaped NIDC (**110**). The array of secondary concentrators (**120**) includes an array of crossed compound parabolic concentrators (**120**) positioned below the concentrator photovoltaic receiver (**170**). The array of crossed compound parabolic concentrators (**120**) and the concentrator photovoltaic receiver (**170**) are held in position with the help of at least one structural support means (**130**). The sunrays are incident (**180**) on the NIDC (**110**), which concentrates the solar energy and a plurality of reflected rays (**190**) are focused to the array of secondary concentrators (**120**) or secondary optics and subsequently to the concentrator photovoltaic receiver (**170**). Thus the amount of incident solar energy per unit area can be increased by using the primary concentrator (**110**) and the array of secondary concentrators (**120**). Thereby each CPV cell of the concentrator photovoltaic receiver (**170**) generates more electrical energy via converting incident solar energy to electrical energy. The arrangement of the primary concentrator such as the NIDC (**110**) allows for more efficient generation of electricity by eliminating sunlight blocking and shadowing effects as well as by minimizing the gap between adjacent facets.

[0031] FIG. **2** illustrates a schematic diagram showing the NIDC (**110**) comprising the plurality of flat facet mirrors (**160**) arranged to form an array according to a preferred embodiment of the present invention. The NIDC (**110**) includes a plurality of flat facet mirrors (**160**) arranged into any form of array. However, FIG. **2** illustrates an exemplary illustration of one possible arrangement of the array of a plurality of flat facet mirrors (**160**). Embodiments of the invention include the plurality of flat facet mirrors (**160**) arranged to form arrays of different shapes and sizes to build the NIDC (**110**). Each flat facet mirror (**160**) is tilted at certain angle in such a way that all the solar images formed by the plurality of flat facet mirrors (**160**) forming the array are superimposed at a destined target, i.e. the entrance surface of array of secondary concentrators (**120**). The height of flat facet mirrors (**160**) are gradually increased from central to peripheral position of the NIDC (**110**) to avoid sunlight blocking and shadowing among adjacent mirrors. Above the NIDC (**110**), there are an array of crossed compound parabolic concentrators (**120**) and concentrator photovoltaic receiver (**170**). The crossed compound parabolic concentrators (**120**) are arranged in 2-D array in such a way that the array dimension is almost same as that of focused solar images formed by NIDC (**110**). The plurality of flat facet mirrors (**160**) positioned at the central region of the NIDC (**110**) is removed so that there is no shadowing from the concentrator photovoltaic receiver (**170**) and the array of secondary concentrators (**120**) cast on any of the facet mirrors. The concentrator photovoltaic receiver (**170**) and the array of secondary concentrators (**120**) are positioned at a predetermined height depending on the size and shape of the arc-shaped NIDC (**110**). The detailed description of the array of crossed compound parabolic concentrators (**120**) is presented in FIGS. **9** and **10**.

[0032] FIG. **3** illustrates a top view of the NIDC (**110**) according to a preferred embodiment of the present invention. The NIDC (**110**) does not follow any specific geometry. The NIDC (**110**) follows a computer generated geometry based on a specially designed computational method or algorithm or computer program operational steps as described in the following FIG. **6**. The NIDC (**110**) employs many identical square or rectangular facet mirrors (**160**) acting as optical aperture to gather the solar irradiance from the sun and to superimpose all the solar images at entrance surface of the array of secondary concentrators (**120**). In a preferred embodiment of the invention, the NIDC (**110**) consists of 2m×2n array of the plurality of identical flat facet mirrors (**160**) arranged at different height to eliminate sunlight blocking and shadowing effects as well as to minimize the gap between the adjacent facets. The concentrator photovoltaic receiver (**170**) and the array of secondary concentrators (**120**) are arranged at an elevated position above the NIDC (**110**). When sunlight falls on this arrangement a shadowing effect is produced and the plurality of flat facet mirrors (**160**) which are affected by the shadowing caused by the concentrator photovoltaic receiver (**170**) and the array of secondary concentrators (**120**) are removed. In addition, embodiments of the present invention, the NIDC (**110**), can also have a higher or lower solar concentration ratio by simply increasing or decreasing the total number of flat facet mirrors (**160**).

[0033] FIG. **4** illustrates a schematic diagram showing how the reflected sunrays (**190**) are focused by the NIDC (**110**) onto the entrance surface of the secondary concentrator (**120**) and subsequently reaching the concentrator photovoltaic receiver (**170**) in the cross-sectional view. The plurality of flat facet mirrors (**160**) is packed together with minimum amount of gap between the adjacent mirrors. The heights of flat facet mirrors (**160**) are increased gradually from central to periph-

eral position of the NIDC (**110**) using suitable mechanical means. The purpose of plurality of flat facet mirrors (**160**) positioned at different levels is to effectively avoid sunlight blocking and shadowing among adjacent flat facet mirrors (**160**). Hence this arrangement of flat facet mirrors (**160**) can maximize the amount of effective sunlight falling on the facet mirrors (**160**) and reflecting to entrance surface of the array of secondary concentrators (**120**). The NIDC (**110**) formed by the array of plurality of flat facet mirrors (**160**) superimposes the solar images formed by individual facet mirrors (**160**) onto entrance surface of the array of the crossed compound parabolic concentrators (**120**) i.e. the secondary concentrators (**120**). The arc-shaped of the NIDC (**110**) formed by the array of the plurality of flat facet mirrors (**160**) arranged at different height helps in superimposing the solar images formed by individual facet mirrors (**160**) onto entrance surface of the secondary concentrators (**120**) and thereafter to the concentrator photovoltaic receiver (**170**). The light concentrated by the primary concentrator (**110**) is further concentrated by the array of secondary concentrators (**120**) before reaching the concentrator photovoltaic receiver (**170**).

[0034] FIG. **5**(*a*) illustrates the Cartesian coordinate system in 3-D representing a coordinate (M_x, M_y, M_z), incident angle (θ_{ij}) and a pair of tilted angles (σ,γ) of a i,j-facet mirror (**160**) where F is the focal distance of the NIDC (**110**) and the origin 'O' is center of the concentrator frame. The locality of each facet mirror (**160**) on the NIDC (**110**) can be indexed as (i, j), where i and j represent the position of the facet mirror (**160**) at i-th row and j-th column of the NIDC (**110**) respectively. $\vec{I}$ is unit vector of the incident sunray (**180**), $\vec{N}_{i,j}$ is unit vector of the normal of i,j-facet mirror (**160**), $\vec{R}_{i,j}$ is unit vector of the reflected sunray (**190**) of i,j-facet mirror. The NIDC (**110**) employs the plurality of identical square or rectangular flat facet mirrors (**160**) acting as optical aperture to gather the solar irradiance from the sun and to superimpose all the images at the receiver. The NIDC (**110**) consists of 2m×2n array of identical flat facet mirrors (**160**) arranged at different height to eliminate sunlight blocking and shadowing effects as well as to minimize the gap between the adjacent facets. In FIG. **5**(*a*), the central line of the NIDC (**110**) starting from the origin denoted as 'O' and lies along the row direction is defined as x-axis. The central line of the NIDC (**110**) from the origin 'O' lies along the column direction is defined as y-axis. Lastly, z-axis is defined from the origin 'O' pointing to the target direction that is also perpendicular to both the x-axis and y-axis. The flat facet mirrors (**160**) in the NIDC (**110**) are fixed at two tilted angles to superimpose the plurality of sunrays (**180**) incident on the NIDC (**110**) onto the array of secondary concentrators (**120**) and then to the concentrator photovoltaic receiver (**170**) associated with the solar concentrator assembly (**100**). The two tilted angles of i,j-facet mirror are represented by, σ is a tilted angle about y-axis, and γ is a tilted angle about x-axis. The angles can be expressed as

$$\sigma = \sin^{-1}\left(\frac{M_x}{2\cos\theta_{i,j}\sqrt{M_x^2 + M_y^2 + (F - M_z)^2}}\right)$$

$$\gamma = \tan^{-1}\left(\frac{M_y}{(F - M_z) + \sqrt{M_x^2 + M_y^2 + (F - M_z)^2}}\right)$$

where M_x, M_y, M_z are the global coordinate of the central point of i,j-facet mirror (**160**) in x-axis, y-axis, z-axis respectively, F is the distance between the center of entrance aperture of the array of secondary concentrators (**120**) and the origin 'O' that is the center of the concentrator frame, which is also known as the focal distance of NIDC (**110**). The incident angle $\theta_{i,j}$ of the sunrays (**180**) can be expressed as

$$\theta_{i,j} = \left[\frac{1}{2}\tan^{-1}\left(\frac{\sqrt{M_x^2 + M_y^2}}{F - M_z}\right)\right]$$

To achieve perfect optical efficiency for transferring the entire reflected rays (**190**) from the facet mirrors (**160**) to the entrance surface of the array of secondary concentrators (**120**), the sunlight blocking and shadowing effects among adjacent facet mirrors (**160**) need to be eliminated. This is done according to a preferred embodiment of the present invention by designing the plurality of facet mirrors (**160**) with gradually increased height along z-direction from the center to the edge of primary concentrator (**110**). Moreover, gaps between the facet mirrors (**160**), G, are also minimized to optimize the total collective area of the primary concentrator or the NIDC (**110**). The locations of facet mirrors (**160**) are computed in both directions along x and y axes to minimize the gap among the facet mirrors (**160**) at a certain distance. FIG. **5**(*b*) shows the initial facet mirror's configuration of the non-imaging dish concentrator (**110**). The concentrator can be divided into four quadrants which are the top-right, top-left, bottom-right and bottom-left.

[0035] FIG. **6** is a flow chart to illustrate how the special computational method or algorithm or computer program operational steps can compute the geometry of the plurality of flat facet mirrors (**160**) in designing the new arc-shaped geometry of NIDC (**110**). According to FIG. **5**(*b*), all facet mirrors in the NIDC (**110**) can be sub-divided into four major quadrants and the origin 'O' is located at the center of the NIDC (**110**). Since the geometrical configuration of facet mirrors (**160**) in the four quadrants is symmetry to each other, the computational algorithm only needs to consider any of the four quadrants in the process of designing the geometry of primary concentrator i.e. the NIDC (**110**) to save the computational time. Therefore, the top-right quadrant of the primary concentrator (**110**) is chosen as a reference for computing the geometry of the NIDC (**110**). Referring to FIG. **5**(*b*), the facet mirror (**160**) located closest to the origin is defined as $M_{1,1}$ and the facet mirror (**160**) located furthest from the origin is defined as $M_{m,n}$, provided that m is the number of column and n is the number of row in the top-right quadrant of the NIDC (**110**). For a convenience of the computational method or algorithm or computer program operational steps in designing the geometry of the NIDC (**110**), a plurality of flat facet mirrors (**160**) is first assumed to be arranged in an array form, where the pivot points for all the facet mirrors (**160**) are defined in the same horizontal plane or in the same height and the orientations of all facet mirrors (**160**) are aligned for superimposing solar images onto the target. In such an arrangement, sunlight blocking and shadowing among adjacent facet mirrors (**160**) are more serious for the facet mirrors (**160**) located further from the central region. Then, according to the computational method or algorithm or computer program operational steps, each of the facet mirrors (**160**) is virtually lifted up one by one from the central toward the

peripheral region of concentrator frame along the x, y, and z directions in order to eliminate the sunlight blocking and shadowing effects while keeping fixed gaps among the facet mirrors (**160**). The final positions of the facet mirrors (**160**) that form a dish will be different from that of the initially defined position in the horizontal plane and the process to determine new mirror positions will cause the variation in the tilted angles of the facet mirrors (**160**) as to maintain the solar images aiming at the target or the array of secondary concentrators (**160**). Hence, in the process of designing the new geometry of the NIDC (**110**), an iterative method is used to calculate the final position as well as the two tilted angles, σ and γ, of each facet mirror (**160**).

[0036] FIG. **7** shows (a) Side view in y-z direction (b) Side view in x-z direction to illustrate the conceptual drawing on how to compute the position of each flat facet mirror (**160**) and to design the arc-shaped geometry of the non-imaging dish concentrator (**110**) using a special computational method or algorithm or computer program operational steps. The computational algorithm starts with defining the initial positions of all facet mirrors (**160**) at the same height and then obtains final positions of facet mirrors (**160**) one by one from the central region towards the peripheral region with gradually increased height as to eliminate sunlight blocking and shadowing among adjacent mirrors (**160**) as well as to minimize the gap between adjacent mirrors (**160**) according to an embodiment of the present invention. This computational algorithm will start to compute final positions of the facet mirrors (**160**) located at the first column, i=1 with row sequence starting from j=1 to j=n. The same procedure is also continued for the following column from i=2 to i=m. The detail of method or algorithm or computer program operational steps to compute the configuration of the facet mirrors (**160**) in the NIDC (**110**) is summarized in the flow chart as shown in FIG. **6**. Let G_i is initial gap between the facet mirrors (**160**) and G is the final gap between the facet mirrors (**160**) obtained from the special computational algorithm.

[0037] FIG. **8** shows the numerical simulation result of solar flux distribution with maximum solar concentration ratio of 435 suns for the case of 22×22 array of facet mirrors (**160**) with each facet dimension of 49.8 cm×49.8 cm and focal distance of 10 m in 3D plot. It is an example of simulated solar flux distribution plot focused by the NIDC (**110**) on entrance surface of array of secondary concentrators (**120**) using ray-tracing technique according to a preferred embodiment of the present invention. From the FIG. **8**, it is clear that each facet mirror (**160**) reflects the incident solar irradiance towards the array of secondary concentrators (**120**) and then to the photovoltaic receiver (**170**).

[0038] FIG. **9** illustrates a schematic diagram showing a cross-sectional view of the arrangement of the array of secondary concentrators (**120**) and the concentrator photovoltaic receiver (**170**). The concentrator photovoltaic receiver (**170**) consists of concentrator photovoltaic cells (**230**), concentrator photovoltaic cell substrates (**240**) and the heat sink (**280**). The secondary concentrator (**120**) is a crossed compound parabolic concentrator (**120**) that is preferably a solid body made from transparent material with high refractive index such as silica in order to increase the acceptance angle of the secondary concentrator (**120**). An array of crossed compound parabolic concentrators (**120**) is proposed as the secondary concentrators (**120**) or lenses due to the geometry allowing high acceptance angle in which the plurality of reflected rays (**190**) may encounter total internal reflection after transmitting into the crossed compound parabolic concentrators (**120**) before absorbed by the concentrator photovoltaic cell (**230**). FIG. **9** also shows a functional side view of the crossed compound parabolic concentrators (**120**) with three exemplary light rays namely **190**, **260**, and **270**, respectively going through three continuous optical phenomena including refraction at the entrance, total internal reflection at the lens interface and absorption by the concentrator photovoltaic cell (**230**). The concentrator photovoltaic cell (**230**) is bonded to a heat conductive substrate (**240**). A clear encapsulant (**220**) is employed to optically couple between the exit face (**210**) of the crossed compound parabolic concentrator (**120**) and the concentrator photovoltaic cell (**230**).

[0039] 'α' is defined as the maximum incident angle relative to the normal of entrance surface of crossed compound parabolic concentrator (**120**) in which the incident ray can still be directed to the exit surface of crossed compound parabolic concentrator (**120**). Here '2α' is the maximum acceptance angle of the crossed compound parabolic concentrator (**120**). The maximum acceptance angle, '2α', must be at least four times of the largest incident angle, '$4\theta_{i,j}$', among all the flat facet mirrors (**160**) of the NIDC (**110**).

[0040] The entrance surface of plurality of second stage or secondary concentrators (**120**) is placed at the focal plane of first stage or primary concentrator (**110**) in such a way that the plurality of second stage concentrators (**120**) further focuses the sunlight concentrated by first stage concentrator (**110**) onto the active area of the solar cell or the concentrator photovoltaic cell (**230**). The solar cell (**230**) converts the incident solar energy into electrical energy. As the amount of incident solar radiation on the solar cell (**230**) is increased the electric power generated is also increased.

[0041] FIG. **10** illustrates a schematic diagram showing (a) a trimetric view for an array of crossed compound parabolic concentrators (**120**). It is just an example of an array with 5×5 pieces secondary concentrators (**120**) but the real design is not limited to this number; and (b) a trimetric view for one of crossed compound parabolic concentrators (**120**). Each crossed compound parabolic concentrator (**120**) consists of two symmetrical compound parabolic concentrator troughs that intersect orthogonally. In various embodiments, the entrance face (**200**) and exit face (**210**) of the crossed compound parabolic concentrator (**120**) can be either rectangular or square in shape dependent on both the dimension of the solar cell (**230**) and the distance between adjacent solar cells (**230**). The largest tilted angle of the flat facet mirror (**160**) of the NIDC (**110**) will determine the acceptance angle of the crossed compound parabolic concentrator (**120**). The area and size of the exit face (**210**) of the crossed compound parabolic concentrator (**120**) is determined in such a manner to match with the size of the concentrator photovoltaic cell (**230**) of the concentrator photovoltaic receiver (**170**).

[0042] FIG. **11** is a flow chart to illustrate a method of operating the solar concentrator assembly (**100**) of the solar electrical power generation system for optimizing efficiency of solar power generation. The method comprises the steps of providing the solar concentrator assembly (**100**) having at least one primary concentrator (**110**), at least one array of secondary concentrators (**120**) and at least one concentrator photovoltaic receiver (**170**) as shown in block **300**. The whole solar concentrator assembly (**100**) is tilted using at least one gear assembly (**140**) to collect maximum amount of sunlight. Then the incident sunlight on the plurality of flat facet mirrors (**160**) of the primary concentrator (**110**) is reflected towards

the destined target. Now as indicated in block **310**, a plurality of reflected rays (**190**) from the at least one primary concentrator (**110**) are superimposed and thereafter directed and focused onto the at least one concentrator photovoltaic receiver (**170**) via at least one array of crossed compound parabolic concentrators (**120**) acting as secondary concentrators (**120**) as shown in block **320**. Finally, as in block **330**, the solar energy is converted to electrical energy by the at least one concentrator photovoltaic receiver (**170**).

[0043] The at least one primary concentrator (**110**) of the solar concentrator assembly (**100**) is non-imaging dish concentrator (**110**) which comprises of a plurality of flat facet mirrors (**160**). The plurality of flat facet mirrors (**160**) are arranged for superimposing plurality of mirror images onto entrance surface of the at least one array of secondary concentrators (**120**). Each plurality of flat facet mirrors (**160**) is arranged at a plurality of levels from central region to peripheral region of the NIDC (**110**) for effectively superimposing the plurality of mirror images onto entrance surface of the array of secondary concentrators (**120**) without sunlight blocking and shadowing on each other. The at least one array of secondary concentrators (**120**) comprises of a plurality of crossed compound parabolic concentrators (**120**) arranged to form a 2D array to match with the size and shape of concentrated solar irradiance formed by the NIDC (**110**). The plurality of crossed compound parabolic concentrators (**120**) forms a plurality of optical funnels having larger area on the entrance surface and smaller area on the exit surface. The larger area on the entrance surface and smaller area on the exit surface allows more spacing among the solar cells (**230**) located at the exit surface for optimal inter-connection of a plurality of solar cells (**230**) in series and/or in parallel forming the concentrator photovoltaic receiver (**170**). The plurality of crossed compound parabolic concentrators (**120**) efficiently concentrates the solar energy to an active areas of array of solar cells (**230**) in a manner of one crossed compound parabolic concentrator (**120**) coupled to one solar cell (**230**). In addition, the at least one array of secondary concentrators (**120**) increases an acceptance angle thereby allowing a higher tolerance to pointing error of sun-tracking of the solar concentrator assembly (**100**). The arc-shaped geometry of the non-imaging dish concentrator (**110**) is designed by using the computational method or algorithm or computer program operational steps as described in FIG. **6** so that it is capable of projecting a reasonably uniform and rectangular pattern of concentrated sunlight onto entrance surface of the array of secondary concentrators (**120**). This result in an optimal and efficient generation of electrical energy compared to the existing solar power generation systems.

[0044] The preferred commercial applications of the solar concentrator assembly (**100**) according to embodiments of the present invention includes use in solar power plant in large scale where multiple units of the solar concentrator assembly (**100**) are arranged and operated in parallel for generating large amount of electrical power. In addition, the solar concentrator assembly (**100**) is employed in building retrofit system for producing electrical power and hot water for domestic usage. For the above application, the solar concentrator assembly (**100**) can be used as grid-connected concentrator photovoltaic system. For off-grid application, solar concentrator assembly (**100**) can also be used as an isolated power generation system for telecommunication tower, street lighting, light house for navigation, etc. Another principal application of the solar concentrator assembly (**100**) is the use in power generation station in rural area, which is usually far from power grid.

[0045] The foregoing description of the specific embodiments will so fully reveal the general nature of the embodiments herein that others can, by applying current knowledge, readily modify and/or adapt for various applications such specific embodiments without departing from the generic concept, and, therefore, such adaptations and modifications should and are intended to be comprehended within the meaning and range of equivalents of the disclosed embodiments. It is to be understood that the phraseology or terminology employed herein is for the purpose of description and not of limitation. Therefore, while the embodiments herein have been described in terms of preferred embodiments, those skilled in the art will recognize that the embodiments herein can be practiced with modification. However, all such modifications are deemed to be within the scope of the claims.

1. A solar concentrator assembly (**100**) of a solar electrical power generation system comprises:

- at least one primary concentrator (**110**) arranged to receive and reflect a plurality of sunrays (**180**), the at least one primary concentrator (**110**) being a non-imaging dish concentrator (NIDC) (**110**) attached to the at least one pedestal (**150**) with the help of at least one gearbox (**140**);
- at least one concentrator photovoltaic receiver (**170**) associated with the solar concentrator assembly (**100**) for converting solar energy to electrical energy;
- at least one array of secondary concentrators (**120**) for focusing and thereafter directing solar energy to the at least one concentrator photovoltaic receiver (**170**); and
- at least one structural support means (**130**) for supporting the array of secondary concentrators (**120**) and the concentrator photovoltaic receiver (**170**).

2. The solar concentrator assembly (**100**) as claimed in claim **1** wherein the non-imaging dish concentrator (**110**) includes a plurality of flat facet mirrors (**160**), and the plurality of flat facet mirrors (**160**) is capable of being arranged into a plurality of forms to create at least one array.

3. The solar concentrator assembly (**100**) as claimed in claim **1** wherein the plurality of flat facet mirrors (**160**) is capable of being tilted at an angle to gather solar irradiance from the sun and thereafter superimposing a plurality of solar images formed by the flat facet mirrors (**160**) at a predefined target to produce reasonably uniform solar irradiance, the predefined target being the entrance surface of the array of secondary concentrators (**120**).

4. The solar concentrator assembly (**100**) as claimed in claim **1** wherein a new non-imaging geometry of the NIDC (**110**) is based on a computer generated geometry determined using at least one method created by a special computational method.

5. The solar concentrator assembly (**100**) as claimed in claim **1** wherein the plurality of flat facet mirrors (**160**) of the NIDC (**110**) is arranged at a plurality of levels for minimizing gap between adjacent flat facet mirrors (**160**).

6. The solar concentrator assembly (**100**) as claimed in claim **1** wherein the plurality of flat facet mirrors (**160**) of the NIDC (**110**) is arranged at a plurality of levels for eliminating sunlight blocking and shadowing effects among adjacent flat facet mirrors (**160**).

7. The solar concentrator assembly (**100**) as claimed in claim **1** wherein the non-imaging dish concentrator (**110**) is

supported on the at least one pedestal structure (**150**), the at least one pedestal structure (**150**) supports a weight of the solar concentrator assembly (**100**).

8. The solar concentrator assembly (**100**) as claimed in claim **1** wherein the non-imaging dish concentrator (**110**) can be tilted by rotational movement towards the plurality of sunrays (**180**) with maximum intensity by employing the at least one gearbox (**140**) coupled with the non-imaging dish concentrator (**110**), the at least one gearbox (**140**) is supported on the at least one pedestal structure (**150**).

9. The solar concentrator assembly (**100**) as claimed in claim **1** wherein the at least one non-imaging dish concentrator (**110**) concentrates the plurality of sunrays (**180**) by directing a plurality of reflected rays (**190**) towards the at least one array of secondary concentrators (**120**) and then subsequently towards the at least one concentrator photovoltaic receiver (**170**).

10. The solar concentrator assembly (**100**) as claimed in claim **9** wherein the at least one array of secondary concentrators (**120**) includes an array of crossed compound parabolic concentrators (**120**) acting as lenses with high acceptance angle, each crossed compound parabolic concentrator (**120**) is a solid body made of transparent material such as silica; wherein the plurality of reflected rays (**190**) may encounter total internal reflection after transmitting into the crossed compound parabolic concentrators (**120**).

11. The solar concentrator assembly (**100**) as claimed in claim **10** wherein the at least one array of crossed compound parabolic concentrators (**120**) acting as secondary concentrators (**120**) guide the plurality of sunrays (**180**) onto active areas of solar cells (**230**) of the at least one concentrator photovoltaic receiver (**170**).

12. The solar concentrator assembly (**100**) as claimed in claim **1** wherein the at least one array of secondary concentrators (**120**) directs the plurality of reflected rays (**190**) to the at least one concentrator photovoltaic receiver (**170**) for transforming solar energy to electrical energy.

13. The solar concentrator assembly (**100**) as claimed in claim **1** wherein the at least one non-imaging dish concentrator (**110**) is held in position with the at least one concentrator photovoltaic receiver (**170**) and at least one array of secondary concentrators (**120**) by employing the at least one of structural support means (**130**).

14. A method of converting solar energy into electrical energy utilizing a solar concentrator assembly (**100**) of a solar electrical power generation system, the method comprising the steps of:

providing the solar concentrator assembly (**100**) having at least one primary concentrator (**110**), at least one array of secondary concentrators (**120**) and at least one concentrator photovoltaic receiver (**170**);

receiving a plurality of sunrays (**180**) incident on at least one array of a plurality of flat facet mirrors (**160**) forming the at least one primary concentrator (**110**);

superimposing the plurality of reflected rays (**190**) from the at least one primary concentrator (**110**) onto the at least one array of secondary concentrators (**120**);

directing and focusing the plurality of reflected rays (**190**) onto the at least one concentrator photovoltaic receiver (**170**) by utilizing at least one array of crossed compound parabolic concentrators (**120**) as secondary concentrators (**120**); and

converting solar energy to electrical energy by the at least one concentrator photovoltaic receiver (**170**).

15. The method of converting solar energy into electrical energy as claimed in claim **14** wherein the at least one primary concentrator (**110**) is a non-imaging dish concentrator (**110**).

16. The method of converting solar energy into electrical energy as claimed in claim **14** wherein the at least one non-imaging dish concentrator (**110**) comprises plurality of flat facet mirrors (**160**), the plurality of flat facet mirrors (**160**) being arranged for superimposing plurality of mirror images at entrance surface of the at least one array of secondary concentrators (**120**) without sunlight blocking and shadowing on each other.

17. The method of converting solar energy into electrical energy as claimed in claim **16** wherein the plurality of flat facet mirrors (**160**) being arranged at a plurality of levels from central position of the non-imaging dish concentrator (**110**) to peripheral position for effectively superimposing the plurality of mirror images on entrance surface of the array of secondary concentrators (**120**) without sunlight blocking and shadowing among adjacent facet mirrors.

18. The method of converting solar energy into electrical energy as claimed in claim **14** wherein the at least one array of secondary concentrators (**120**) comprises a plurality of crossed compound parabolic concentrators (**120**) arranged to form at least one array.

19. The method of converting solar energy into electrical energy as claimed in claim **18** wherein the plurality of crossed compound parabolic concentrators (**120**) forms a plurality of optical funnel having a larger area on an entrance surface and a smaller area on an exit surface.

20. The method of converting solar energy into electrical energy as claimed in claim **18** wherein the plurality of crossed compound parabolic concentrators (**120**) having the larger area on the entrance surface and the smaller area on the exit surface allows more spacing for optimal inter-connection of a plurality of solar cells (**230**) of the concentrator photovoltaic receiver (**170**) located at the exit surface in series and/or in parallel for minimizing current mismatch loss.

21. The method of converting solar energy into electrical energy as claimed in claim **18** wherein the plurality of crossed compound parabolic concentrators (**120**) having the larger area on the entrance surface and the smaller area on the exit surface allows a plurality of solar cells (**230**) of the concentrator photovoltaic receiver (**170**) receiving higher intensity of solar irradiance with the ratio dependent on the entrance surface area to exit surface area.

22. The method of converting solar energy into electrical energy as claimed in claim **18** wherein each of the plurality of crossed compound parabolic concentrators (**120**) efficiently concentrates the solar energy to an active area of each solar cell (**230**) in the concentrator photovoltaic receiver (**170**).

23. The method of converting solar energy into electrical energy as claimed in claim **14** wherein the at least one array of secondary concentrators (**120**) increases an acceptance angle thereby allowing a higher tolerance to pointing error of sun-tracking of the solar concentrator assembly (**100**).

24. The method of converting solar energy into electrical energy as claimed in claim **14** wherein the at least one non-imaging dish concentrator (**110**) is capable of projecting reasonably uniform irradiance and either square or rectangular pattern of concentrated sunlight onto entrance surface of the at least one array of secondary concentrators (**120**).

* * * * *

APPENDIX C

Dense-Array Concentrator Photovoltaic System Using Non-Imaging Dish Concentrator and Crossed Compound Parabolic Concentrator

Kok-Keong Chong*, Tiong-Keat Yew, Chee-Woon Wong, Ming-Hui Tan, Woei-Chong Tan, An-Chow Lai, Boon-Han Lim, Sing-Liong Lau, Faidz Abdul Rahman

Faculty of Engineering and Science, Universiti Tunku Abdul Rahman, off Jalan Genting Kelang, Setapak, 53300 Kuala Lumpur, Malaysia

Abstract. Solar concentrating device plays an important role by making use of optical technology in the design, which can be either reflector or lens to deliver high flux of sunlight onto the Concentrator Photovoltaic (CPV) module receiver ranging from hundreds to thousand suns. To be more competitive compared with fossil fuel, the current CPV systems using Fresnel lens and Parabolic dish as solar concentrator that are widely deployed in United States, Australia and Europe are facing great challenge to produce uniformly focused sunlight on the solar cells as to reduce the cost of electrical power generation. The concept of non-imaging optics is not new, but it has not fully explored by the researchers over the world especially in solving the problem of high concentration solar energy, which application is only limited to be a secondary focusing device or low concentration device using Compound Parabolic Concentrator. With the current advancement in the computer processing power, we has successfully invented the non-imaging dish concentrator (NIDC) using numerical simulation method to replace the current parabolic dish as primary focusing device with high solar concentration ratio (more than 400 suns) and large collective area (from 25 to 125 m^2). In this paper, we disclose our research and development on dense array CPV system based on non-imaging optics. The geometry of the NIDC is determined using a special computational method. In addition, an array of secondary concentrators, namely crossed compound parabolic concentrators, is also proposed to further focus the concentrated sunlight by the NIDC onto active area of solar cells of the concentrator photovoltaic receiver. The invention maximizes the absorption of concentrated sunlight for the electric power generation system.

Keywords: non-imaging dish concentrator, crossed compound parabolic concentrator, optical analysis, concentrator photovoltaic, concentrating solar power, ray-tracing technique.
PACS: 42. Optics, 88.40fr Concentrator collectors, 88.40jp Multijunction solar cells, 42.79Ek Solar collectors and concentrators

INTRODUCTION

The cost of photovoltaic system is mostly associated with the cost of solar cell. This cost can be reduced by increasing the output power per unit solar cell and this could be done by replacing expensive solar cell with low cost optical material such as reflector or lens. The solar energy can be concentrated ranging from hundreds to thousand suns onto solar cell by a concentrator. The invention and development of much higher efficiency concentrator photovoltaic (CPV) cell compare to conventional photovoltaic cell had encouraged the development of concentrator systems. Furthermore, concentrator system can be more efficient when used in hybrid photovoltaic/thermal system which produces electricity and hot water simultaneously.

Current commercial CPV systems, using Fresnel lens and parabolic dish, are facing two great challenges: to produce uniform focused sunlight on the solar cells and to reduce the cost of solar concentrator. Recently, Chong et al. have been exploring different optical technology namely non-imaging optics aimed to produce much more reasonable uniform solar flux distribution cost effectively [1-3]. One of their inventions, non-imaging dish concentrator (NIDC), has been verified to be capable of producing uniform solar flux and is very suitable for the application of CPV system for minimizing current mismatch problem in the array of solar cells to achieve higher system efficiency [4-5]. NIDC consists of multiple identical square or rectangle facet mirror acting as optical apertures to gather the solar irradiance from the sun and to superimpose all the images at the common receiver.

On the other hand, compound parabolic concentrator (CPC) has been widely used in flat panel PV system as low concentration concentrator as it has a few advantages. One of the advantages is the use of CPC concentrator can

National Physics Conference 2014 (PERFIK 2014)
AIP Conf. Proc. 1657, 030009-1–030009-7; doi: 10.1063/1.4915159

eliminate the necessity of diurnal tracking of the sun with its big acceptance angle. CPC had been widely studied since the invention by Hinterberger and Winston in USA, Baranov and Melinikov in Soviet Union, and Ploke in Germany independently in 1970s. The detail studies had shown the geometry is giving the highest geometrical concentration ratio, thus the geometry is chosen for the design of the secondary concentrator in our study. A CPC lens can be formed by rotating the 2D CPC geometry around its axis of symmetry. The fabrication of solar cell in square or rectangle shape is not suitable to use with the CPC lens which the entrance and exit aperture of the CPC lens is circular. This problem can be improved by intersecting two symmetrical 2D CPCs orthogonally to form a crossed compound parabolic concentrator with square or rectangle entrance and exit aperture. The method had been adapted by Mammo et al. in UK and it was used as reflective concentrator for building integrated photovoltaic applications with low concentration [6].

Packing factor is defined as the percentage of active area of CPV per total module area. In the assembly of dense array CPV module, it is impossible to achieve 100 percent packing factor. This is due to the present of the physical connection required to connect the cells in series and parallel to produce a desirable power output as shown in Figure 1. The concentrated sunlight that fall on the area without active solar cell material will become loss to the system and thus reduce the system efficiency.

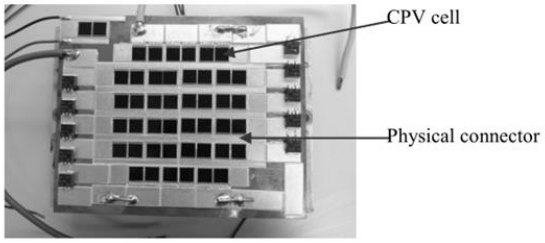

FIGURE 1. The assembly of dense array CPV module in University Tunku Abdul Rahman

In addition to the primary concentrator, a secondary concentrator namely crossed compound parabolic concentrator (CCPC) lens is proposed to further concentrate and guide the sunlight onto the active area of CPV cells. The introduction of the CCPC lens is to increase the absorption of the solar irradiance by the each solar cell. Although secondary concentrator is widely used and studied in a single cell CPV system such as Fresnel lens system but it is not widely discussed and studied for the application of dense-array CPV system. So we would like to propose the use of CCPC as secondary concentrator integrated with the primary concentrator, NIDC, for the application of dense array CPV system. Therefore the introduction of CCPC lens will act as an optical funnel as shown in Figure 2, which guides the sunlight falling on the non-active area of the CPV module onto the active area of CPV cells, in order to increase the absorption of sunlight by CPV cells. An array of CCPC lenses can be arranged closely to each other at the receiver of the dense-array concentrator system to further concentrator the sunlight onto the CPV cells and to increase the packing factor of dense-array CPV module.

Instead of utilizing hollow body with reflective wall for CCPC, a solid body filled with transparent dielectric CCPC lens working by the means of refraction and total internal reflection is proposed to be integrated with NIDC. The dielectric-filled CCPC has certain practical advantages. The acceptance angle of dielectric-filled CCPC is larger compared to that of hollow reflective CCPC with the same geometry. Total internal reflection is 100% efficient, whereas it is difficult to get more than about 90% reflectivity from metalized surfaces [7]. Sunlight reflected by NIDC arrives at entrance aperture of CCPC at various incident angles. CCPC designed with acceptance angle larger than the largest incident angle will be able to concentrate most of the sunlight onto the CPV cell.

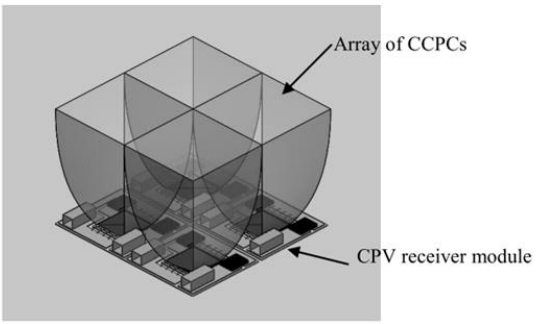

FIGURE 2. CCPC lens mounted on a single cell CPV module

NON-IMAGING DISH CONCENTRATOR (NIDC)

NIDC employs multiple identical square or rectangular facet mirrors acting as optical apertures to gather the solar irradiance from the sun and to superimpose all the images at the common receiver. The configuration of the facet mirrors is determined using a newly developed computational algorithm which finds the best configuration that will eliminate blocking and shadowing effects from the adjacent facet mirrors. This can be done by gradually increase the height of facet mirrors located from the central to peripheral region as shown in Figure 3. The NIDC discussed in this paper consists of 96 square facet mirrors with each facet 20 cm × 20 cm arranged into an array of 10×10 with 4 mirror in the central area is removed due to the blocking by the receiver mounted at the focal of the NIDC. The total reflective area formed is 3.84m^2 and the focal distance of the NIDC is 210 cm.

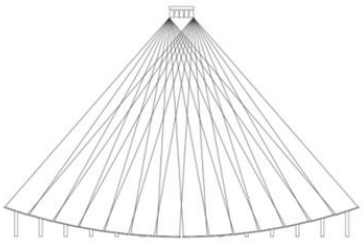

FIGURE 3. The configuration of facet mirrors of NIDC to prevent shadowing and blocking from adjacent mirror

DIELECTRIC FILLED CCPC GEOMETRY

CCPC is formed by intersecting two symmetrical 2D CPCs orthogonally. Therefore a CCPC with square entrance and exit aperture is formed to match the shape of solar cell. CCPC lens is a solid body filled with transparent substrate such as B270 glass. The CCPC lens is designed in a way to match the size and shape of solar cell and the incident angles of sunlight reflected by NIDC and incident on the secondary concentrator. In our study, the CCPC lens has square exit aperture, $2a'$, of 9.8 mm, which is slightly smaller than the dimension of the solar cell used. The CCPC geometry has half acceptance angle, θ_i', of 24.1° in free space. However, the angular half acceptance angle, θ_i, of CCPC lens becomes 37.77° due to dielectric medium B270 glass with refractive index, n, of 1.5. The refraction between the air and dielectric interface has significantly increased the angular half acceptance angle of CCPC lens. The size of entrance aperture, 2 a, can be calculated with Equation 1 and the length, L, of the lens is calculated with Equation 2. Therefore, the size of entrance aperture of the CCPC lens is 24.0 mm and the length is 37.78 mm.

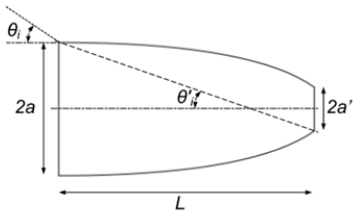

FIGURE 4. Schematic diagram of the geometry of 2-D CPC

$$2a = \frac{2a'}{\sin\theta'_i} \tag{1}$$

$$L = \frac{a'(1+\sin\theta'_i)\cos\theta'_i}{\sin^2\theta'_i} \tag{2}$$

The geometrical concentration ratio, CR, is given by Equation 3. CCPC lens in this study has geometrical concentration ration of 5.998.

$$CR = \left(\frac{a}{a'}\right)^2 = \left(\frac{1}{\sin\theta'_i}\right)^2 = \left(\frac{n}{\sin\theta_i}\right)^2 \tag{3}$$

Figure 5 shows the flow chart of the procedure to determine the geometry of CCPC lens. The size of the exit aperture of CCPC lens is determined according to the dimension of the solar cell used and follows by the half acceptance angle of CCPC lens according to the largest incident angle of light ray reflected from NIDC. Finally the entrance aperture size and height of CCPC lens is calculated according to the exit aperture size and half acceptance angle. Figure 6 shows the CCPC lens design with dielectric filled body.

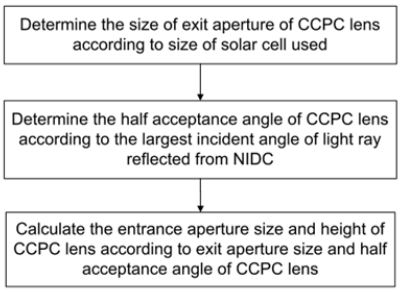

FIGURE 5. Flow chart shows the procedure of determining the geometry of CCPC lens during the design.

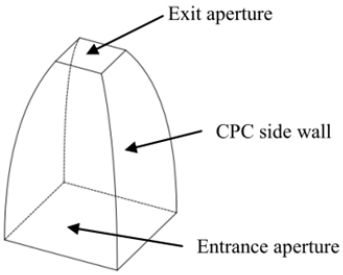

FIGURE 6. Crossed compound parabolic concentrator (CCPC) lens

The size of image formed by the NIDC is about 20 cm × 20 cm, hence an array of 8 × 8 CCPC lenses is arranged closely to each other where the total surface area of the entrance aperture formed can match the size of the image as shown in Figure 7. The entrance aperture surface plane is located at the focal plane of NIDC to collect concentrated sunlight from NIDC and then further focus them onto an array of 8 × 8 CPV cells.

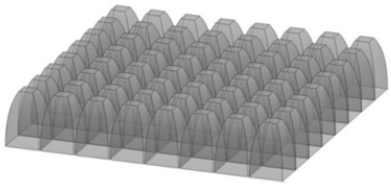

FIGURE 7. 8×8 array of CCPC lenses

SIMULATION AND ANALYSIS

Ray-tracing is carried out using the optical simulation software LightTools to investigate the behavior of light ray incident from 0° to 38.45°. All light rays with incident angle from 0° to 26° will be transmitted to the exit aperture. When the incident angle of light ray is more than 26°, some of the light rays will escape from the side walls that are near to the exit aperture without reaching the exit aperture as shown in Figure 8(c). The percentage of light rays escape gradually increases to 13.8% as the incident angle increases from 26° to 38.45°.

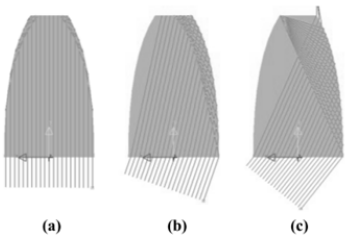

FIGURE 8. (a) 0° incidence angle (b) 19° incidence angle (c) 38.45° incidence angle

Figure 9 depicts schematic diagram of NIDC and the array of 8 × 8 CCPC lenses to show some light rays in the ray-tracing simulation using LightTools. A total of 12 million rays were traced in our simulation.

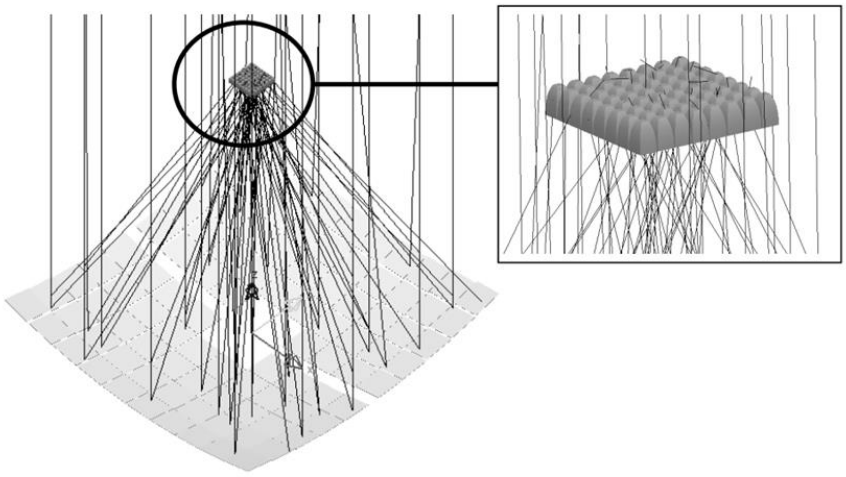

FIGURE 9. Ray-tracing model of NIDC with 8 × 8 array of CCPC lenses as secondary concentrator.

Figure 10 discloses the simulation result of solar flux distribution at the exit aperture of CCPC lens. The distribution of solar flux is not highly uniform and the value of parameter peak to average ratio (PAR) of the flux profile is 2.052. According to the study by Baig et al., the non-uniformity with PAR of 2 will not significantly reduce the fill factor of CPV cell [8]. Figure 11 illustrates the difference in IV characteristics of a multi-junction solar cell exposed to a uniform and non-uniform illumination obtained by Baig et al. in their study. Their measurement result shows that the fill factor difference between PAR of 1 and 1.95 is less than 0.01.

From our simulation result for NIDC with 8 × 8 array of CCPC lenses, the concentration ratio is 5.781 and 96.39% of energy will be transferred from entrance aperture to exit aperture. The total concentration ratio is 498.85.

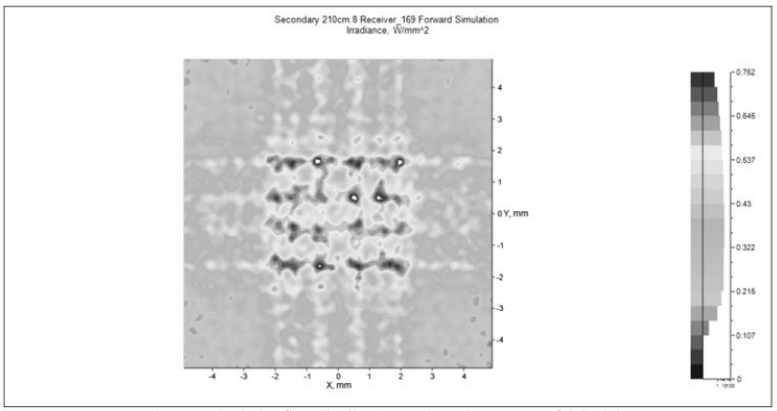

FIGURE 10. Solar flux distribution at the exit aperture of CCPC lens

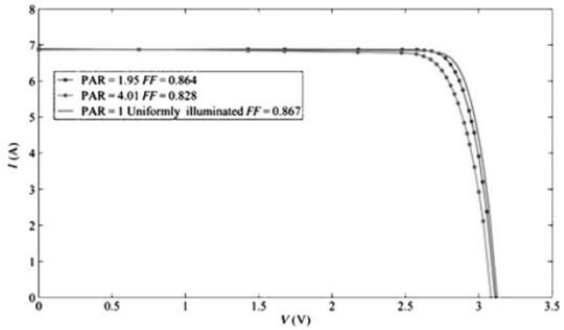

FIGURE 11. Difference curves of IV characteristics for a single multi-junction solar cell exposed to a uniform and non-uniform illumination by Baig et al. [8].

ACKNOWLEDGMENTS

The authors would like to express their gratitude to the Ministry of Energy, Green Technology and Water (AAIBE Trust Fund) and the Ministry of Science, Technology and Innovation (e-Science Fund with project number 03-02-11-SF0143) for their financial support. In addition, we are also grateful to Dr Wong Kok Fye from Dow Corning for supplying optical materials.

REFERENCES

1. M. H. Tan, K. K. Chong, C. W. Wong, *Applied Optics* **53(3)**, 475 (2014).
2. K. K. Chong, W. C. Wong, F. L. Siaw, T. K. Yew, *Journal of Solar Energy Engineering* **132: 011011**, 1-9 (2010).
3. K. K. Chong, F. L. Siaw, C. W. Wong, G. S. Wong, *Renewable Energy* **34**, 1364–1370 (2009).
4. K. K. Chong, C. W. Wong C, T. K. Yew, M. H. Tan, US Patent, Application no: 13/901,519 (pending) filed on 23rd May 2013.
5. K. K. Chong, T. K. Yew, M. H. Tan, US Patent, and Application no: 14/462,891 (pending) filed on 19th August 2014.
6. E. Mammo N. Sellami N, T. Mallick, "Performance analysis of a reflective 3D crossed compound parabolic concentrating photovoltaic system for building façade integration", Progress in Photovoltaics: Research and Applications. 2012.
7. R. Winston, J. Miñano, P. Benítez, W. Welford, *Nonimaging Optics*. 1st ed. Burlington, Mass.: Elsevier Academic Press; 2005.
8. H. Baig, K. Heasman, T. Mallick, *Renewable and Sustainable Energy Reviews* **16(8)**, 5890-5909 (2012).

APPENDIX D

Available online at www.sciencedirect.com

ScienceDirect

Solar Energy 120 (2015) 296–309

SOLAR ENERGY

www.elsevier.com/locate/solener

Performance study of crossed compound parabolic concentrator as secondary optics in non-imaging dish concentrator for the application of dense-array concentrator photovoltaic system

Tiong-Keat Yew, Kok-Keong Chong *, Boon-Han Lim

Lee Kong Chian Faculty of Engineering and Science, Universiti Tunku Abdul Rahman, Bandar Sungai Long, 43000 Kajang, Selangor, Malaysia

Received 29 March 2015; received in revised form 21 May 2015; accepted 7 July 2015
Available online 7 August 2015

Communicated by: Associate Editor Brian Norton

Abstract

Optical and electrical analyses of non-imaging dish concentrator (NIDC) with secondary concentrator for the application in dense-array concentrator photovoltaic (CPV) system are presented. Array of crossed compound parabolic concentrator (CCPC) lenses is selected as secondary concentrator due to high acceptance angle, larger entrance aperture to provide more space for high flexibility of inter-connection among CPV cells, and square exit aperture matching well with commercial CPV cell. Electrical performance of integrated CPV cells with CCPC lenses (CPV + CCPC) assembly module is analyzed for different pointing errors: 0°, 0.1°, 0.2°, 0.3° & 0.4°, and the results are compared to that of dense-array CPV (DACPV) module. It was found that overall electrical performance of CPV + CCPC assembly module is better than that of DACPV module despite using 77% less CPV cells than that of DACPV module.

Keywords: Crossed compound parabolic concentrator; Non-imaging dish concentrator; Concentrator photovoltaic; Ray-tracing; Secondary concentrator; Numerical simulation

1. Introduction

Concentrating solar power has been getting more important as an alternative green solution to reduce the cost of electrical and thermal power generation. The recent achievement in the technology of multi-junction concentrator photovoltaic (CPV) cell with conversion efficiency of more than 41% and still in the stage of improving have stimulated the development of concentrator optics (King et al., 2012). Solar concentrator with appropriate optical design is deployed to concentrate sunlight onto the CPV cell that is capable to work efficiently under highly concentrated solar irradiance for generating electricity (Zubi et al., 2009; Chong et al., 2013b). Solar concentrator made of less costly materials can offset the price of highly efficient CPV cell made from a more expensive semiconductor material so that the whole system can be more cost effective. Fresnel lens is one the most widely used optical devices in CPV system wherein each Fresnel lens focus sunlight onto a single CPV cell (Sonneveld et al., 2011; Ryu et al., 2006). One of the shortcomings of Fresnel lens CPV system is the incapability of capturing solar energy that is not converted to electricity. In this design, each solar cell is attached to a passive heat sink for rejecting the waste heat to surrounding without heat recapturing mechanism in order to maintain the cell at optimal operation

* Corresponding author. Tel.: +603-90860288; fax: +603-90198868.
E-mail addresses: chongkk@utar.edu.my, kokkeong_c@yahoo.com (K.-K. Chong).

http://dx.doi.org/10.1016/j.solener.2015.07.026
0038-092X/

temperature. For large point focus system, parabolic dish is employed to concentrate sunlight onto a receiver plane where either thermal convertor or CPV receiver can be placed for energy conversion. In the case of CPV receiver in dish system, active cooling system is required to maintain the operation temperature of CPV cell by circulating cooling fluid through the heat sink for heat removal. The waste heat collection via the cooling fluid can then be utilized for thermal applications or power generation. Therefore, the overall system efficiency is much higher as compared to that of flat PV panel or Fresnel lens CPV system, etc., when both electricity and thermal outputs are considered. In spite of parabolic dish system capable of generating both electrical and thermal power simultaneously, the nature of its optical property is not so suitable for the application of CPV system that requires uniform illumination (Baig et al., 2012). Parabolic dish is an imaging device that produces sharp, circular shape and non-uniform Gaussian distribution focusing spot.

To overcome the challenges faced by parabolic dish, Chong et al. invented a computer generated dish geometry that is constituted of many flat facet mirrors aimed to produce uniform focusing spot, non-imaging dish concentrator (NIDC) (Chong et al., 2012, 2013a, 2013b; Tan et al., 2014). Dense-array CPV (DACPV) receiver is placed at the focal plane of NIDC to convert concentrated sunlight into electricity. The assembling of DACPV module requires small gap among solar cells for interconnection both in parallel and series and thus there will be some physical area illuminated by concentrated sunlight without active solar cell material. Furthermore, the present of build-in bus bars on the surface of CPV cell (about 1 mm in both sides of CPV cell) has further increased non-active area of the incident surface. As a result, it is impossible to achieve 100% packing factor where the packing factor of the DACPV module is defined as the ratio of usable active area of solar cells to the total solar illumination area on the incident surface. Low packing factor will affect overall conversion efficiency of whole system since those concentrated sunlight fallen on non-active area of the receiver will not be converted to electricity. In this article, we would like to propose a method to increase the percentage of incident rays that impinge on the active area of solar cells by introducing a secondary concentrator. The solar cell is attached directly to the exit aperture of the secondary concentrator, which acts as optical funnel tailored to guide the concentrated sunlight from primary concentrator to solar cells. In addition, the introduction of secondary concentrator can provide more space for the interconnection among solar cells that allow more flexibility in the ways to connect solar cells in both series and parallel for minimizing the current mismatch in the circuitry of DACPV cells. Each CPV cell can also have individual bypass diode for protecting the cell and improving the fill factor of the CPV system.

Compound parabolic concentrator (CPC) was first invented by Welford and Winston (1978). CPC is a type of non-imaging concentrators that can concentrate all the incident sunrays from the entrance aperture within the acceptance angle to the exit aperture. Compound parabolic concentrator had long been used as solar collector for both photovoltaic and thermal application (Mallick et al., 2004; Oommen and Jayaraman, 2002). As most of the commercially available CPV cells are in the shape of either square or rectangle, the design of secondary concentrator must take the shape of receiver into consideration. Mammo et al. (2012), Sellami et al. (2010), Sellami and Mallick (2013) and Baig et al. (2014) discussed on how to match exit aperture of a reflective 3-D crossed compound parabolic concentrator (CCPC) to a solar cell in both size and shape. Micheli et al. (2014) had discussed technical issues and challenges in the fabrication of densely packed concentrating photovoltaic receiver in which one compound parabolic concentrator coupled with a homogenizer is placed onto each cell but there was no detailed study on the optical design. In our study, an array of 3-D dielectric filled CCPCs as secondary concentrator with each of them coupled to a single CPV cell to form a good optical combination with NIDC was proposed and filed for patent (Chong et al., 2012, 2013a, 2013b, 2014a, 2014b, 2014c). In this paper, both optical and electrical performances of integrated optical system of NIDC and dielectric filled CCPC have been analyzed and studied in the application of CPV system. Then, the performance of integrated optical system is compared with that of NIDC without secondary concentrator in DACPV system.

2. System description

2.1. Primary optics: Non-imaging dish concentrator

Non-imaging dish concentrator (NIDC) with the aim of producing uniform flux distribution across rectangular focusing spot was first proposed by Chong et al. and further analyzed by Tan et al. (Chong et al., 2012, 2013a, 2013b, 2014a, 2014b, 2014c; Tan et al., 2014). Fig. 1 shows primary concentrator NIDC comprised of ninety-six identical flat facet mirrors acting as optical apertures to gather solar irradiance from the sun and to superimpose all the facet images at the focal plane to form a primary focused image. The geometrical configuration of the facet mirrors is determined using a newly developed computational algorithm, which is capable to eliminate blocking and shadowing effects among the adjacent facet mirrors (Chong et al., 2012, 2013a, 2013b; Tan et al., 2014). It can be done by gradually increasing the height of facet mirrors located from the central to peripheral regions. The optical configuration of facet mirrors forms a reflective surface of dish contour. In the study, we consider NIDC configuration consisted of an array 10×10 facet mirrors with a dimension of $20\ \text{cm} \times 20\ \text{cm}$ each and four facet mirrors in the central region are omitted due to shadowing by the receiver. The total reflective area of the NIDC is $3.84\ \text{m}^2$, projection area of the facet mirrors is $3.76\ \text{m}^2$ and the focal distance of the NIDC is 210 cm. Sun-tracking system is

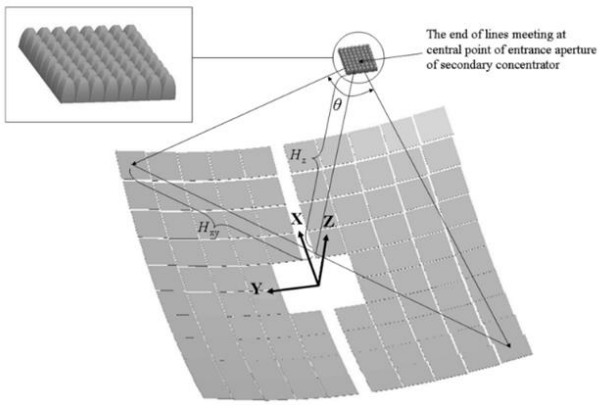

Fig. 1. Schematic diagram to show an integrated optical system consisted of two major elements: the primary concentrator, non-imaging dish concentrator (NIDC) and secondary concentrator, an array of dielectric filled crossed compound parabolic concentrator, where the rim angle of NIDC is defined as θ.

employed to ensure incident sunlight always aligned with the optical axis of the NIDC. Each flat facet mirror is tilted at two orientation angles based on its location in NIDC to reflect incident sunrays to a common target and thus different facet mirrors reflects incident sunlight at different angles of reflection.

The sunrays reflected by the facet mirrors at four corners have the largest incident angle relative to the receiver plane and thus the rim angle of NIDC is defined as angle subtended by the light rays reflected by the two most distant facet mirrors, which are located at the top-left corner and bottom-right corner. Fig. 1 shows a facet mirror located at one corner of the NIDC where its distance from center of the NIDC in *X*-direction and *Y*-direction are 92.25 cm and 96.25 cm respectively. The shortest vertical distance in *Z*-direction from central point of entrance aperture of secondary optics to the line joining the central points of two most distant facet mirrors is 183.86 cm. The rim angle is calculated as 71.9° by using the following equation.

$$\text{Rim angle, } \theta = 2\tan^{-1}\left(\frac{H_{xy}}{H_z}\right) = 2\tan^{-1}\left(\frac{\sqrt{92.25^2+96.25^2}}{183.86}\right) \quad (1)$$

2.2. Secondary optics: Crossed compound parabolic concentrator

There are two major requirements for the geometrical design of secondary concentrator. The first requirement is to ensure an exit aperture can match well with the shape and dimension of CPV cell. The second requirement is to ensure acceptance angle of the secondary concentrator is larger than the rim angle of NIDC so that the aperture of secondary optics is sufficiently large to subtend the all the sunrays reflected by NIDC and maximizing the sunlight to be concentrated onto CPV cell.

High efficiency multi-junction CPV cell, which is commercially available, is mostly either square or rectangle in shape. The CPV cells used in our study are product of Spectrolab with mechanical dimension of 11 mm × 10 mm and active area of 9.85 mm × 9.89 mm and the detailed specifications are listed in Table 1 (Spectrolab, 2010). Thus, square exit aperture is highly recommended instead of circular exit aperture in order to map the concentrated sunrays across the CPV cell for aiming to produce uniform illumination throughout the whole active surface area. For this reason, a typical candidate for the secondary concentrator with a square exit aperture would be crossed compound parabolic concentrator (CCPC), which is formed by intersecting two symmetrical 2-D compound parabolic concentrators (CPC) orthogonally. In the perspective of geometrical optics for CCPC, all the sunrays that successfully enter the CCPC within the acceptance angle will emerge at the exit aperture.

A dielectric filled CCPC with square cross sections in both entrance and exit apertures are tailored to match the dimension of CPV cell assembly as shown in Fig. 2. Each CPV cell assembly consists of CPV cell, by-pass diode and direct bonded copper with Au/Ni surface plating (front and back surfaces) on Al_2O_3 substrate. On the other hand, B270 superwite is selected as dielectric material for CCPC lens as it is a clear high transmission crown glass (modified soda-lime glass) available in various forms and affordable in cost. A systematic process as shown in the

Table 1
Specifications of non-imaging dish concentrator, crossed compound parabolic concentrator lens, secondary concentrator, CPV cell assembly, and CPV cell.

Primary concentrator: Non-imaging dish concentrator (NIDC)	
Type of reflector	3 mm mirror with back metallic coating
Number of facet mirror	96 units
Dimension of facet mirror	20 cm × 20 cm
Array arrangement	Facet mirrors arranged into 10 rows and 10 columns with 4 facet mirrors in central region are removed
Focal distance	210 cm
Total reflective area	3.84 m^2
Total projection area of reflector	3.76 m^2
Range of solar rays reflected angle	8.6–36.7°
Crossed compound parabolic concentrator (CCPC) lens	
Dimension of entrance aperture	24 mm × 24 mm
Dimension of exit aperture	9.8 mm × 9.8 mm
Length, L	37.78 mm
Geometrical concentration ratio	5.998
Half acceptance angle, θ'_i	24.1°
Angular half acceptance angle, θ_i	37.77°
Dielectric material	B270 superwite
Refractive index of dielectric material	1.5
Transmittivity of dielectric material	87.5%
Secondary concentrator: Array of CCPC lenses	
Array of CCPC lenses	8 × 8
Entrance aperture size	195.5 mm × 195.5 mm
Gap spacing between CCPC lenses	0.5 mm
CPV cell assembly (Spectrolab product: CCA 100 C3MJ Concentrator Cell Assembly)	
Dimension of CPV cell assembly	25 mm × 21 mm (Note: Original size is 25.5 mm × 21.0 mm as provided in the specification but we trim it to 25 mm × 21 mm)
Typical performance efficiency	38.5%
Ceramic Carrier	Direct bonded copper with Au/Ni surface plating (front and back surfaces) on a Al_2O_3 substrate
By-pass diode	12A Schottky
CPV cell (Spectrolab product: CDO 100 C3MJ)	
Typical performance efficiency	38.5%
Dimension of cell aperture (active area)	9.85 mm × 9.89 mm (98.9 mm^2)
Mechanical dimension of cell (including bus bar, etc.)	11 mm × 10 mm
V_{OC} (1000 W/m^2 irradiance)	2.77 V
I_{SC} (1000 W/m^2 irradiance)	14 mA
Operating temperature of CPV cell	−40 °C to 100 °C

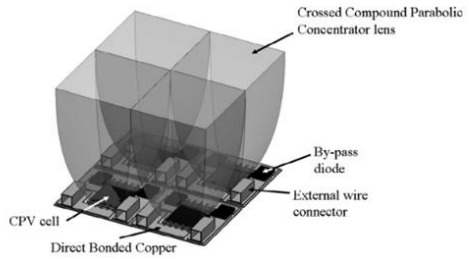

Fig. 2. A 2 × 2 array of CPV + CCPC assembly sets. Each CPV + CCPC assembly set is an integrated concentrator photovoltaic cell assembly and crossed compound parabolic concentrator lens. Each concentrator photovoltaic (CPV) cell assembly consists of triple-junction CPV cell, by-pass diode and direct bonded copper with Au/Ni surface plating (front and back surfaces) on Al_2O_3 substrate.

flow chart described in Fig. 3 has been applied to design the dimension of CCPC lens well tailored to our application.

Referring to Fig. 4, Eqs. (2), (3) and (5) were derived by Winston et al., and Eq. (4) can be derived from Snell Law (Winston et al., 2005).

$$2a = \frac{2a'}{\sin\theta'_i} \tag{2}$$

$$L = \frac{a'\left(1+\sin\theta'_i\right)\cos\theta'_i}{\sin^2\theta'_i} \tag{3}$$

$$\theta_i = \sin^{-1}\left(n\sin\theta'_i\right) \tag{4}$$

$$C_R = \left(\frac{a}{a'}\right)^2 = \left(\frac{1}{\sin\theta'_i}\right)^2 = \left(\frac{n}{\sin\theta_i}\right)^2 \tag{5}$$

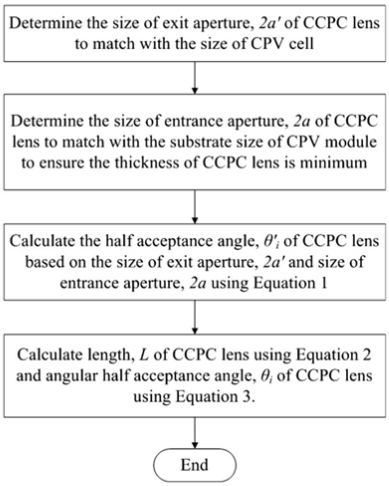

Fig. 3. Flow chart to show systematic process in designing dielectric filled CCPC geometry.

In our design, the CCPC lens should have exit aperture size, $2a' = 9.8$ mm, which is slightly smaller than the active area of the solar cell, 9.85 mm × 9.89 mm, so that all sun-rays arriving at exit aperture can reach the active area of solar cell including the sunlight exiting near the edge of the exit aperture. In the case study, the size of entrance aperture, $2a = 24$ mm, is selected in order to match the dimension of CPV cell assembly, 25 mm × 21 mm, as listed in Table 1 with the configuration as shown in Fig. 4. The purpose of this selection is to ensure the CPV cell assembly can be arranged closely to each other with small tolerance of 0.5 mm in every side and to minimize the thickness of CCPC lens because the absorptivity of sunlight by the dielectric material of CCPC is proportional to the thickness of the lens. The entrance aperture size of CCPC must be either the same or larger than the size of CPV cell assembly so that all CCPC lenses can be arranged tightly to each other. The integrated design of CCPC and CPV is more efficient compared to that of DACPV in terms of packing factor by reducing the percentage of sunlight fallen on non-active area that incurs losses to the whole system.

The final geometrical design of CCPC lens is shown in Fig. 4. The half acceptance angle, θ'_i of CCPC geometry can be computed using Eq. (2) as 24.1°. For dielectric filled CCPC lens made of B270 glass material with refractive index, n, 1.5, the angular half acceptance angle, θ_i of CCPC lens can be calculated as 37.77° using Eq. (4). There are two advantages of CCPC lens against reflector: it increases the acceptance angle due to refraction effect at the air-dielectric interface and it allows total internal reflection without any reflectivity loss. Since the focal distance is inversely proportional to the rim angle based on Eq. (1), the rim angle can be reduced by increasing the focal distance in the case of the rim angle (θ) larger than the acceptance angle of CCPC ($2\theta_i$). By fixing the acceptance angle of CCPC, the adjustment of focal length is necessary to ensure that all the concentrated sunlight from NIDC can be fully guided to the exit aperture. The length, L of the lens is 37.78 mm calculated with the use of Eq. (3). The geometrical concentration ratio of CCPC, defined as C_R, is expressed in Eq. (5) and is determined as 5.998. The sunlight concentrated by NIDC will be further concentrated by CCPC lens.

Secondary concentrator is comprised of CCPC lenses arranged into row and column to form 2-D array as shown in Fig. 5. Primary focused image size of 22.6 cm × 22.6 cm produced by the NIDC can be obtained from the simulated result as plotted in Fig. 6. The entrance aperture is placed at the focal plane of NIDC for collecting the concentrated sunlight from NIDC and each of CCPC lenses will further focus the sunlight on their respective CPV cell. An array of 8 × 8 dielectric filled CCPC lenses is arranged closely with a gap spacing of 0.5 mm between two adjacent lenses to form a secondary concentrator so that total surface area 19.55 cm × 19.55 cm of the entrance aperture can match with the primary focused image of NIDC. The entrance aperture of secondary concentrator is purposely designed to be slightly smaller size than that of primary focused image. Due to solar disc effect, peripheral region of the primary focused image with much lower solar concentration ratio as compared to that of the central region is omitted.

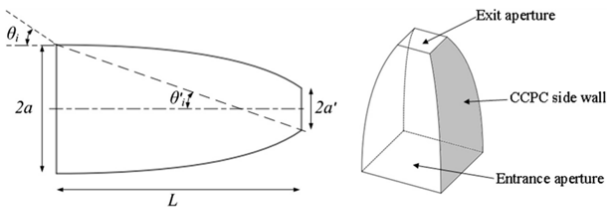

Fig. 4. Dielectric filled crossed compound parabolic concentrator with angular half acceptance angle, θ_i of 37.77°. The square entrance aperture size, $2a$ is 24 mm; square exit aperture size, $2a'$ is 9.8 mm; and the total length, L is 37.78 mm.

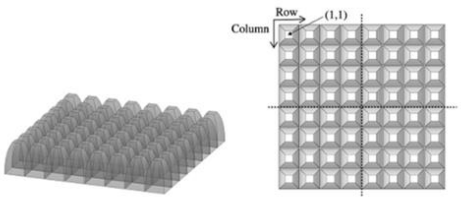

Fig. 5. An array of 8 × 8 dielectric filled CCPCs is arranged closely with a gap spacing of 0.5 mm between two adjacent lenses to form a secondary concentrator so that total surface area 19.55 cm × 19.55 cm of the entrance aperture can match with the primary focused image of NIDC. The lenses are divided into four symmetrical quadrants.

It is to avoid imbalance in current generation by those CPV cells located in the peripheral region as compared to that of the central region and to subsequently cause current mismatch problem affecting overall conversion efficiency of the whole module.

3. Optical performance study

3.1. Methodology of optical performance study

The optical performance is carefully evaluated by using commercial ray-tracing software, called LightTools. The optical system consists of two major elements: the primary concentrator, which is NIDC and secondary concentrator, which is an array of CCPC lenses with the specifications as listed in Table 1 and the 3-D optical layout design is illustrated in Fig. 1. In our numerical modeling using LightTools, a light source with dimension slightly larger than the dimension of NIDC is generated to generate parallel cone rays with solar disc half angle of 4.65 mrad. The slightly larger light source is important to guarantee that the ray-tracing of sunrays has covered the entire facet mirrors of NIDC in the simulation. In the setting of simulation program, all the flat facet mirrors involved in the ray-tracing program are made of 3 mm thick dielectric glass with back-coated reflective surface. The properties of dielectric filled CCPC is set according to the specifications given by B270 superwite datasheet with refractive index of 1.5 and transmittance of 87.5% (Schott Desag, 2000).

A receiver plane is fixed at the focal plane of NIDC to study the solar flux distribution before the sunrays are further concentrated by CCPC lenses to their respective exit apertures. Moreover, each exit aperture of CCPC is also assigned with a receiver plane to study the concentrated flux distribution. The ratio of flux density at the receiver plane to flux density at the light source is defined as Solar Concentration Ratio (SCR). In each simulation, twelve million rays were traced to obtain the simulated result, and the simulated flux distribution patterns are plotted as shown in the Figs. 6a–d.

For the case of off-tracking, the light source was rotated around the *X*-axis, *Y*-axis and both *X*, *Y* axes with pointing

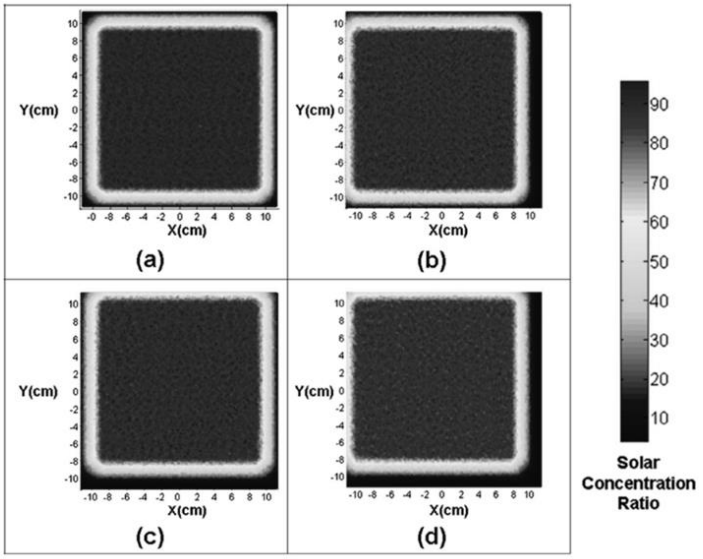

Fig. 6. Solar flux distribution of primary focused image by NIDC: (a) no pointing error (b) pointing error of 0.3° counter-clockwise rotation about *Y*-axis (c) pointing error of 0.3° counter-clockwise rotation about *X*-axis (d) pointing error of 0.3° counter-clockwise rotation about both *X*-axis and *Y*-axis.

error ranging from 0° to 0.4° with increment of 0.1°. The choice of range for pointing error takes into consideration of practical tracking accuracy as if a 12-bits optical encoder is employed as feedback sensors in the tracking algorithm (Chong et al., 2009a, 2009b). After setting all the parameters for primary concentrator, secondary concentrator and receiver planes, the ray-tracing program is initiated to plot the flux distribution pattern on the receiver planes for both NIDC and exit apertures of CCPC lenses.

3.2. Result and discussion of optical performance study

Fig. 6a depicts the simulated result of primary focused image formed by NIDC without pointing error. The simulated solar flux distribution is consisted of flat top region with maximum SCR of 88 suns located in the central region covering the area of 18.2 cm × 18.2 cm and surrounded by steep decrease from 88 suns to 0 within 2 cm near the edge to form a total primary focused image size of 22.6 cm × 22.6 cm. The percentage of energy within the uniform illumination area is 79%. With such uniformity, it can minimize current mismatch problem, which has made it suitable for dense array concentrator photovoltaic (DACPV) application.

Pointing error is caused by inaccurate sun-tracking system and incident sunrays relative to NIDC should be parallel with Z-axis (optical axis of NICD) if there is no pointing error exists. To study the effect of inaccurate sun-tracking towards the electrical performance of CPV system, we simulate the cases of pointing error by rotating the light source from 0 to 0.4° with 0.1° increment in counter-clockwise direction about X-axis, Y-axis, and both X & Y axes concurrently. For pointing error of 0.3° counter-clockwise about Y-axis as shown in Fig. 6b, the primary focused image has shifted to negative direction of X-axis without any obvious distortion in both flux distribution pattern and image dimension. For pointing error of 0.3° counter-clockwise about X-axis as shown in Fig. 6c, the primary focused image has shifted to positive direction of Y-axis without any obvious effect to both flux distribution pattern and image dimension. Finally, the study also includes the case of off tracking in both axes $X = 0.3°$ counter-clockwise & $Y = 0.3°$ counter-clockwise simultaneously. From the simulated result as shown in Fig. 6d, the whole image has shifted in both X & Y directions without affecting the distribution pattern and dimension. According to the simulated results, the image has shifted about 6 mm towards the corresponding direction for each 0.1° of pointing error.

Fig. 7 shows the simulated solar flux distribution on the receiver planes at the exit apertures of CCPC lenses located in top-left quadrant of the full array. The flux distribution pattern and solar concentration ratio of the other three quadrants are similar to the simulated result in which their relationship are mirror symmetry to each other. Among all the concentrated flux at exit apertures, SCR for the exit aperture of CCPC at the four corners of the complete array is the lowest when it is compared to the SCR for other CCPC lenses. It was reflected by the flux distribution pattern of primary focused image with the lowest average SCR at the corner. Total average SCR at the CCPC position (4,4) or central region of the secondary concentrator is 416 suns whilst the SCR is lower for those CCPC lenses located in outermost ring with the lowest SCR at four

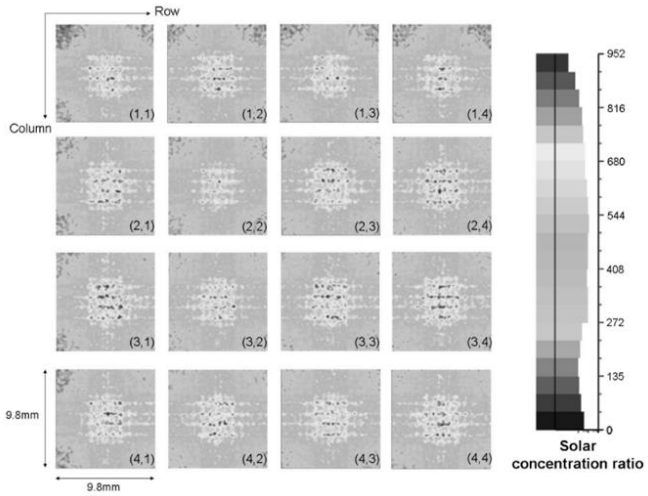

Fig. 7. Solar flux distribution at the exit aperture of top left quadrant (first 4 rows and first 4 columns) of CCPC array for the case of without pointing error during sun-tracking.

Table 2
The position of crossed compound parabolic concentrator (CCPC) lens in the top left quadrant of full array and its corresponding peak-to-average ratio (PAR).

CCPC position	PAR	CCPC position	PAR
(1,1)	2.35	(3,1)	2.14
(1,2)	2.26	(3,2)	2.22
(1,3)	2.35	(3,3)	2.09
(1,4)	2.33	(3,4)	2.08
(2,1)	2.21	(4,1)	2.20
(2,2)	2.16	(4,2)	2.17
(2,3)	2.14	(4,3)	2.14
(2,4)	2.11	(4,4)	2.11

corners. The overall uniformity of solar flux distribution pattern is acceptable, in which the value of peak to average ratio (PAR) of the all exit apertures ranges from 2.08 to 2.35 as listed in Table 2. For the solar flux distribution in the full CCPV array, the average SCR for 6×6 array of CCPC located in the central region of receiver is 416 suns, but the average SCR ranges from 346 to 381 suns for CCPCs located at four edges of the 8×8 array.

Baig et al. (2012, 2013) had done an extensive study on the non-uniform illumination in both concentrating solar cell and module. According to Baig et al., the non-uniform incident flux illuminated on solar cell would affect the fill factor (FF) of solar cell, which can reduce the maximum power output. In fact, it is very difficult to obtain uniform illumination as there are many factors that can cause non-uniformity such as the imperfection of optical geometry, aberration, geometrical error of concentrator profile caused by manufacturing defect, inaccurate sun-tracking, optical misalignment of solar concentrator, and mechanical failures. To quantify different profiles of non-uniformity, Herrero et al. (2012) had introduced a parameter called peak-to-average ratio (PAR). They had characterized the non-uniform light patterns produced by optical systems and reproduced them on CPV cells in experiment to obtain the fill factor under different profiles of non-uniformity in which the percent variation of fill factor (FF) versus PAR of multi-junction (MJ) solar cell is provided in Fig. 8 (Herrero et al., 2012). Considering CCPC located at (4,4) with peak SCR of 952 suns and average SCR of 416 suns, the peak-to-average ratio (PAR) is only $952 \div 416 = 2.29$. The PAR of illumination at the exit apertures of the CCPC lenses ranges from 2.08 to 2.35 in our study. From Fig. 8, the non-uniformity with PAR below 2.5 will not significantly affect the fill factor of CPV cell.

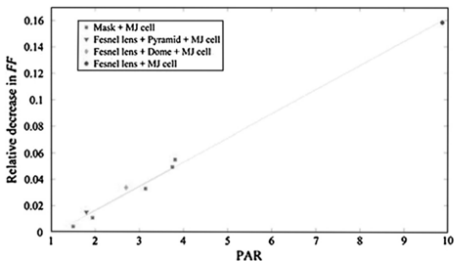

Fig. 8. Percent variation of fill factor (FF) versus peak-to-average ration (PAR) of multi-junction (MJ) solar cell. (Herrero et al., 2012).

4. Electrical performance study

4.1. Methodology of electrical performance study

We have adopted numerical modeling method by using Simulink to analyze the electrical performance of two different electrical layout designs of CPV cells: (1) dense array concentrator photovoltaic (DACPV) module based on solar flux distribution of primary focused image, and (2) array of integrated CPV cells and CCPC lenses (CPV + CCPC) assembly module based on solar flux distribution at CCPC exit apertures. As proposed by Siaw et al. (2014), a circuit with three current sources connected in series is applied in our study to represent a comprehensive equivalent circuit model for a triple-junction CPV cell. The triple-junction CPV cell circuit model is then simplified into a single-diode model, which is equivalent to a CPV cell block in SimElectronics, which is the function block in Simulink. CPV cell block represented by a single CPV cell as current source with one exponential diode, a parallel resistor of resistance R_P, and a serial resistor of resistance R_S are arranged into subsystems in Simulink to form an array. The five-parameter model is chosen as it is good enough to perform a sensibly accurate analysis and it was successfully verified in the field test conducted by Siaw et al. (2014).

Short circuit current of CPV cell under one sun, I_{SC}^1 and open-circuit voltage under one sun, V_{OC}^1 can be determined from the Spectrolab datasheet for CPV cell (Spectrolab, 2010). The formulas of short-circuit current, I_{SC}, and open-circuit voltage, V_{OC}, of CPV cell are expressed in Eqs. (6) and (7) respectively (Siaw and Chong, 2013; Siaw et al., 2014). Solar irradiance at solar concentration ratio of one sun is equivalent to 1000 W/m^2. For this study, the ideality factor of CPV cell and series resistance are assumed to be $N = 3$ and $R_S = 0\,\Omega$ respectively. The default temperature for the modeling is 25 °C and the solar concentration ratio (SCR) is represented by C_R.

$$I_{SC} \cong I_{SC}^1 \times C_R \tag{6}$$

$$V_{OC} \cong V_{OC}^1 + N(kT/q)\ln C_R \tag{7}$$

The efficiency data of CPV cell provided by the datasheet of Spectrolab is only limited to SCR ranging from 350 to 900 suns (Spectrolab, 2010). For the SCR below 350 suns, the maximum power efficiency can be simulated by using Simulink and based on five parameters extracted from Spectrolab datasheet, i.e. $I_{SC}^1 = 14.0$ mA,

$V^1_{OC} = 2.77$ V, 1 sun = 1000 W/m^2, $N = 3$, and $R_S = 0\ \Omega$ at temperature of 25 °C. For the completeness of electrical performance study, we have modeled and plotted the graph of the maximum power efficiency against solar concentration ratio ranging from 1 to 1000 suns for single CPV cell as shown in Fig. 9. The simulated maximum power efficiencies from the Simulink modeling are also verified with the data given in the Spectrolab datasheet with acceptable deviation between both results ranging from −0.15% to 0.81% for SCR of 350–900 suns and the details are listed in Table 3.

The maximum power efficiency of CPV cell is calculated using the following equation:

$$\text{Maximum power efficiency} = \frac{\text{Maximum output power}}{\text{Active area of CPV cell} \times C_R \times 1000\ \text{W m}^{-2}} \times 100\% \quad (8)$$

Before the optimization process begins, the sizes of the both modules are set to be the same, which are 20 cm × 20 cm based on the size of a single flat facet mirror in NIDC. It also provides a fair comparison for both DACPV and CPV + CCPC assembly modules by using the same area of primary focused image for the electrical performance analyses. One major concern in the comparison for both DACPV and CPV + CCPC assembly modules is that the electrical conversion efficiency is SCR dependent parameter in which the SCR for DACPV is in the range of 88 suns whilst the SCR for CPV + CCPC is in the range of 400 suns. Referring to Fig. 9, the conversion efficiencies for 88 suns and 400 suns are 38.2% and 38.7% respectively with the difference of only 0.5% and hence it is still acceptable for an academic study to understand the advantage of inserting secondary optics into the system. The primary focused image size formed by NIDC is 22.6 cm × 22.6 cm, which is a slightly larger than the size of module that we set. The external region beyond the boundary of 20 cm × 20 cm of the primary focused image is ignored in our electrical simulation as the SCR is less than half of the highest SCR in the central region.

Fig. 10 shows a detailed algorithm for optimizing the electrical layout for both DACPV and CPV + CCPC assembly modules. From the optical simulation results presented in previous section, the values I_{SC} and V_{OC} of every CPV cell or CPV + CCPC assembly set are calculated according to the solar concentration ratio mapped to them. In the process of optimizing the electrical layout, the CPV cells or CPV + CCPC assembly sets are divided into four

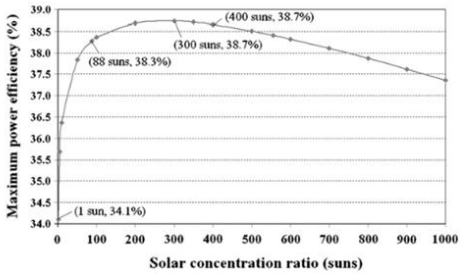

Fig. 9. Maximum power efficiency of CPV cell obtained from the numerical modeling using Simulink and five parameters extracted from Spectrolab datasheet ($I^1_{SC} = 14.0$ mA, $V^1_{OC} = 2.77$ V, 1 sun = 1000 W/m^2, $N = 3$, $R_S = 0\ \Omega$ at temperature 25 °C). Note: The maximum power efficiency with SCR of 350–900 suns obtained from our simulation is very close to that of the datasheet provided by Spectrolab as shown in Table 3.

Table 3
Comparison of the maximum power efficiency between the numerical modeling and Spectrolab datasheet for Spectrolab CPV cell.

Solar concentration ratio	Maximum power efficiency of Spectrolab CPV cell (%)		Difference (%)
	Spectrolab datasheet	Numerical modeling	
350	38.56	38.71	−0.15
555	38.51	38.41	0.10
700	38.51	38.10	0.41
900	38.48	37.62	0.86

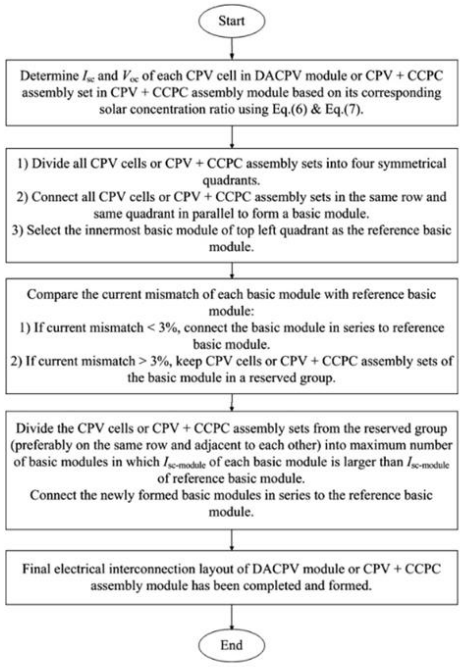

Fig. 10. Flow chart to show an algorithm for optimizing the electrical layout for both DACPV module and CPV + CCPC assembly module.

symmetrical quadrants. All CPV cells or CPV + CCPC assembly sets of the same row and quadrant are connected in parallel to form a basic module at first. In our study, there are 32 basic modules to form a complete DACPV module and 16 basic modules to form a complete CPV + CCPC assembly module. The innermost basic module of the top-left quadrant is selected as the reference basic module to form the complete DACPV or CPV + CCPC assembly module. The short circuit current of basic module, $I_{SC\text{-module}}$ is defined as a sum of short circuit currents of all CPV cells or CPV + CCPC assembly sets in the same basic module. Then, $I_{SC\text{-module}}$ of all other basic modules is compared to $I_{SC\text{-module}}$ of reference basic module to determine the amount of current mismatch. If the amount of current mismatch is less then 3%, the basic module will be connected in series with the reference basic module. Otherwise, the CPV cells or CPV + CCPC assembly sets of the basic module will be kept in a reserved group. After the first optimizing process is completed, the CPV cells or CPV + CCPC assembly sets in the reserved group are divided into a maximum possible number of basic modules in which $I_{SC\text{-module}}$ of each basic module must be larger than that of the reference basic module. The selection criterion for CPV cells or CPV + CCPC assembly sets in the reserved group to form a basic module is that those cells or assembly sets must be located in immediate adjacent to each others for a convenience of practical assembling process. Last but not least, all the basic modules from the reserved group are connected in series to the reference basic module to form a complete DACPV module or CPV + CCPC assembly module as shown in Fig. 11 or Fig. 12.

Figs. 11 and 12 show the optimized electrical layout for CPV + CCPC assembly and DACPV modules respectively. In the design of the electrical interconnection layout for DACPV module, two criteria must be fulfilled to include the practical consideration of physical assembling process for the module. First criterion is that the CPV cells from the same row of the array must be connected in parallel except those cells from the rows in both ends. Second criterion is that each basic module must contain at least one CPV cell located at the outermost ring of the array to allow each basic module connected to a by-pass diode for protecting the cells from reverse bias voltage breakdown. The mechanical dimension of CPV cell used in this study is 11 mm × 10 mm. Considering the requirements of preparing more space for both die attachment of solar cells on direct bond copper (DBC) substrate and interconnection between cells via ribbon bonding process, gap spacing between adjacent CPV cells are 1 mm along row direction and 2 mm along column direction.

4.2. Result and discussion of electrical performance study

The optimized electrical layouts of the CPV + CCPC assembly module and DACPV module used for electrical performance study using Simulink are shown in Figs. 11 and 12 respectively. Fig. 13 illustrates flow chart of the modeling process using Simulink to obtain the electrical performance results of CPV module by plotting *I–V* and *P–V* curves. Fig. 14 shows simulated *I–V* and *P–V* curves of CPV + CCPC assembly module without pointing error and maximum power output, P_{mp} can be extracted from *P–V* curve. Similarly, *I–V* and *P–V* curves for both CPV + CCPC assembly module and DACPV module are also plotted under different conditions includes pointing error 0, 0.1°, 0.2°, 0.3°, 0.4° in the cases of *X*-axis, *Y*-axis and *X* & *Y* axes concurrently. Maximum output power (kW) and system efficiency (%) are extracted from the aforementioned simulated results to plot against pointing error.

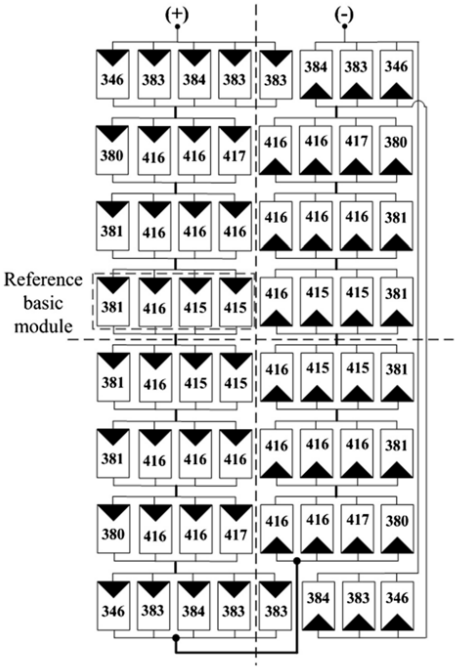

Fig. 11. Optimized electrical layout design with average solar concentration ratio assigned to each CPV cell for CPV + CCPC assembly module under perfect sun-tracking condition.

System efficiency of the DACPV module and CPV + CCPC assembly module is calculated using Eq. (9) as follow,

$$\text{System efficiency} = \frac{\text{Maximum output power of DACPV module or CPV + CCPC assembly module}}{\text{Total projection area of NIDC} \times 1000\,\text{W m}^{-2}} \quad (9)$$

Fig. 15 depicts a comparison of maximum output power and system efficiency between DACPV module and

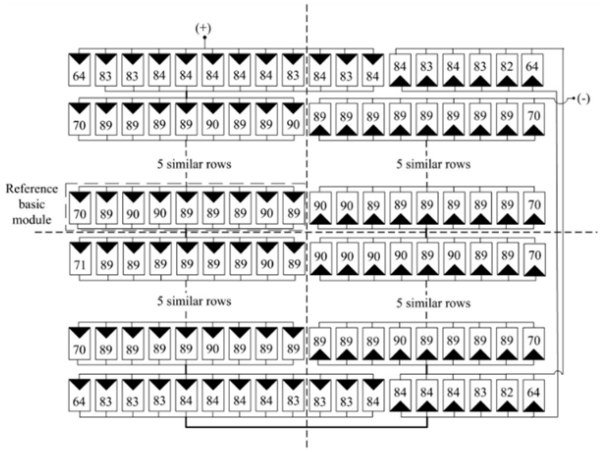

Fig. 12. Optimized electrical layout design with average solar concentration ratio assigned to each CPV cell for DACPV module under perfect sun-tracking condition.

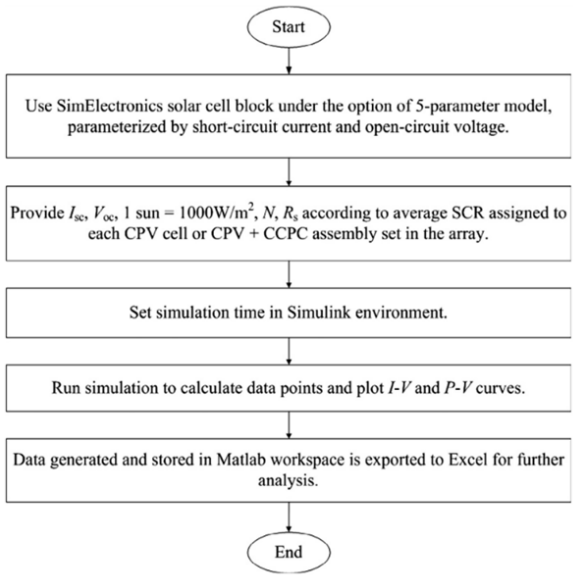

Fig. 13. Flow chart to show Simulink algorithm for electrical performance modeling of CPV module.

CPV + CCPC assembly module for different pointing errors ranging from 0° to 0.4° by rotating the light source about X-axis, Y-axis and both X & Y axes concurrently. In overall, the maximum output power of CPV + CCPC assembly module is better than that of DACPV module for all angles of pointing error about any axis even though the absorption loss of dielectric filled secondary concentrator as high as 12.5% was introduced.

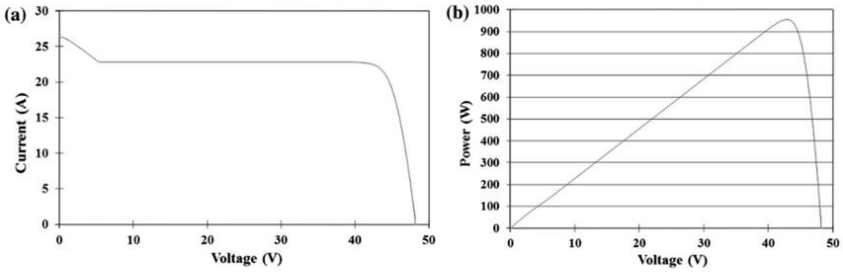

Fig. 14. (a) *I–V* curve, (b) *P–V* curve of CPV + CCPC assembly module without pointing error.

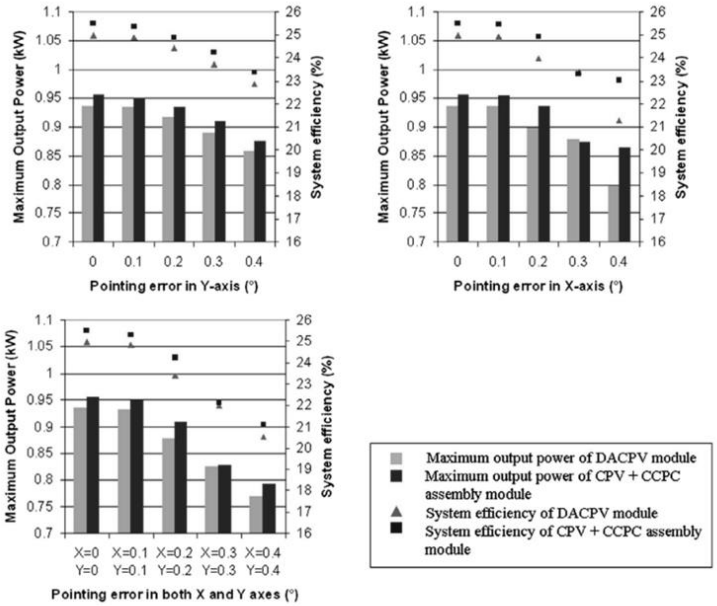

Fig. 15. Comparison of maximum output power (kW) and system efficiency (%) for DACPV module and CPV + CCPC module with pointing error ranging from 0° to 0.4° caused by rotating light source about *Y*-axis (top left), *X*-axis (top right) and both *X* & *Y* axes (bottom).

By increasing pointing error about *X*-axis, the primary focused image will gradually shift along *Y*-direction and it will cause a drastic drop in the maximum output power when the pointing error has reached 0.3° because the outermost basic module is no longer illuminated and current mismatch becomes more severe owing to serial connection of all the basic modules in *Y*-direction. According to Fig. 15, there is indeed a drastic drop in maximum power output of CPV + CCPC assembly module when the pointing error about *X*-axis has increased from 0.2° to 0.3°. It is also revealed in the percentage of current mismatch between outermost basic module and reference basic module in which the current mismatch is only 5% when pointing error is 0.2° but it has increased steeply to 20% when pointing error is 0.3°. For DACPV module, steep increase in current mismatch between outermost basic module and reference basic module only happens when the pointing error about *X*-axis has increased from 0.3° to 0.4° in which the percentage of current mismatch at pointing error 0.3° and 0.4° are 23% and 55% accordingly. Consequently, the decrease in maximum power output for DACPV module at pointing error about *X*-axis 0.3° is less than that of

CPV + CCPC assembly module. In this case, the maximum power output of DACPV module is 5 W more than CPV + CCPC assembly module.

CPV + CCPC assembly module can reduce the usage of CPV cells by 77% in which a total of 282 CPV cells was employed in DACPV module but only 64 CPV cells was utilized in CPV + CCPC assembly module. The packing factor of DACPV is only 0.7 and hence 30% of solar energy is concentrated on the non-active area of receiver without converted to electricity. The major cause of low packing factor in DACPV module are: the two stripes of bus bar with the width of 0.5 mm each on the surface of CPV cell, the adjacent CPV cells cannot be arranged too close to each other to avoid short circuit current and 1 mm of gap spacing is introduced for the sake of the die attachment process of CPV cells on the DBC, the limitation of DBC substrate where the size of alumina layer is always larger than the size of copper layer to create 2 mm of gap spacing when the DBCs are attached onto a heat sink.

5. Conclusion

Optical and electrical analyses of NIDC with an array of CCPC lenses as secondary concentrator for the application in CPV system are presented. For optical performance of CPV + CCPC module, the overall uniformity of solar flux distribution pattern is acceptable in which the value of peak to average ratio (PAR) of the all exit apertures ranges from 2.08 to 2.35. The modeling of electrical performance has also shown that the maximum output power of CPV + CCPC modules is better than that of DACPV module in overall despite absorption loss of 12.5% in CCPC lens. In addition, CPV + CCPC module can reduce the usage of CPV cells by 77% as compared with DACPV module. The use of CCPC lenses as secondary concentrator can provide more space to ease the electrical interconnection among CPV cells and to allow by-pass diode connected to each CPV cell as compared to DACPV module with very limited electrical connection. Furthermore, any damaged or faulty CPV cell assembly in CPV + CCPC module is easily replaceable without affecting others unlike the DACPV module where any faulty cell can cause unrecovered damaged to the whole module.

Acknowledgements

The authors would like to express their gratitude to the Ministry of Energy, Green Technology and Water (AAIBE Trust Fund) and the Ministry of Science, Technology and Innovation (e-Science Fund with project number 03-02-11-SF0143) for their financial support. The authors would also like to thank Synopsys for providing evaluation license of their optical solution product: LightTools, and Dr Wong Kok Fye from Dow Corning for providing the adhesive materials for our research work.

References

Baig, H., Heasman, Keith C., Mallick, Tapas K., 2012. Non-uniform illumination in concentrating solar cells. Renew. Sustain. Energy Rev. 16 (8), 5890–5909.

Baig, H., Sarmah, N., Heasman, Keith C., Mallick, Tapas K., 2013. Numerical modelling and experimental validation of a low concentrating photovoltaic system. Sol. Energy Mater. Sol. Cells 113, 201–219.

Baig, H., Sellami, N., Chemisana, D., Rosell, J., Mallick, Tapas K., 2014. Performance analysis of a dielectric based 3D building integrated concentrating photovoltaic system. Sol. Energy 103, 525–540.

Chong, K.K., Siaw, F.L., Wong, C.W., Wong, G.S., 2009a. Design and construction of non-imaging planar concentrator for concentrator photovoltaic system. Renew. Energy 34 (5), 1364–1370.

Chong, K.K., Wong, C.W., Siaw, F.L., Yew, T.K., Ng, S.S., Liang, M.S., Lim, Y.S., Lau, S.L., 2009b. Integration of an on-axis general sun-tracking formula in the algorithm of an open-loop sun-tracking system. Sensors 9 (10), 7849–7865.

Chong, K.K., Wong, C.W., Yew, T.K., Tan, M.H., 2012. Solar Concentrator Assembly, Malaysian Patent. No. PI 2012002439 (pending) filed on 31st May 2012.

Chong, K.K., Wong, C.W., Yew, T.K., Tan, M.H., 2013a. Solar Concentrator Assembly. US Patent, Application No.: 13/901,519 (pending) filed on 23rd May 2013.

Chong, Kok-Keong, Lau, Sing-Liong, Yew, Tiong-Keat, Tan, Philip Chee-Lin, 2013b. Design and development in optics of concentrator photovoltaic system. Renew. Sustain. Energy Rev. 19, 598–612.

Chong, K.K., Yew, T.K., Tan, M.H., 2014a. Dense-Array Concentrator Photovoltaic System Utilising Non-Imaging Dish Concentrator and Array of Crossed Compound Parabolic Concentrators. Malaysian Patent, No. PI 2014000210 (pending) filed on 23rd January 2014.

Chong, K.K., Yew, T.K., Tan, M.H., 2014b. Dense-Array Concentrator Photovoltaic System Utilising Non-Imaging Dish Concentrator and Array of Crossed Compound Parabolic Concentrators. US Patent, Application No.: 14/462,891 (pending) filed on 19th August 2014.

Chong, K.K., Yew, T.K., Tan, M.H., 2014c. Dense-Array Concentrator Photovoltaic System. China Patent. Application No./Patent No.: 201410529913.2 Date of Filing: October 9, 2014.

Herrero, R., Victoria, M., Domínguez, C., Askins, S., Antón, I., Sala, G., 2012. Concentration photovoltaic optical system irradiance distribution measurements and its effect on multi-junction solar cells. Prog. Photovoltaics Res. Appl. 20, 423–430.

King, R., Bhusari, D., Larrabee, D., Liu, X., Rehder, E., Edmondson, K., Cotal, H., Jones, R., Ermer, J., Fetzer, C., Law, D., Karam, N., 2012. Solar cell generations over 40% efficiency. Prog. Photovoltaics Res. Appl. 20 (6), 801–815.

Mallick, T.K., Eames, P.C., Hyde, T.J., Norton, B., 2004. The design and experimental characterisation of an asymmetric compound parabolic photovoltaic concentrator for building facade integration in the UK. Sol. Energy 77, 319–327.

Mammo, Eliyas Debebe, Sellami, Nazmi, Mallick, Tapas Kumar, 2012. Performance analysis of a reflective 3D crossed compound parabolic concentrating photovoltaic system for building façade integration. Prog. Photovoltaics Res. Appl. 21, 1095–1103.

Micheli, L., Sarmah, N., Fernandez, E.F., Reddy, K.S., Mallick, T.K., 2014. Technical issues and challenges in the fabrication of a 144-Cell 500× concentrating photovoltaic receiver. In: Photovoltaic Specialist Conference (PVSC), 2014 IEEE 40th, pp. 2921, 2925.

Oommen, Rachel, Jayaraman, S., 2002. Development and performance analysis of compound parabolic solar concentrators with reduced gap losses—'V' groove reflector. Renew. Energy 27, 259–275.

Ryu, Kwangsun, Rhee, Jin-Geun, Park, Kang-Min, Kim, Jeong, 2006. Concept and design of modular Fresnel lenses for concentration solar PV system. Sol. Energy 80, 1580–1587.

Schott Desag, 2000. Specification: Physical and Chemical Properties B270 Superwite. Datasheet. Date Release: 02 May 2000. 04.00, 14 pages.

Sellami, Nazmi, Mallick, Tapas K., 2013. Optical efficiency study of PV crossed compound parabolic concentrator. Appl. Energy 102, 868–876.

Sellami, N., Mallick, T., McNeil, D.A., 2010. Optical performance modeling of a typical 3-D cross compound parabolic photovoltaic concentrator using ray trace technique. Paper Presented at 6th Photovoltaic Science, Applications and Technology Conference, Southampton, United Kingdom, 24/03/10–26/03/10.

Siaw, Fei-Lu, Chong, Kok-Keong, 2013. A systematic method of interconnection optimization for dense-array concentrator photovoltaic system. Sci. World J. Article ID 275169, 11 pages.

Siaw, F.-L., Chong, K.-K., Wong, C.-W., 2014. A comprehensive study of dense-array concentrator photovoltaic system using non-imaging planar concentrator. Renew. Energy 62, 542–555.

Sonneveld, P.J., Swinkels, G.L.A.M., van Tuijl, B.A.J., Janssen, H.J.J., Campen, J., Bot, G.P.A., 2011. Performance of a concentrated photovoltaic energy system with static linear Fresnel lenses. Sol. Energy 85, 432–442.

Spectrolab Inc., 2010. CCA 100 C3MJ Concentrator Cell Assembly. Datasheet. <www.spectrolab.com>.

Tan, M.H., Chong, K.K., Wong, C.W., 2014. Optical characterization of nonimaging dish concentrator for the application of dense-array concentrator photovoltaic system. Appl. Opt. 53 (3), 475–486.

Welford, W.T., Winston, R., 1978. Optics of Nonimaging Concentrators. Light and Solar Energy. Academic Press Incorporated, New York, United States.

Winston, R., Miñano, J.C., Benítez, P., 2005. Nonimaging Optics. Elsevier Academic Press, Burlington, Mass., pp. 50–57.

Zubi, Ghassan, Bernal-Agustin, Jose L., Fracastoro, Gian Vincenzo, 2009. High concentration photovoltaic systems applying III–V cells. Renew. Sustain. Energy Rev. 13, 2645–2652.